A Morphological Study of PFCB-Ionomer/ Poly(Vinylidene Fluoride) Copolymer Blends for Fuel Cell Applications

Nathanael May

Thesis submitted to the faculty of the Virginia Polytechnic Institute and State University in partial fulfillment of the requirements for the degree of Master of Science In Materials Science and Engineering

Robert B. Moore, Chair
David A. Dillard
Robert W. Hendricks
Abby Whittington

8-11-2011

Blacksburg, VA

Key terms: Small Angle X-ray Scattering, Perfluorocyclobutane, Proton Exchange Membrane, Partially Fluorinated Ionomer, Sulfonated Aromatic Hydrocarbon, Solution Casting, Morphology

A Morphological Study of PFCB-Ionomer/ Poly(Vinylidene Fluoride) Copolymer Blends for Fuel Cell Applications

Nathanael May

Abstract

A new material for use as a proton exchange membrane in fuel cells has been developed: a blend of a perfluorocyclobutane-based block ionomer (S-PFCB) and Poly (vinylidene-co-hexafluoropropylene) (Kynar Flex, KF). This thesis details the work done thus far to characterize the morphology of this material, using small angle x-ray scattering, differential scanning calorimetry, atomic force micrscopy, and some other techniques to a lesser extent.

Small angle x-ray scattering (SAXS) of pure S-PFCB showed a strong block copolymer-associated phase separation, on the order of 25 nm. Differential scanning Calorimetry (DSC) confirmed this finding. SAXS also revealed the presence of a peak representing individual ionic aggregates on the order of 3 nm. Finally, it was shown with DSC that no crystallinity develops in the S-PFCB block copolymer, while one of the blocks, known as 6F, crystallizes extensively.

SAXS of incremental blend compositions of KF and S-PFCB revealed a steady increase in size of the block copolymer phase separation peak in SAXS, demonstrative of the miscibility of KF and the non-sulfonated 6F block of S-PFCB. Furthermore, this incremental study determined the scattering vector range relevant for comparing amounts of KF crystallinity. DSC of incremental blend compositions revealed two phases of KF crystallinity develops upon cooling a membrane, independent of cooling rate.

Atomic force microscopy (AFM), small angle x-ray scattering (SAXS), and differential scanning calorimetry (DSC) corroborate to suggest a nonuniform morphology through the thickness of solution cast membranes. Also, the effect of different casting temperatures and after-casting anneals on morphology was assessed.

Future work on this project involves morphological studies at various relative humidities and temperatures, as well as following up on discoveries already made. Finally, transmission electron micrscopy (TEM) should be performed to provide a visual analog, which will greatly help in developing an accurate morphological model.

Acknowledgements

I would first like to thank the sponsor of this project, General Motors, for its financial, technical, and material support in understanding this new material system. I appreciate General Motors willingness to invest in this still growing field, and hope that, ultimately, its investments prove both financially and environmentally significant. Specifically, I would like to thank Yeh-Hung Lai and Ron Li, for their regular input and guidance.

My graduate committee, consisting of Professors David Dillard, Robert Hendricks, and Abby Whittington, all have my thanks for providing me with guidance. I am particularly very grateful to my advisor and graduate committee chair, Professor Robert Moore. Throughout my master's studies, he has remained patient with me while I waded deeply into a subject not entirely familiar to me, in polymer morphology and chemistry. Thank you for putting up with my learning experiences throughout this project. I hope this document and my understanding of the subject matter measures up to the standards to which you hold all of your students; I know I have learned much from you and the MoRG.

Speaking of the MoRG, I would like to thank the Moore Research Group as well. From their individual skills and knowledge bases, I learned much of what I needed to complete this project. In particular, I would like to express heartfelt thanks to Mingqiang Zhang, the operator and resident expert for SAXS in the MoRG. He did a good deal of work to help me collect the relevant SAXS data for this project, and was crucial in the completion of my work. Other fellow research colleagues within the GM project also deserve my thanks. Without the help of Katherine Finlay, Ashley Gordon, Chase Siuta, or Jessica <3 Wright, I would not have been able to do the work I have. Thank you all, and I wish you all good hunting.

Contents

Table of Figures

Chapter 1: Introduction to PEM Fuel Cells

1.1 Fuel Cell Operation

Fuel cell technology has potential to offer an alternative energy storage mechanism to gasoline in the energy industry, specifically for automobiles, but also for a variety of other mobile and stationary devices.

Today's dominant technology, the internal combustion engine (ICE), extracts chemical energy from petroleum-based fuels through igniting it to produce mechanical energy. This energy both drives the vehicle and may be converted into electricity to run an automobile's various electronic systems. A fuel cell converts energy through an entirely different mechanism [5].

Take the example of a hydrogen fuel cell. Hydrogen, if ignited with oxygen, combusts violently. This results from electrons associated with the chemical bonds of hydrogen (H-H) and water (O=O) achieving a lower energy state by forming bonds with each other (O-H). The difference in energy in these two states is rapidly converted into heat, light, and mechanical energy, much like how gasoline ignites in an ICE. A fuel cell, however, extracts this energy in an entirely different way. Instead of igniting the two species (oxygen and hydrogen gases), hydrogen gas molecules are first split into two protons and two electrons each via a catalyst, at the surface of a proton exchange membrane (PEM) [5a]. This membrane allows protons to pass through it, but insulates electrons. Thus, electrons are forced to travel through a connected circuit to recombine with the protons on the other side of the membrane. Driving this reaction in one direction is the presence of oxygen on the far side of the PEM. When the protons and electrons arrive at the opposite end of the PEM, they react with oxygen and form water. As protons on the cathode side of the reaction are consumed, the concentration gradient drives more protons across the PEM; as more protons travel through the PEM, more electrons are forced around it to continue the reaction. The movement of electrons around the PEM represents a current, and the energy potential between the cathode (hydrogen side) and anode

(oxygen/water side) constitutes a voltage. Therefore, this chemical reaction directly generates electrical energy [6]. The electrochemical steps of this process are shown in Figure 1-1.

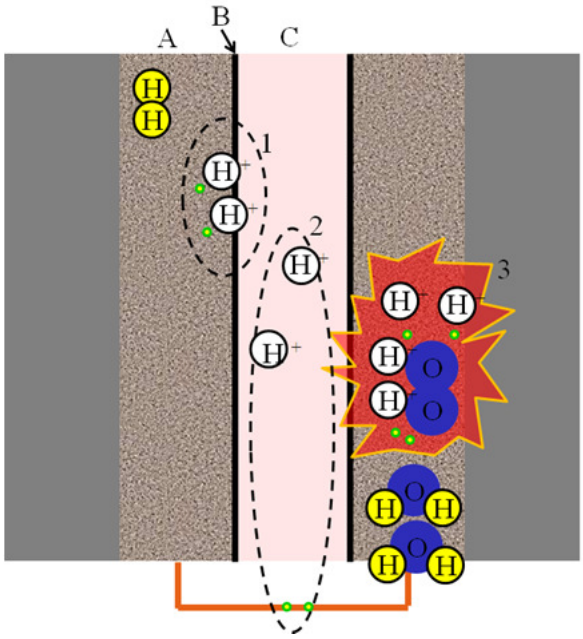

Figure 1-1: Basic PEM fuel cell operation

Fuel cells lack moving parts besides fuel transport mechanisms, which are generally simple air pumps. Thus, maintaining them for long periods of time is mechanically simple. Furthermore, their demonstrated efficiency (40-50%) exceeds that of internal combustion engines (roughly 30%) [7].

1.2 Current PEM Materials

However, many scientific and engineering hurdles still prevent PEM fuel cells (PEMFCs) from being competitive in the current petroleum-based economy. The PEM in particular provides many challenges to making marketable fuel cell-powered products. The case of Nafion® (registered trademark of DuPont, Figure 1-3), the current "benchmark" PEM material, illustrates many of the requirements of an ideal PEM, both in its strengths and shortcomings. Nafion® (Figure 1-3) is an ionomer, a polymer with chemically attached ionic groups;

specifically, Nafion® contains sulfonic acid groups (SO_3^-) that can be neutralized by various cations, from protons to alkalines and more. These sulfonic acid anions tend to form clusters, as shown in

Figure 1-2.

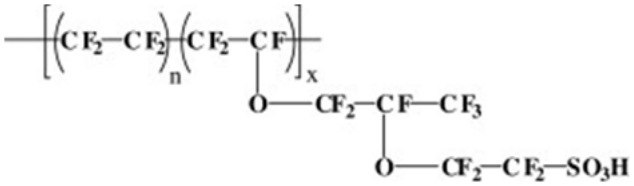

Figure 1-3: Chemical structure of Nafion®

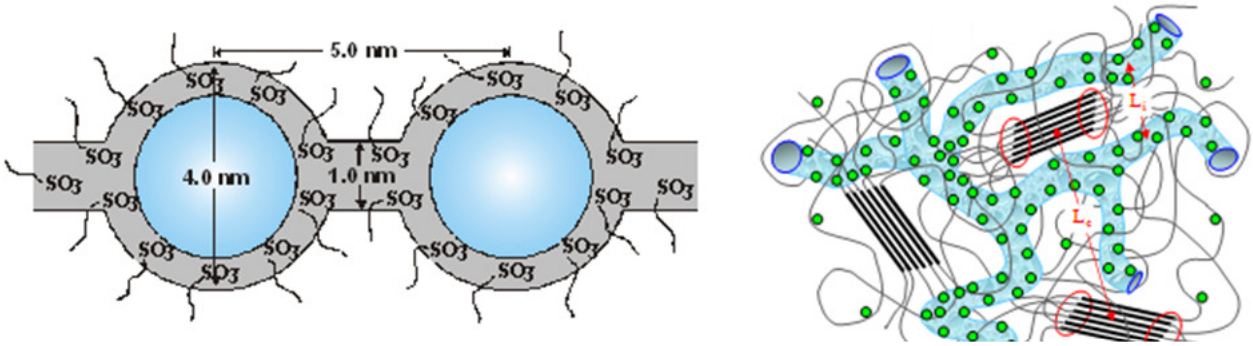

Figure 1-2: Two models for how sulfonic acid aggregates to form water channels [4]

These clusters absorb water, and some other hydrogen-bonding fluids, causing Nafion® to swell visibly in water[8]. When filled with water, these sulfonic-acid aggregates allow for conduction of protons through Nafion®[8]. However, deionized water does not transport electrons. Thus, electrons do not pass through Nafion®, even in its wet state. This means that Nafion® fits the fundamental requirement of a PEM: conductive to protons, but insulating to electrons [8].

Nafion® is perfluorinated, meaning that, every spare carbon bond is associated with a fluorine atom. The C-F bond is extremely chemically stable, giving Nafion® both chemical and

thermal stability. In addition, C-F bonds are hydrophobic, and so water does not tend to permeate the solid polymer chain network. This, in turn, prevents water from degrading a Nafion® membrane.

While possessing the desirable properties of good proton conductivity, thermal and mechanical stability, and resistance to degradation in water, Nafion® also falls short in some material properties. Notably, Nafion®'s high methanol crossover rate prevents is from being used in direct methanol fuel cells, a class of fuel cells receiving great attention for portable applications. Also, high processing costs for Nafion® makes up a large percentage of the total cost of a PEM fuel cell. In fact, some of Nafion®'s desirable properties lead to its high cost. Its high thermal and chemical stability prevent it from being cheaply melt-processed or solution-cast, respectively. Finally, Nafion®'s ionic conductivity tends to drop significantly above 80 °C, while PEMFCs tend to operate at or above this temperature [9]. Thus, both academic and industrial researchers are actively searching for Nafion® alternatives for PEM materials.

A class of polymer known as "aromatic hydrocarbon polymers" possess many of the advantages of Nafion® and other perfluorinated ionomers, having adequate chemical and thermal stability. Aromatic hydrocarbon polymers incorporate aromatic molecules into their structure. The most common type of aromatic group in aromatic hydrocarbon polymers is benzene, but others are occasionally found, as shown in Figure 1-4.

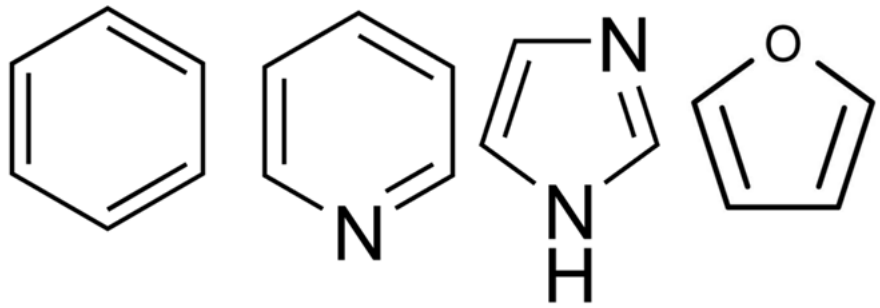

Figure 1-4: Some common aromatic molecules: (from left to right) benzene, pyridine, imidazole, furan

The hydrogens bonded to carbons which are involved in an aromatic structure are considered "aromatic hydrogens"; all other hydrogens involved in hydrogen-carbon bonds are considered

"aliphatic." Aromatic hydrogens cannot be chemically extracted by water under normal conditions like aliphatic hydrogens can, and thus are resistant to degradation in water. Several such polymers, such as sulfonated polyether ether ketone (SPEEK) and sulfonated polystyrene (SPS), beat Nafion® out in proton conductivity at elevated temperatures [10]. SPEEK and several other simple aromatic hydrocarbon ionomers considered for PEM applications are shown in Figure 1-5.

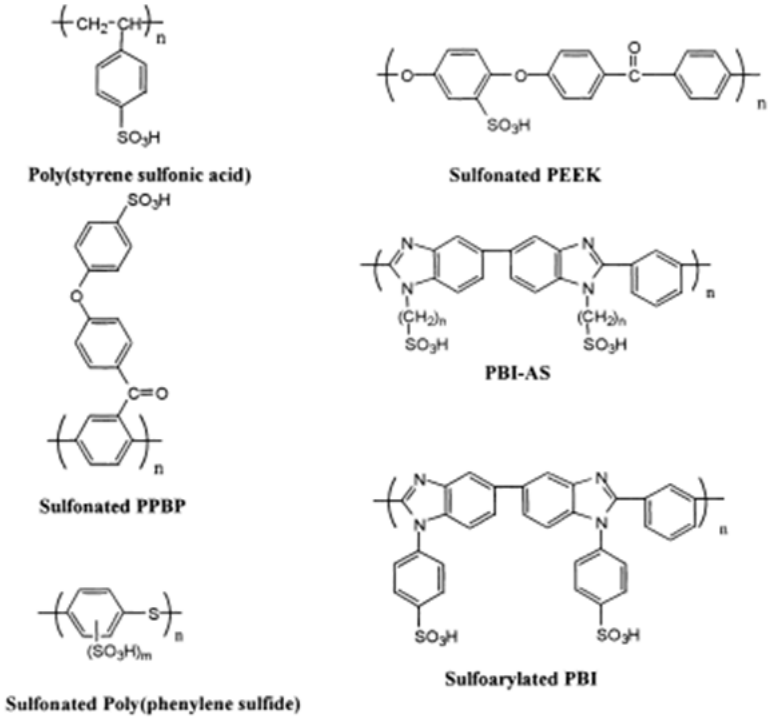

Figure 1-5: Some aromatic hydrocarbon-based ionomers researched for PEM applications [11]

In addition to these traditional polymers, some more recent aromatic hydrocarbon polymers containing perfluorinated groups have been developed [12].

1.3 Development of S-PFCB

As previously discussed, Nafion®'s perfluorinated chains give it many desirable properties such as thermal and chemical stability, properties that also increase its processing costs. Including perfluorinated groups into aromatic hydrocarbon polymer repeat units yields a

material with good stability under many conditions that can be processed easily. Perfluorocyclobutane (PFCB), as in Figure 1-7, achieves these desirable properties by combining both perfluorinated and aromatic groups into its backbone. This backbone, due to its aromaticity, is rather stiff, and hinders organization of sulfonic acid groups bonded directly to it (main chain sulfonated, MCS). Therefore, placing sulfonic acid groups at the end of a relatively flexible side chain (side chain sulfonated, SCS) allows for lower energy organization of sulfonic acid groups into ionic aggregates. GM initially used an MCS polymer, but moved to SCS after studies showed phase separation between the S-PFCB and KF in MCS polymers under exposure to humidity and elevated temperature (both sulfonated blocks shown in Figure 1-7) [13].

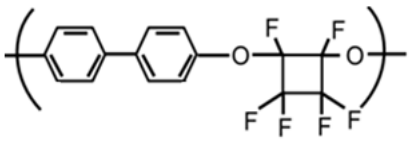

Figure 1-7: Biphenyl vinyl ether-pefluorocyclobutane (BVPE-PFCB, or simply PFCB)

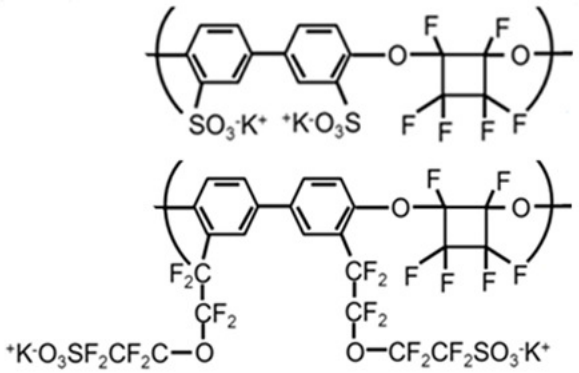

Figure 1-7: "Gen-1", MCS (top) and "Gen 2", SCS (bottom) S-PFCB, sulfonated block only

Sulfonated aromatic polymers such as these show even greater proton conductivity in the block form, as opposed to a random copolymer form [14]. It is thought that the block structure brings sulfonated groups closer together, and allows for better organization of ionic channels and finer control of morphology [15].

However, current aromatic hydrocarbon ionomers (including PFCB) exhibit great dimensional changes with elevated water content, a phenomenon known as hygral expansion; this occurs as the polymer's ionic aggregate network takes in water molecules. An unconstrained membrane would swell significantly when hydrated (i.e. when in use) and contract when hydration levels decrease (i.e. when not in use). However, when inside of an actual fuel cell, the PEM is sandwiched between two gas diffusion layers, constraining it locally in two dimensions; these constraints induce stress cycles when the hydration of the PEM changes. Therefore, significant hygral expansion, combined with their brittleness, often causes

aromatic hydrocarbon ionomers to fail under hydration cycling. Because PEMFCs in vehicular use undergo regular hydration cycling (as the vehicle is turned on and off), the mechanical performance of such ionomers must be improved.

One such way to improve mechanical and hygral stability is to promote crystallinity, but complex polymers such as PFCB do not tend to crystallize. However, one particular PFCB-based polymer, known as 6F (Figure 1-8), shows crystallinity despite having a bulky backbone [3].

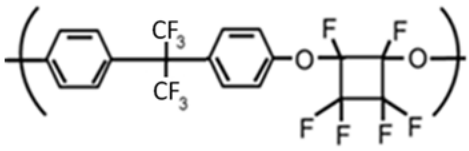

Figure 1-8: "6F" PFCB-BVPE polymer, a PFCB that shows significant crystallinity

Using 6F as a non-sulfonated block, and combining it with blocks of sulfonated PFCB, a polymer with outstanding properties results. However, despite a theoretical increase in stability from incorporating 6F, a block copolymer of 6F and sulfonated PFCB remains brittle, with unacceptably high hygral expansion.

1.4 KF Blends

Research has been done into blending tough, rubbery polymers into these brittle ionomers to provide a low cost, high conductivity, and mechanically stable PEM. Any material blended in these ionomers must likewise have great resistance to chemical attack (i.e. water) and must not degrade at temperatures within the fuel cell's operation range. Polyvinylidene fluoride (PVDF) and related polymers, as shown in Figure 1-9, fit these criteria, and are often blended into brittle ionomers to improve their mechanical properties [16].

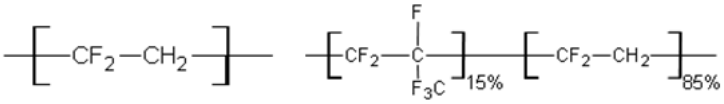

Figure 1-9: PVDF, l (Kynar) and PVDF-co-hexafluoropropylene, r (Kynar Flex, KF)

General Motors is currently investigating a blend of PFCB-based ionomers and Kynar Flex (KF) for its next generation fuel cell vehicles. In order to predict lifetime behavior of this new PEM material, GM needs mechanical models to calculate the extent to which cycling the membrane with respect to temperature and water content will compromise its performance. Typically, mechanical failure manifests as pinholes or thinning through the PEM that act as a short circuit for hydrogen gas to escape through, drastically decreasing its efficiency. In addition to mechanical characterization, GM must understand the morphology of the polymer, as morphology dictates the material's conductive and mechanical properties. Furthermore, GM desires the ability to predict performance based on processing, which comes from thorough understanding of the processing-morphology relationship.

This thesis relays in detail the current understanding of the morphology of these blends, based on studies involving several techniques, and centered heavily on small angle x-ray scattering. We have probed the blocky phase separation of this material, and shown how changes in both Kynar Flex content as well as several processing parameters influences the pure ionomer, S-PFCB and its blends.

Chapter 2: Literature Review: Morphological Development and Characterization of Ionomers

2.1 Perfluorinated Polymer Property-Morphology-Processing Relationship

Understanding the performance of the benchmark perfluorinated ionomer (PFSI), Nafion®, begins with understanding the most basic perfluorinated polymer: polytetrafluoroethylene (PTFE). The degree of crystallinity of PTFE in particular influences its mechanical properties. Crystallinity in PTFE can be easily manipulated using various heat treatments to vary between 25 and 65%, as measured by DSC (which considers fraction of chains involved in crystalline regions). Furthermore, increased molecular weight has a detrimental effect on the amount of crystallinity attained by identical heat treatments [17].

It is well known that the stress-strain behavior of PTFE varies little with respect to degree of crystallinity, with only a few percent difference at most, for high temperature and strain. Interestingly, samples with low crystallinity are stiffer in this case than those with high crystallinity. It is hypothesized that slip in crystalline regions allow for deformation at high strains, when amorphous regions have oriented, and surrendered all the strain they will[18]. In addition, elongation to failure in uniaxial stress decreases with increased crystallinity, as crystalline regions of PTFE cannot realign in the tensile direction like amorphous regions can. However, even for high degrees of crystallinity (X_c=65%) PTFE has a maximum elongation of nearly 300% strain [17b].

2.1.1 Nafion®

The effect of thermal history of Nafion® membranes on both their physical and transport properties has been previously studied. In hydrolyzed (sulfonated form) N111-F membranes, annealing at temperatures from 130 ^{o}C to 165 ^{o}C has little discernable effect on proton conductivity; in such tests, the membranes' proton conductivities varied from approximately 50 to 90 mS/cm. While annealed membranes consistently showed several percent increase in proton conductivity, the difference between annealed and unannealed

samples most often fell within experimental error. The same trends were also observed with water sorption values for all membranes, and in water flux values for thick (N115-N117) membranes. In thin (N111-N112) membranes, the same time and temperature treatments resulted in noticeable increases in water flux (34%-45%), which fell well outside of experimental error. Thermal annealing of the same membranes under the same time and temperature conditions had little impact on the EW as measured by a titration method.

Annealing Nafion® membranes, ranging from thicknesses of N111 to N117 at 165 ^{o}C for 3 hours, showed little trends in crystallinity of the polymer, as measured by peak fitting XRD data. Nafion® membranes with thicknesses ranging from N112 to N117 showed small decreases in measured crystallinity, while N111 membranes showed small increases. This suggests that any changes in mechanical or transport properties of the Nafion® membranes are not due to changes in the crystallinity of PTFE segments in the polymer. In general, the XRD fits showed greater crystallinity in thin membranes compared to thicker ones. However, the lower solubility of thicker membranes in DMSO calls this into question, as solubility has been thought to increase with decreases in crystallinity. This suggests that larger structure than short-term crystallinity may be responsible for changes in solubility of Nafion® membranes processed in different ways. Concurring with this assessment is SAXS data, which shows little change with annealing for any membrane thickness, though in N112 shows some visible distinction in its annealed state[19].

The most significant effect annealing has on transport in Nafion® membranes appears when studying proton self-diffusion through PGSE NMR analysis. Annealed membranes show greatly increased proton self-diffusion for every thickness. It is speculated that the annealing process used (in ambient, slightly humid air), allows for increases in free volume and segmental mobility, which promote proton self-diffusion, or the movement of protons [20].

The effect of solution processing parameters on resultant films has been extensively studied for Nafion® perfluorosulfonated ionomers. In particular, processes that yield very mechanically and chemically stable membranes have been developed.

Solution casting procedures involving room temperature evaporation of typical solvents generally yield membranes with poor mechanical and chemical properties. For instance, membranes dissolved in an ethanol-water mixture, and with solvent evaporated at room temperature, yield brittle membranes that can be dissolved in warm water. Clearly, such membranes are of little practical use in fuel cells. However, using a modified procedure, in which stronger solvents are used, and evaporated, at higher temperature, membranes that are mechanically comparable to as-received Nafion® 117, and only slightly dissolved when ultrasonicated in ethanol-water, result.

For membranes dissolved in DMSO, evaporation at 130 ^{o}C resulted in membranes that lost nearly 80% of their mass when ultrasonicated in ethanol-water. Increasing the evaporation temperature to 190 ^{o}C resulted in membranes that lost less than 5% of their mass under the same conditions. The researchers also showed the effect of changing solvents on membrane properties.

In order to test the effect of solvent on resulting solution cast films' properties, a single type of solvent was initially used to dissolve the material. Then, to replace this original solvent (EtOH, water) with a new, low boiling point one, the original solution was evaporated down from 10 to 2 mL, and 8 mLs of new solvent were added. This process was repeated several times until only a small amount of original solvent remained. For high boiling point solvents, the new solvent was added to the original solution, and the original solvent was removed by evaporation at 100 ^{o}C. Membranes were then cast from different solvents at different temperatures, and ultrasonicated as described previously. The data demonstrated that, in general, solvents with higher solubility parameters required higher temperature evaporation to produce high quality membranes. Also, for every solvent tested, increasing solvent evaporation temperature decreased mass loss.

SAXS studies also help to compare the morphologies of membranes solution processed or recast using different procedures. Simple SAXS scans show near perfect morphological comparison between as-received Nafion®, and high-temperature cast membranes.

DCS helps connect morphological changes with casting processes to its mechanical quality. Agreeing with SAXS data, DSC shows much more significant crystalline peaks in high-temperature cast materials to compared to room-temperature ones. It, therefore, becomes obvious that a loss in degree of crystallinity comes along with decreased membrane quality [21].

2.2 The Effect of Thermal Treatment on Other Ionomers

While the effect of thermal treatment on Nafion® deals mainly with changes in crystallinity, aromatic hydrocarbon ionomers, whose bulky backbones do not tend to crystallize, in general experience different morphological change with various anneals. For the same block SPS shown in , thermal annealing at 120 C for 168 hours disrupts a highly periodic hexagonal structure, replacing it with one more resembling lamellae, with a characteristic spacing of approximately 23 nm [22]. Crucially, these sample were prepared by freeze drying, and not processed at elevated temperature or cast from solution.

2.3 PEM Material Morphologies

2.3.1 Nafion® Morphological Models

Nafion® is considered the benchmark PEM material due to its outstanding properties of mechanical, thermal, and oxidative stability, as well as its relatively high proton conductivity at temperatures below 80-100 °C [1, 5b, 6-8, 23].

Nafion®'s ionic aggregate morphology gives it its unique PEM properties, and gives us a basis of comparison to evaluate the performance-morphology relationship of many PEM materials. Though the nature of these ionic aggregates has been studied extensively, there is currently no consensus on their exact arrangement. Many commonly cited models include the Gierke sphere-channel model [23a, 24], the core-shell model of MacKnight and Fujimura [25], the Eisenberg-Hird-Moore (EHM) model[26], the shell-core sandwich model from Haubold [2], the branched channel model of Kreuer [1, 27], Rubatat's rod structure [28], and the parallel channel model of Schmidt-Rohr et.al. [29], among others. Much speculation of Nafion®'s morphology centers on SAXS data, an example of which is given in Figure 2-1.

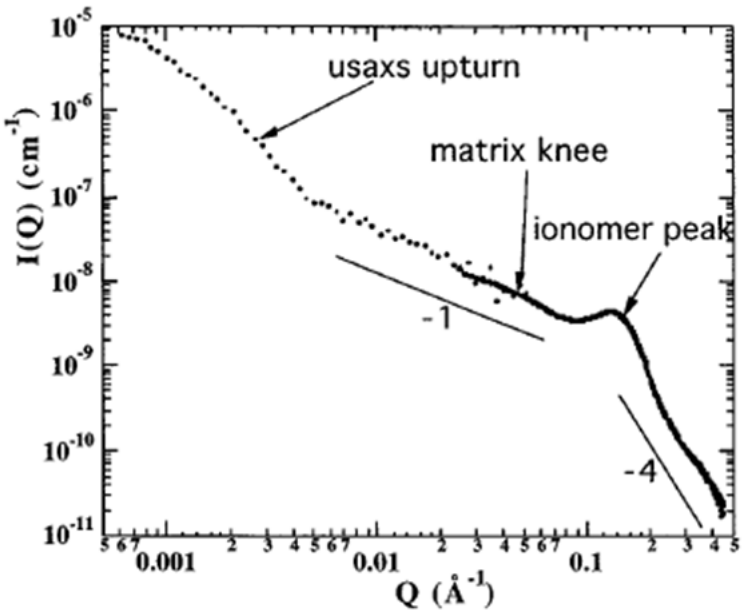

Figure 2-1: Example of Nafion® SAXS profile, with both the "ionomer peak" and a crystalline "matrix knee" called out [28]

The first attempt to describe the shape of Nafion®'s ionic aggregates comes from Gierke and Munn. The SAXS data collected in this study showed significant molecular order at approximately 5 nm for acid form Nafion®; Gierke attributed it to ionic aggregation due to the fact that it only appeared after the perfluorinated base polymer had been hydrolyzed (i.e. converted from SO_2F to $SO_3^-H^+$ form). This peak's intensity is shown to decrease with increasing counterion size in the alkaline series, with no appreciable change in the scattering angle. The ionic aggregate peak's intensity also decreases with increasing molecular weight; it also slightly shifts in position from d≈5 nm to d≈4 nm when equivalent weight varies from 970 to 1790. The shape of the ionic aggregates was concluded to be spherical, based on the fact that this allowed every sulfonic acid group to be hydrated, while minimizing interaction between hydrophobic backbone segments and hydrophilic sulfonic acid groups [23a].

Fujimura proposed a modification of the sphere-model, considering the ether side chains to form a shell around sulfonic acid spheres. Figure 2-2 shows both the sphere and shell-core models.

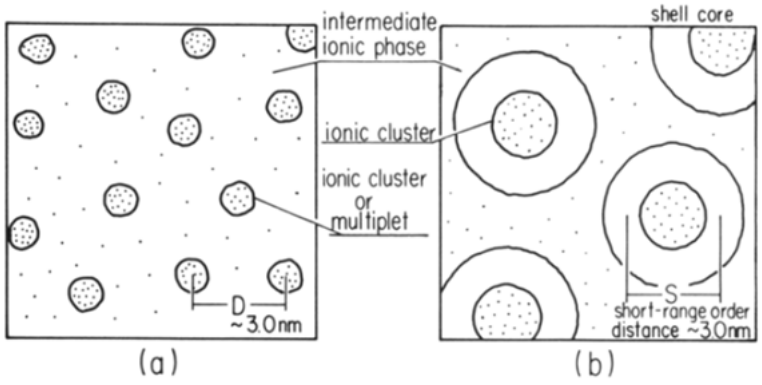

Figure 2-2: Two early models of Nafion®: the hard sphere model (a) and the core-shell (or modified hard sphere) model (b) [25a]

This particular understanding arose from interpretation of the change in SAXS response of Nafion® with increased water content. If the "ionic peak" exhaustively studied in SAXS were the result of an interparticle distance (as in the sphere model), the d-spacing would decrease or remain constant with increasing water content (i.e. as the sphere swelled). However, the d-

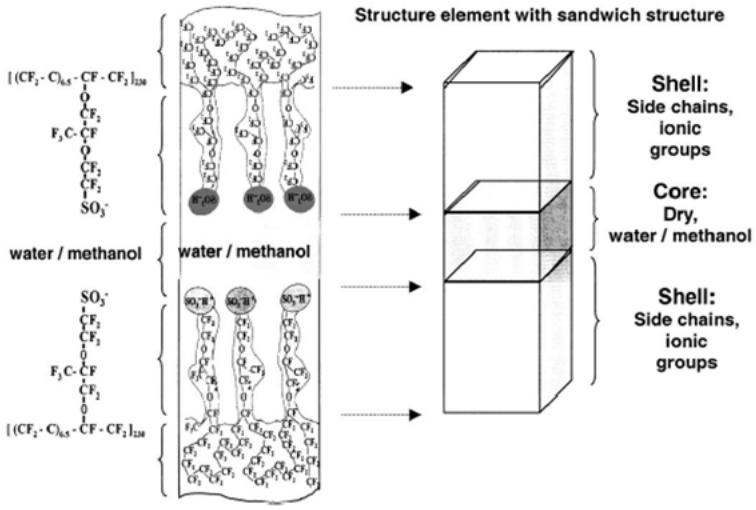

Figure 2-3: Haubold's sandwich-like ionic aggregate structure [2]

spacing of the ionic peak decreases with increasing water content, more strongly supporting a core-shell model, where the peak represents intraparticle distance [25c].

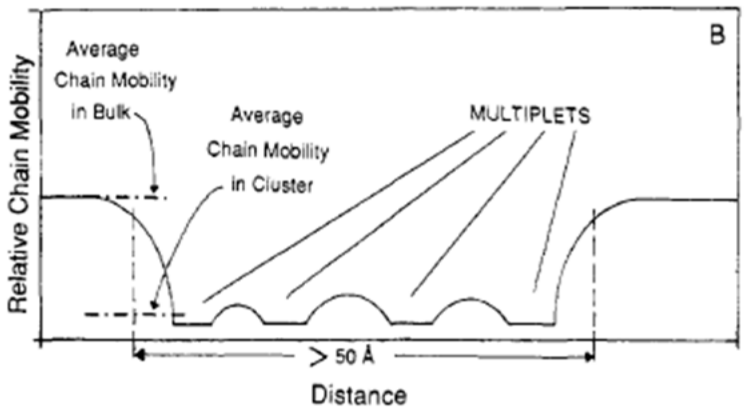

Figure 2-4: EHM model of restricted chain mobility around ionic aggregates [26]

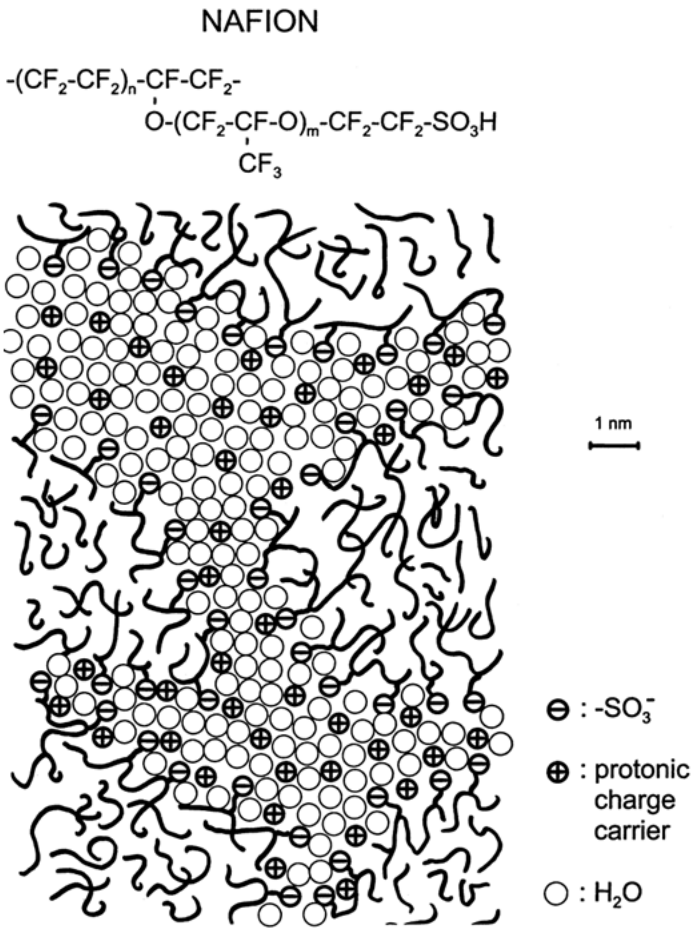

Figure 2-5: Kreuer's branched-channel model of Nafion [1]

The Eisenberg-Hird-Moore [26] model considers morphology from a perspective of chain mobility rather than electron density differences. They first acknowledge the strong interactions of ions will group them together in clusters. Around these clusters, to a radius of at least the reputation length of the polymer backbone, will be a region of restricted mobility, as shown in Figure 2-4 [26]. This model has many ramifications, both for morphological considerations as well as predictive power for the relationship

between mechanical properties and ionic aggregation.

Haubold[2] later used theoretical fits to SAXS data to refine understanding of Nafion®'s ionic structure. Beginning with a sandwich-like model (Figure 2-3), he developed equations using the structure and form factor of this model to describe its SAXS response. He then fit the parameters of shell thickness, core thickness, and scattering contrast of each region. The fits quite adequately describe the real SAXS response. While shell dimensions increase with increasing methanol content (35 to 50 Å), the fit core size counter intuitively decreases with added methanol (28 to 12 Å) [2].

Kreuer[1] further examined these concepts using SAXS. Ise[27] first speculated that SAXS data could be interpreted to determine the ratio of surface area of a channel-like system to volume of the channels. Therefore, knowing the average spacing of a channel, and also the surface area-to-volume ratio of the network, Kreuer constructed a Nafion® model, the SAXS simulations of which matched extremely well to experimental data.

Rubatat[28] provided the next morphological model, consisting of parallel water channels, each an "inverted micelle," with hydrophobic backbone constituting a cylindrical shell, and sulfonic acid side chains collecting in the middle. Furthermore, Rubatat conjectures no major structural reorganization with the addition of water, instead suggesting a change in peak position and intensities due to dilution of scattering features.

The most recent Nafion® morphological models extensively use SAXS simulation for validation. One of the most important recent results comes from Schmidt and Rohr, who have provided the model that fits to experimental SAXS data for Nafion® swelling with water.

These morphological models for Nafion® form the basis of interpretation of SAXS data for other ionomers.

2.3.2 Morphological Models of Other Ionomers

The morphology of other ionomers, including sulfonated aromatic hydrocarbon polymers, has also been studied. For instance, Kreuer extended his work on Nafion® to SPEEK,

determining that both a higher surface area-to-volume ratio existed for this ionomer, as well as a narrower average channel size. This model, then results in a more branched morphology, with a slightly higher average distance between each sulfonic acid group[1].

Block copolymers in particular have unique, controllable morphologies based on sulfonated block length. Block sulfonated polystyrene (SPS) has been theorized to form cylindrical ionic aggregates, similar to Rubatat's parallel channel model, but more ordered due to more organized sulfonation [30]. In other SPS-based block copolymers, two degrees of ordering has been seen using Small-angle neutron scattering: one small feature analogous to ionic aggregates found in Nafion®, and a higher structure composed of concentrations of these smaller aggregates due to the distance between sulfonated blocks in the copolymer, as shown in Figure 2-6 [31].

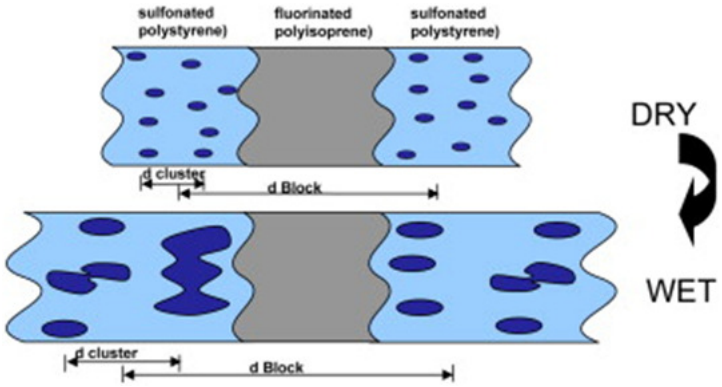

Figure 2-6: Proposed model for triblock copolymer including block sulfonated polystyrene, showing two degrees of ordering [31]

Smaller aggregates ranged in size from 3.2 to 4.7 nm, and the larger block had an average size of 20.3 to 35.5 nm. It is important to note that researchers in this study assumed a polystyrene block length of 16 monomer units, which corresponds to a block length of approximately 1.89 nm, which is much smaller than the block structure speculated.

Other SPS block copolymers show two distinct heterogeneities in SAXS. SPS-block-poly(ethylene ran-butylene)-block PS samples with different degrees of sulfonation all showed both a small feature, a few nm in size, and a larger feature, closer to 20 nm in size. These

feature sizes did not change substantially among samples with different degrees of sulfonation [32]. Also, polystyrene-block-(PVdF-co-HFP) membranes have been synthesized, with the intent of sulfonating the PS blocks to different degrees; this essentially results in a series of polymers in a spectrum from randomly sulfonated to block sulfonated. In the less sulfonated form, and thus, the form with more randomly spaced sulfonic acid groups, no ordering was observed for a scale from 0 to 100 nm. However, as the amount of sulfonation in these polymers increased, and thus, the sulfonated polystyrene segments took on a more blocky nature, clear phase separation from 20-40 nanometers was observed [33]. In these same polymers, which are fluorous in the non-sulfonated block, proton conductivity increase dramatically over comparable block sulfonated polystyrene samples that incorporated non-fluorinated hydrophobic blocks. It is speculated that the degree of phase separation in more significant when fluorinated segments are involved. Therefore, while not necessarily causally linked, the distinctness of separated phases in a block sulfonated copolymer is correlated to an increase in proton conductivity.

However, while some polymers experience an increase in ordering when block sulfonated groups are incorporated, some highly ordered polymers have their ordering disrupted by sulfonation. For instance, a PS-block-poly(ethylene-alt-propylene) (PS-PEP) polymer sulfonated to different degrees initially contained highly periodic phases, but took on a different phase nature with even small amounts of sulfonation, (Figure 2-7) [34]. This suggests that ionic interactions overcome other types of ordering in sulfonated polymers.

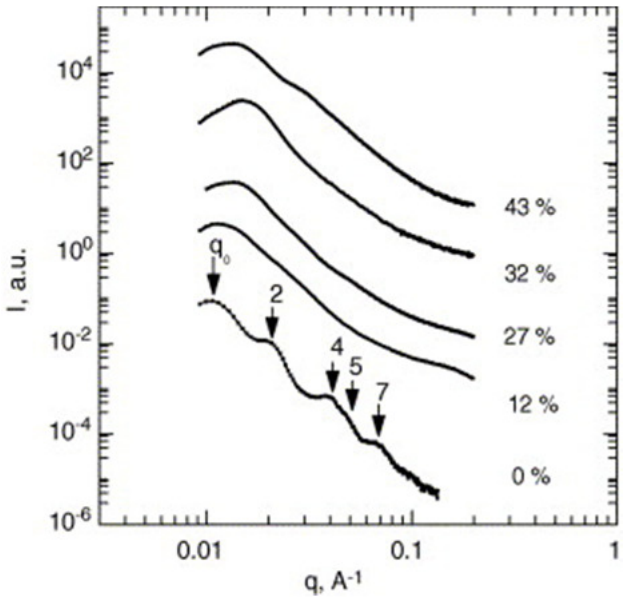

Figure 2-7: The SAXS profile of PS-PEP sulfonated to different degrees [34]

Block sulfonated poly(ether ether ketone), SPEEK, also shows ordering with an average of approximately 31 nm, while comparable random SPEEK polymers have much less ordering at this scale [35].

The difference between randomly sulfonated ionomers and block sulfonated is best illustrated with a combination of SAXS and TEM data. The change in morphology of disulfonated poly(aryl ether sulfone) polymers as the sulfonated block length increases has been studied in this manner. In these polymers, block copolymer morphology appears for as low as 5K sulfonated block sizes, and goes from a cluster-like morphology for these low block lengths, to a channel-like structure for block sizes of 15K, as shown in TEM micrographs presented in Figure 2-9.

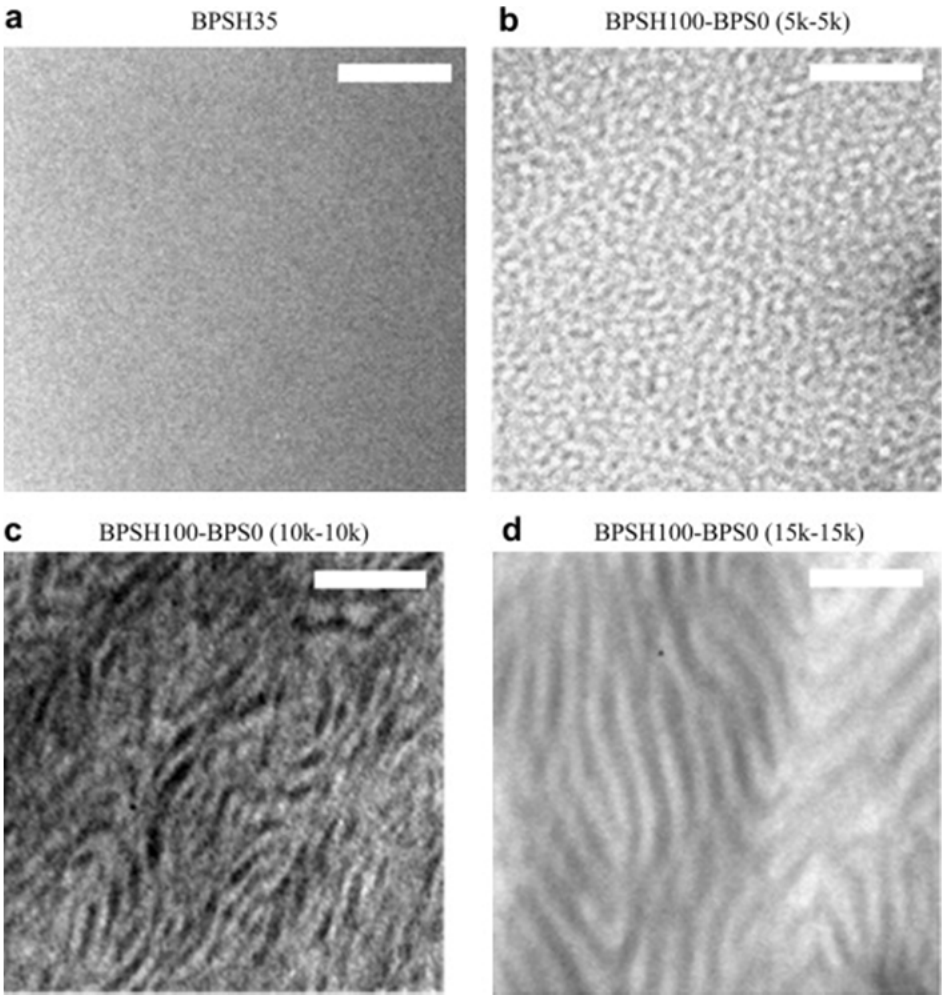

Figure 2-8: TEM micrographs of S-PAES with increasing block length, scale bar 100 nm; (a) randomly sulfonated, (b) 5K block MW, (c) 10K block MW, (d) 15K block MW[14]

SAXS also reveals these changes, with a change in q ranges to smaller vectors, or larger sizes, as sulfonation increases, as shown in Figure 2-9[14].

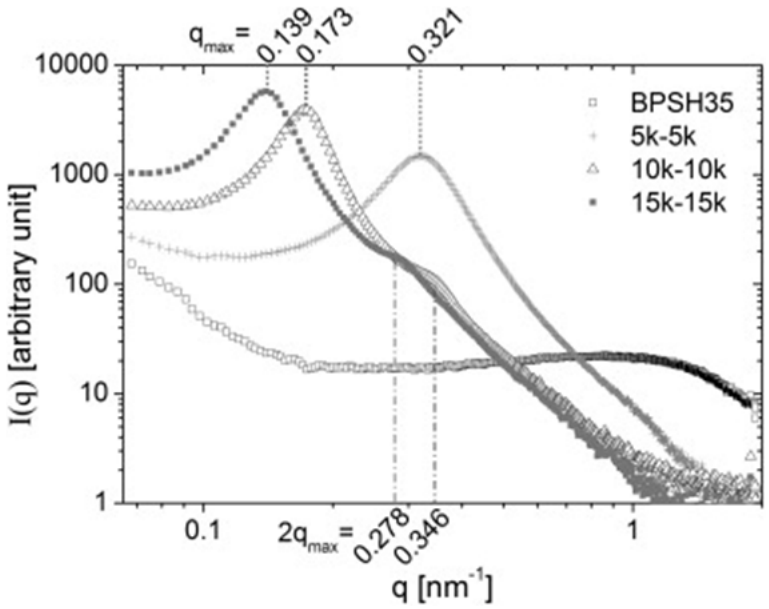

Figure 2-9: SAXS scans of S-PAES with various sulfonated block lengths[14]

The size and distribution of this "block copolymer" feature is crucial to the conductive and mechanical properties of these ionomers.

2.3.3 Poly (vinylidene difluoride) Homopolymer and Copolymer Morphology

PVdF is a well-characterized polymer, known for its rubbery toughness, crystallinity, and piezoelectric properties [36].

The crystallinity of PVdF has been shown to decrease significantly when blended with other ionomers. For instance, 50/50 S-PEEK/PVdF blends have been shown to contain less than 50% of the crystallinity of pure PVdF [16].

2.3.4 Sulfonated Polymer/PVdF-Based Polymer Blends

In order to improve the mechanical properties and hygral stability of aromatic hydrocarbon polymers, several have been blended with PVdF and related tough, hydrophobic copolymers. PVdF, a rubbery polymer at room temperature, and thus can promote the mechanical properties of other polymers by blending them together. This kind of addition has been shown to greatly reduce material strain in the presence of methanol and water [16].

Addition of PVdF or PVdF-co-HFP has also been shown to decrease the maximum mechanical elongation of a thin membrane before break, while increasing the maximum stress at break [37].

2.3.5 6F Characterization

Quite surprisingly, 6F homopolymer crystallizes up to 35%, despite its bulky chemical structure; these crystallites have spacing of approximately 5.6 Å, and melt at approximately 185 °C, as shown in DSC [3]. Figure 2-10 shows the wide angle x-ray diffraction (WAXD) response of pure 6F polymer.

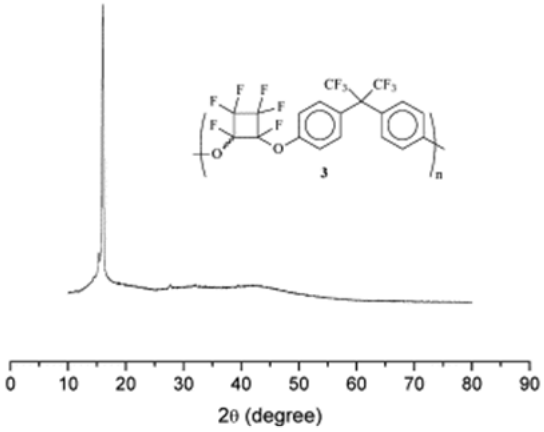

Figure 2-10: WAXD response of 6F homopolymer, along with its structure[3]

2.3.6 Perfluorocyclobutane (PFCB) Containing Ionomers Studied for Fuel Cell Applications

Some limited studies have been performed on PFCB-based ionomers for fuel cell applications, though most have focused on mechanical and conductive properties, not morphology. Several PFCB-based ionomers have been synthesized with the same equivalent weight (EW), or concentration of sulfonic acid groups per mass of Nafion 117. They have been shown to have higher proton conductivity and similar water uptake to 1100 EW Nafion® [38]. However, the nature of the ionic aggregation of such polymers has not been studied. Likewise, the nature of blocky phase separation has not been probed. Finally, the effect of blending in a tough, hydrophobic polymer on the polymer's phase and ionic aggregation behavior has not yet been reported for any of these materials. Neither have the effects of varying solution casting parameters on morphology of these polymers been studied.

Chapter 3:

3.1 Materials

3.1.1 S-PFCB

S-PFCB is a block copolymer, consisting of sulfonated and non-sulfonated blocks. The sulfonated block consists of poly (Biphenyl vinyl ether-Perfluorocyclobutane) (BVPE-PFCB), with perfluoroether side chains capped with sulfonic acid groups. The non-sulfonated block is also a BVPE-PFCB polymer, with two trifluouromethyl groups inserted between the aromatic rings, known in its homopolymer form as "6F" PFCB. S-PFCB is polymerized with the addition of sulfonated blocks of molecular weight MW=8,000 g/mol (polydispersity index ≈ 2) and non-sulfonated monomer, in a ratio of 2 sulfonated monomer units to every non-sulfonated monomer unit. A thorough description of the synthesis of this material can be found in its patent [39]. The resulting structure is given in Figure 3-1.

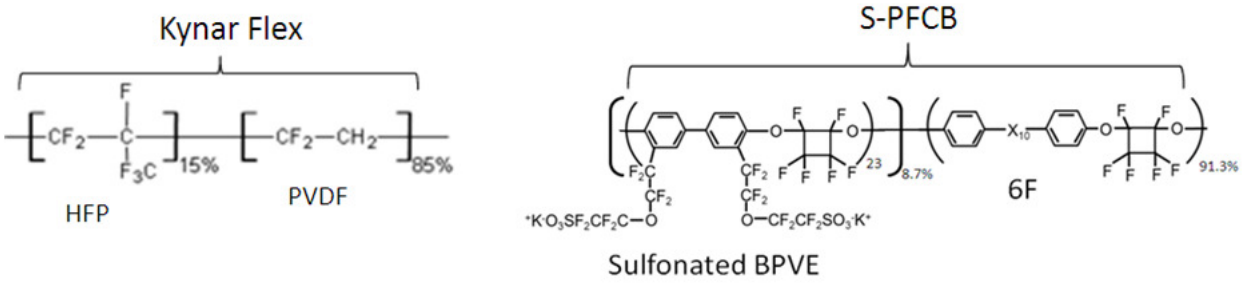

Figure 3-1: Chemical structure of Kynar Flex (L) and Gen 2 S-PFCB (R)

For S-PFCB, two different polymers were used, with the only difference between the two being molecular weight (for "TAKS 115C", M_n=45,000-50,000 g/mol; for "TCT 840B," M_n=75,000 g/mol). In a limited number of studies, an older "Gen 1" S-PFCB polymer was used for comparison purposes. Its chemical structure is identical to the structure given, except for the lack of perfluorovinyl ether side chains; sulfonic acid groups in Gen 1 are directly bonded to the BVPE backbone; it is also known as main-chain sulfonated (MCS) PFCB. In addition, non-sulfonated PFCB was used in comparison studies. Its chemical structure is identical to the structure given, except for a lack of both perfluorovinyl ether side chains and sulfonic acid

groups; instead, a bromine atom occupies the site where a sulfonic acid side chain would bond to the main chain.

3.1.2 Kynar Flex

Kynar Flex is a random copolymer of Poly-vinylidine difluoride (85 mol%) and Poly-hexafluoropropylene (15 mol%). We received this material in powder form (product KF 2751), which has a molecular weight of 380,000 g/mol. The structure of KF is given in Figure 3-1.

3.2 Membrane Casting

Some membranes for morphological studies were provided by GM (GM cast), and some were cast in-house (VT cast). VT cast membranes were all prepared, cast, and processed in the same way, except for single factor variations that were used to study the morphology. A "control" procedure is given below.

3.2.1 VT Cast Membranes

First, 10 wt% of polymer solids was added into 90 wt% of solvent, N,N-dimethylacetamide unless otherwise specified. The polymer solids were comprised of S-PFCB and Kynar Flex, with the weight fraction of KF varying from 0 to 1 for different batches. Next, the mixture was homogenized at 17,000 RPM for 5 minutes, and 24,000 RPM for 30 seconds using an IKA T-25 Digitial Ultra-Turrax. It was then filtered through an ePTFE filter with 5 µm pore diameter. Solutions were used for casting from 1 to 70 days after the initial filtering.

Polymer membranes were cast onto various substrates using an in-house fabricated casting block. For flexible substrates, a thick paper backer was put on the casting block, followed by the substrate itself. Vacuum was then applied to smooth the substrate across the surface of the block. When using glass as a rigid substrate, no paper backer was used, and vacuum was applied. Next, a rectangular masking tape shim was applied to designate the area where a membrane would be cast. The solution was laid down along the top inside edge of the shim (3-4 mils thick). The solution was then drawn down by a casting knife with a 3 mil gap.

The casting block was then rapidly heated to 80 °C (< 15 minutes) and held isothermally for 1 hour before being allowed to air cool back to room temperature, which took approximately 1 hour. Sample heat treatments are given in Figure 3-2.

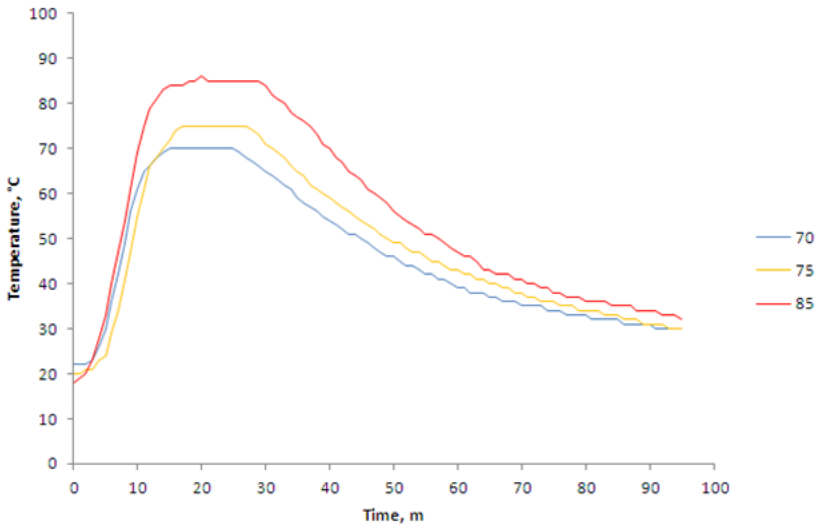

Figure 3-2: Experimental temperature profiles for casting a membrane from solution, given for temperature holds of 70, 75, and 85 °C

Next, the substrate with polymer cast onto it was submerged in RO water, and the membrane allowed to float off its substrate. Each membrane was then bathed in water at 50 °C for 1 hour, either biaxially constrained in tension by a PTFE frame, or free of constraint, as specified in individual specimen descriptions. They were then dried in a desiccator for a minimum of 12 hours. The last processing applied to the membrane before characterization was a 2 hour isothermal hold at 100 °C. This removed residual stresses induced by localized hygral strain in the water bath.

3.2.2 Commercially Cast (GM Cast)

Prior to being sent to us for characterization, commercially cast membranes were cast using the same nominal thermal history as VT cast membranes. Specifically, a 10 wt% solids solution was laid down onto a substrate at room temperature. The substrate was then rapidly heated to

80 °C, held for 1 hour, and allowed to air cool to room temperature. Samples of varying KF content were produced, and the S-PFCB used was either TAKS 115C or TCT 840B.

Commercially cast membranes were received from GM on the substrate onto which they were cast. They were first removed from the substrate by peeling, and fixed into a rigid PTFE frame. The membrane/frame system was then bathed in water at 50 °C for 1 hour. The membrane was then dried in a desiccator while still in the frame for at least 12 hours. After being removed from the frame, all commercially cast membrane samples were held isothermally at 100 °C for 2 hours to remove residual stresses, as with the VT cast membranes.

3.2.3 Ion Exchange Procedure

Some membranes underwent an ion exchange procedure, which replaced sulfonic acid protons with another counterion, such as sodium or cesium.

First, the membrane was placed in methanolic CsOH (or NaOH for sodium ion exchange). The concentration of CsOH was calculated such that there were 5 times as many moles of Cs+ ions as there were sulfonic acid groups in the polymer, assuming 1100 g polymer per mol SO_3^-. The membrane was stirred in solution for twelve hours. The membrane was then removed, and washed with DI water. Finally, it was stirred in DI water for 12 hours and desiccated overnight. This procedure follows common guidelines used for Nafion® counterion exchanges, and resulting SAXS data verifies successful exchange [1][40].

3.3 Membrane Characterization

In order to probe this new polymer's morphology, many characterization tools offer different and synergetic looks. Differential scanning calorimetry (DSC), atomic force microscopy (AFM), and small angle x-ray scattering (SAXS) in particular help piece together a very detailed picture of the way the different components of the ionomer blend interact.

- SAXS: Probes d-spacing of ordering features from ~2.5-100nm
- DSC: Helps to probe glass transition temperatures, exothermic events (melting), and freezability of the water bound within the ionomer

- AFM: Gives information about surface phase heterogeneities down to the nanometer scale

3.3.1 Small-Angle and Wide Angle X-ray Scattering

SAXS targets a collimated x-ray beam through a polymer sample, such as a membrane or liquid-filled cell, in order to develop a scattering pattern approximately based around 2-100 nm sizes. These x-rays are then scattered elastically in all directions by heterogeneities in the sample. When diffracted by a particle, some x-rays end up interfering with each other, either positively or negatively, as shown in Figure 3-3. The relationship of a peak's scattering angle with sample feature size is described by Bragg's law, $n\lambda=2d*\sin(\theta)$, where n is the number of repeated feature lengths represented by an interference event, λ is the wavelength of an incident, monochromatic beam, d is the size of a features, and θ is half of the angle between the incident x-ray and the diffracted x-ray. The result is a scattering pattern, as shown in Figure 3-4. Radial integration of this scattering pattern gives a plot of intensity vs. scattering angle, or, more commonly, intensity vs. scattering vector $q= 4\pi*\sin(\theta)/\lambda$. This scattering vector therefore accounts for

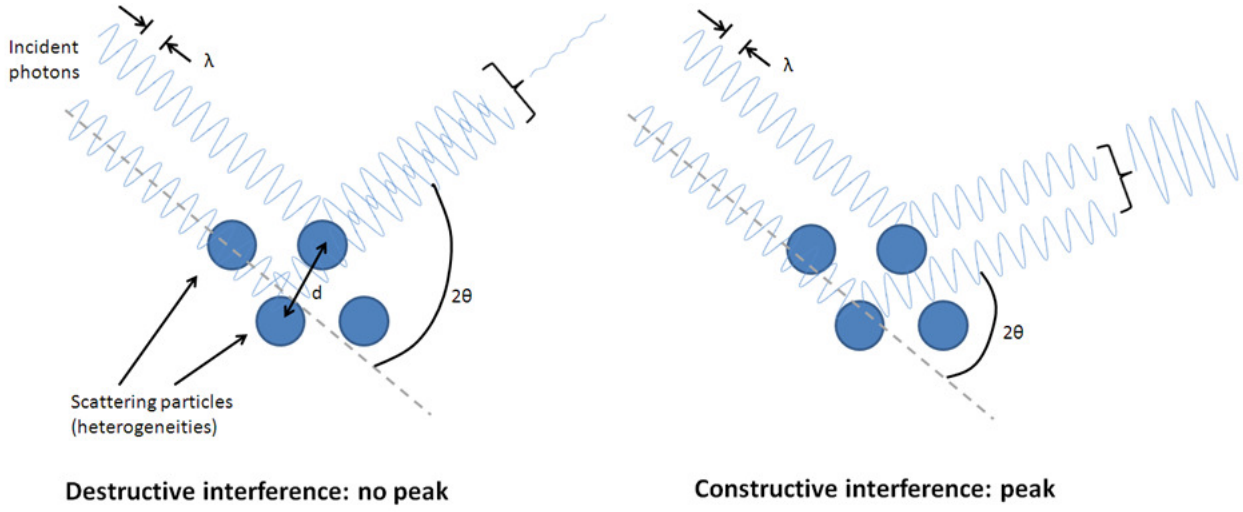

Figure 3-3: Constructive interference of waves helps reveal the average size or interparticle distance of a material's heterogeneities

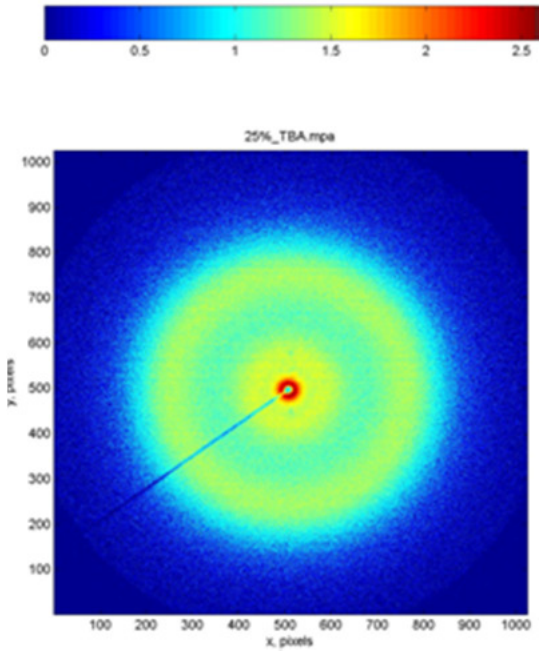

Figure 3-4: An example SAXS scattering pattern (Nafion 117)

Scattering intensity is influenced by several factors. A more common heterogeneity will scatter more strongly, leading to a more intense peak. In addition, a feature with significant difference in electron density than its surroundings will also scatter more strongly. A thicker sample gives x-rays a higher probability of interacting with a given feature, making thicker samples scatter features more strongly. The difference between a single layer of a given sample and several layers of that samples is a scalar factor increase in intensity. On a plot of the log of intensity, this appears as a vertical shift. Figure gives an example of a sample's SAXS response, with 1-10 sample layers.

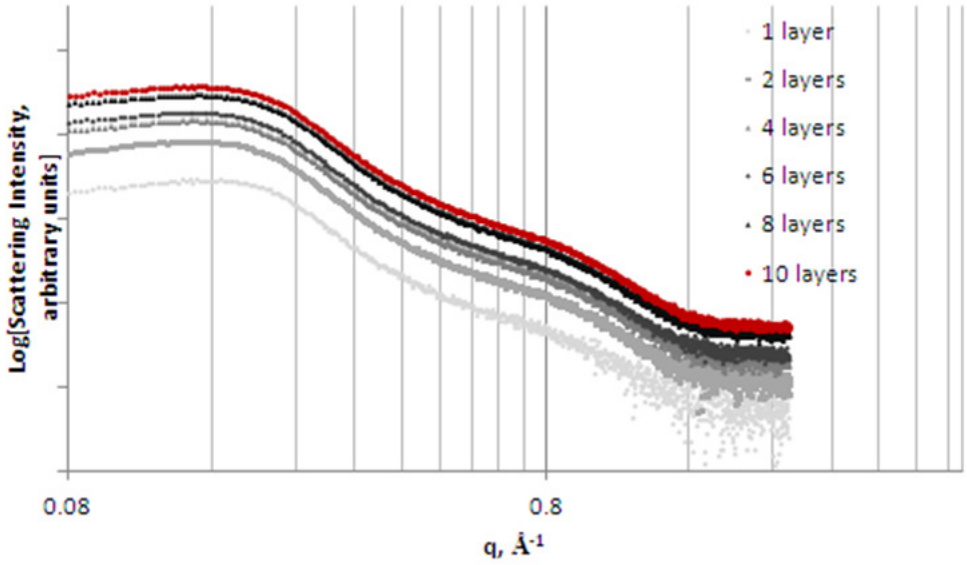

Figure 3-5: SAXS response of a membrane, stacked in various number of layers

If these responses are divided by their thicknesses, they all collapse nearly completely on top of each other, as seen in Figure 3-6: SAXS scans of Figure 3-5, divided by their thicknesses.

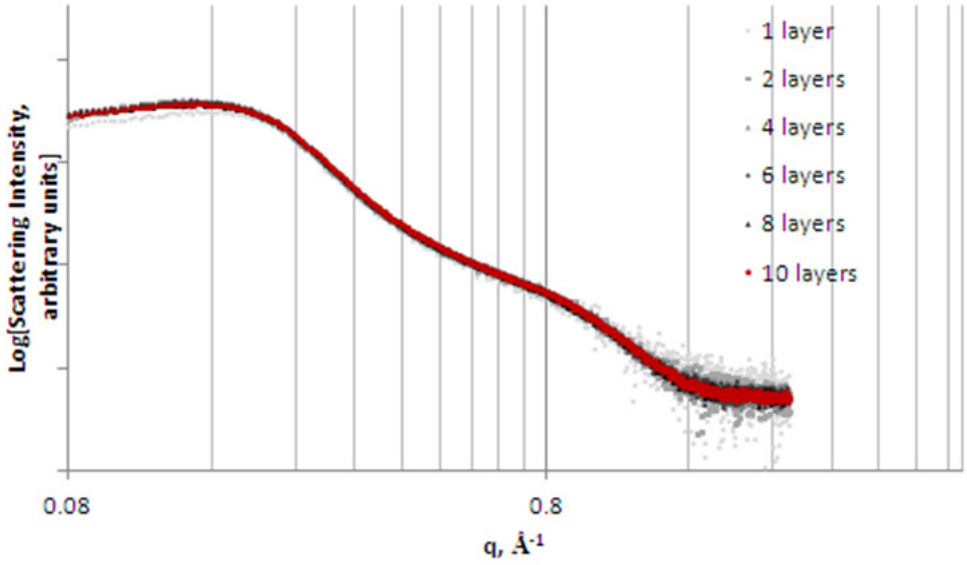

Figure 3-6: SAXS scans of Figure 3-5, divided by their thicknesses

Using these several curves to generate a standard deviation for each data point, we are able to determine the error across several samples independently processed and handled in the same way. Figure 3-7 shows the resulting error.

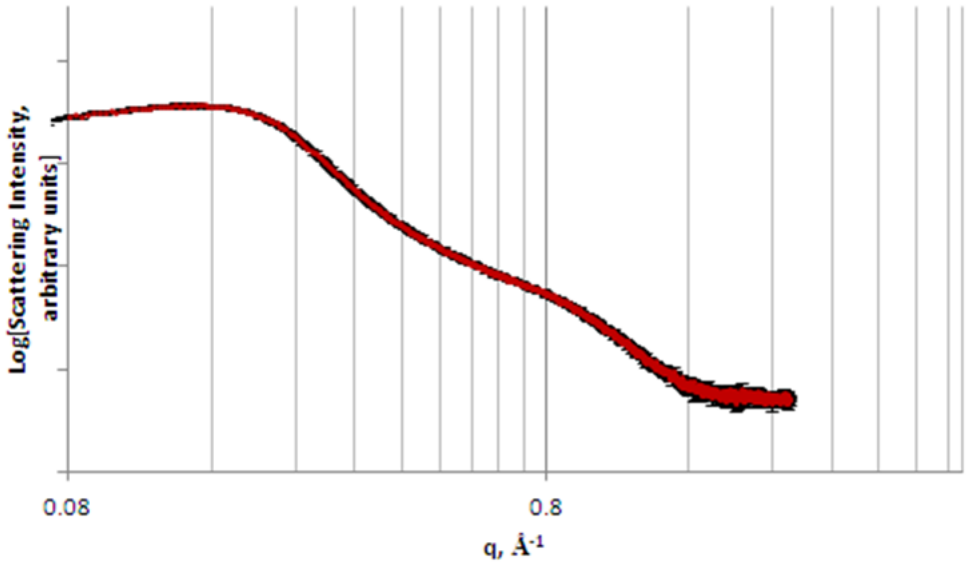

Figure 3-7: SAXS data, including error bars (± 1 standard deviation) generated from samples nominally processed and handled in the same way

However, the way these factors influence scattering pattern cannot always be captured by a scalar factor. For instance, in Figure 3-8, SAXS patterns of S-PFCB of three different casting thicknesses are given.

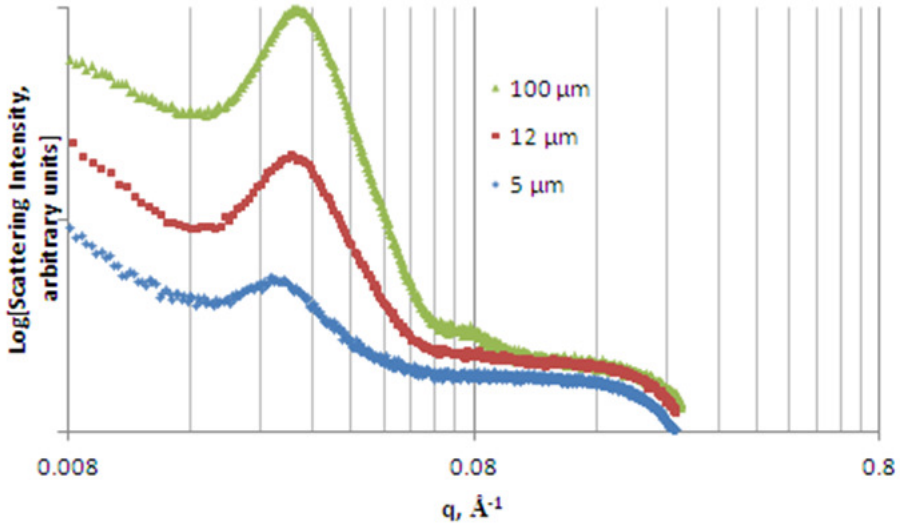

Figure 3-8: SAXS profile of VT cast Gen 2 PFCB, with different thicknesses

Although these samples represent the same polymer, with the only difference being the thickness to which they were cast, these profiles will not vertically shift to superimpose onto each other. Therefore, these samples contain different morphologies.

The most important analyses of the SAXS scans reported in this document contain comparisons of the form and position of different peaks. For instance, the following two profiles (Figure 3-9) show S-PFCB with no KF (0%) and in a blend with 30 wt% KF; this plot represents changes in form that can be interpreted without necessarily considering relative intensities.

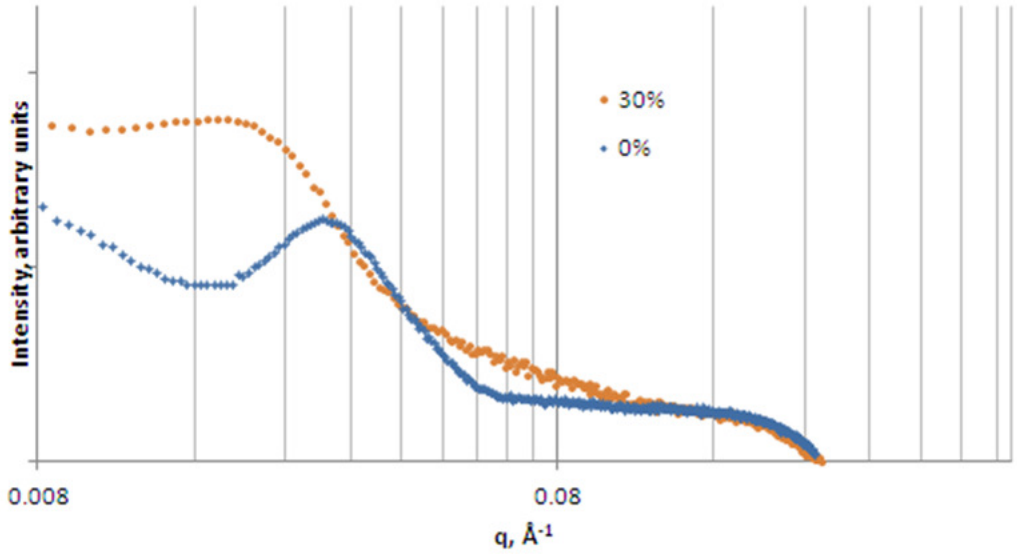

Figure 3-9: SAXS of two different KF contents in S-PFCB (wt % KF)

The peak that dominates the profiles (a block copolymer phase feature, called out in Figure 3-9), appears broader and centered over a smaller q range in the 30% KF sample. However, the region of the curve immediately following the peak is more difficult to interpret; without a peak and q_{max} to locate a feature, the difference in slope cannot be definitively explained. Therefore, for the purpose of this study, the amount of Kynar Flex was varied incrementally. This allows for a trend to be established, and generally strengthens our conclusions. The data from this incremental study is found in Figure 3-10.

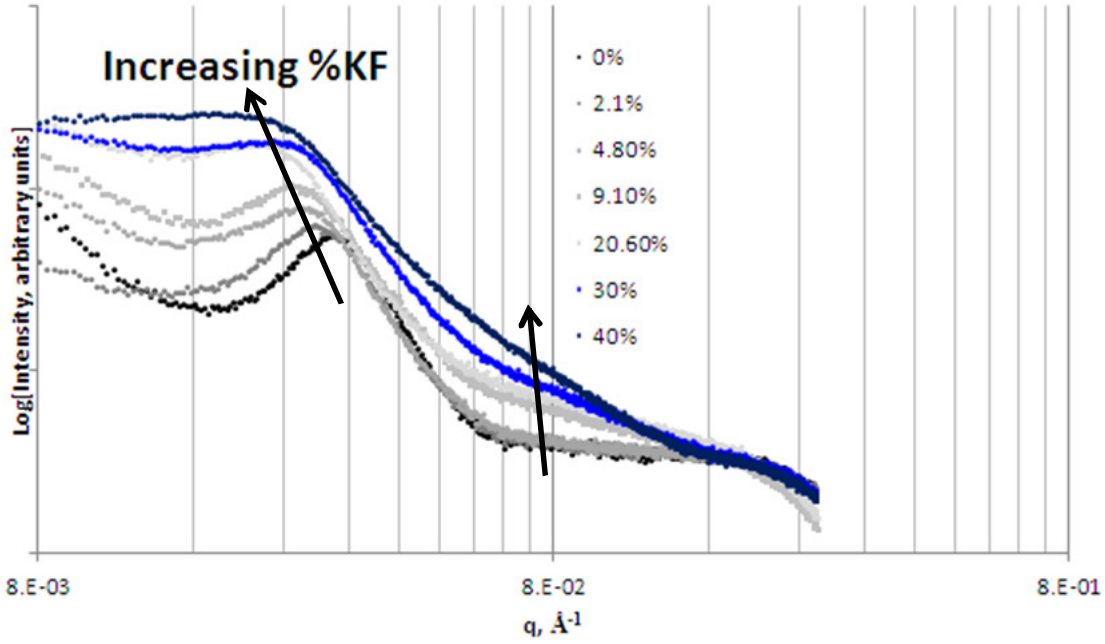

Figure 3-10: SAXS of incremental variation in KF content (wt%)

With both a trend in the block copolymer peak and the region at approximately q=.08, we can conclude that features in both of those ranges change gradually as KF is added. For every comparative study, care was taken to ensure thicknesses were within 5% for every sample.

There are corrections that can be used to account for variations in thickness of a sample, converting the intensity from arbitrary units to absolute units. In order to perform these transformations, three basic steps are applied. First, a SAXS scan is taken without a sample, and this response subtracted from the sample scan. This step is known as a background correction. Next, the response is divided by sample thickness, a step known as thickness correction. Finally, the response is corrected for beam flux and counting time, in order to make the response comparable to data taken on other instruments, which may be taken on an instrument with different beam flux, and counted for a different time. This type of SAXS data is called absolute units and can, in theory, be compared to each other with respect to q ranges and intensities, regardless of instrument, samples thickness, or total number of data counts [41].

These corrections were used for a small portion of the samples in this study, where specified. Typically, samples had thickness approaching 10 μm, and the counting time necessary on our laboratory instrument to overcome background subtraction was prohibitively long.

3.3.1.1 Peak Fitting

Many models exist for the interpretation of SAXS responses in ionomers, each with different assumptions and generalizations meant to illustrate a tangible representation of the arrangement of ionic clusters and other polymer features. These models are discussed extensively in Chapter 2: Review of Literature. They generally begin assuming a shape of ionic aggregates (e.g. sphere, cylinder, etc.), and then develop equations for intensity vs. scattering vector q, as functions of different structural sizes and scattering coefficients. While these models can offer more accurate descriptions of dimensions of different morphologies, they necessarily depend on assumptions that may prove inadequate, and are constantly being refined or replaced. For example, the SAXS response in Figure 3-11 illustrates both the raw data and two fits: a simple hard sphere model and a modified hard sphere model, illustrated in Figure 3-12.

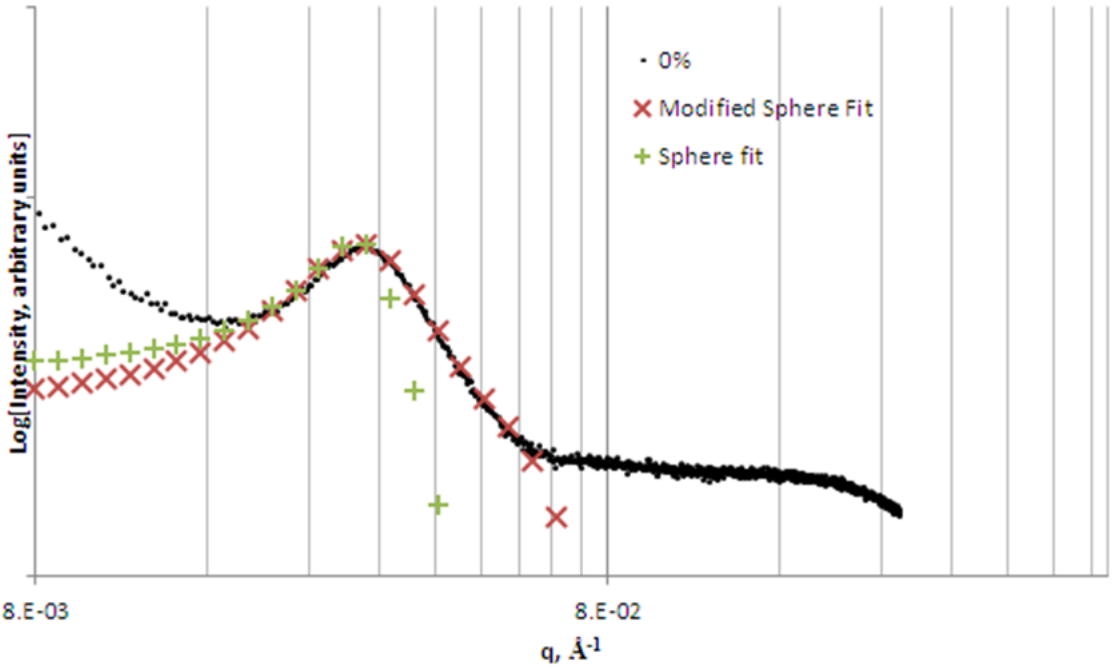

Figure 3-11: SAXS response of pure S-PFCB, peak fit with two simple models

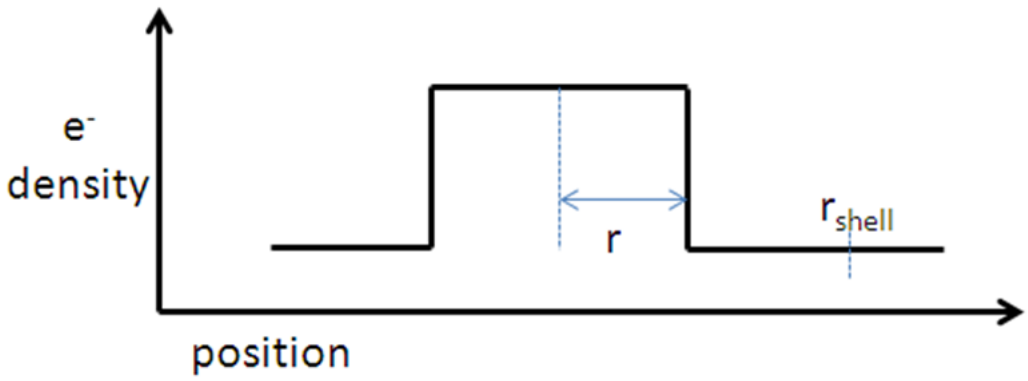

Figure 3-12: graphical model of the modified hard sphere model for SAXS; r represents feature radius and r_{shell} represents an outer core that prevents hard spheres from coming closer than $2*r_{shell}$ from each other

The theoretical SAXS response for these models, intensity as a function of q range, is well documented [23a, 42].

Some simpler models, such as the ones shown, are most useful for fitting individual peaks, and do not consider scattering by anything other than simple features. As of yet, there has been no model developed for fitting SAXS data of block sulfonated copolymers. However, it is occasionally useful to identify peaks more precisely than estimating q_{max} can obtain. Therefore, a modified hard sphere fit is used to determine peak positions, and this often gives different results than picking q_{max} and calculating d spacing using Bragg's law ($d = 2\pi/q$). For instance, in the example shown, Bragg's law gives a mean feature size of 22 nm, while both fits give 19 nm.

3.3.1.2 SAXS, Experimental Parameters

All small angle x-ray scattering scans were performed on a Rigaku S-Max 3000 instrument. For most specimens, the evacuated sample chamber induces dry, room temperature conditions. Every sample was held in a desiccator for at least 12 hours before being scanned in SAXS. When specified, scans were performed at varied temperature and/or humidity as well. Also, this instrument has three options for scattering angle range: small angle, mid-angle, and wide angle. For small angle scans, the sample is placed in a chamber far away from the detector, and data ranges from .006<q<.24 $Å^{-1}$. For mid-angle scans, specimens are placed in a chamber closer to the detector, and data ranges from .01<q<.4 $Å^{-1}$. Finally, for wide angle scans, a detector plate is placed directly in front of the sample, giving a very small sample to detector distance. This gives data from .5<2θ<25. All samples were counted for 1 hour.

3.3.2 Differential Scanning Calorimetry

A differential scanning calorimeter simultaneously heats two pans at a constant rate- one empty pan, and one with a sample in it- measuring the difference in the energy absorbed by each. The excess energy absorbed by the sample pan represents the energy taken in by the sample while it undergoes structural, phase, and morphological changes. The technique is often used in polymer systems to determine their glass transition temperature, the melting temperatures of crystallites, and the energy associated with each thermal event. Glass

transitions in polymers appear as a step change in the energy enthalpy curve, while melting events appear as bumps or spikes, as shown in Figure 3-10.

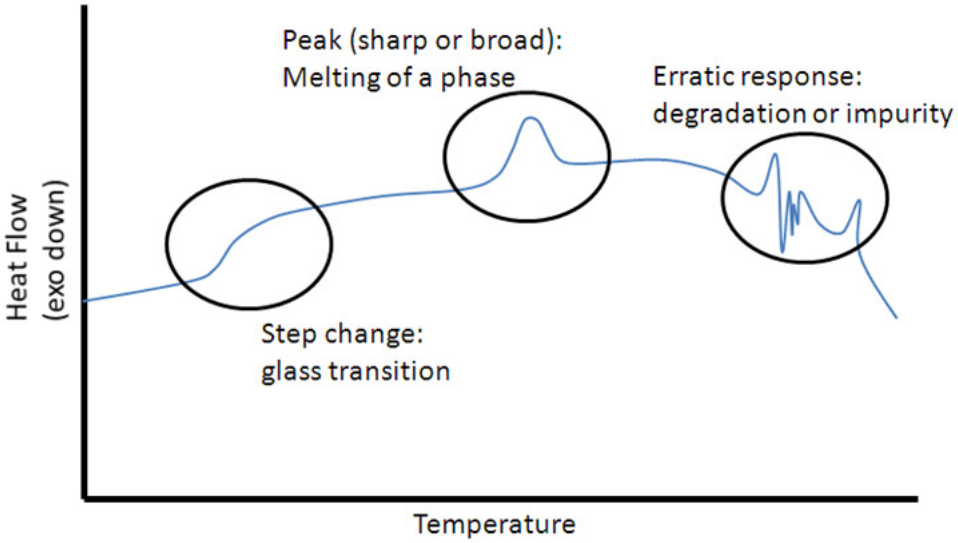

Figure 3-13: Hypothetical polymer DSC scan

The broadness or sharpness of these events is influenced by the rate at which the material is heated. Thus, for our systems, we conducted heating at several rates to assess its effect on our response.

DSC responses can also depend on thermal history. For instance, a polymer that is quenched to below its T_g will not contain crystallites, while one processed at elevated temperature may show more crystallinity. Therefore, a second scan after the sample has cooled in a controlled manner only includes the thermal history imposed by the controlled cool. For ionomers, however, more than simple thermal-morphological history can change between first and second scans. S-PFCB absorbs significant amounts of water, which leaves the material upon heating, and very quickly as the temperature approaches 100 C. Therefore, water content can change irreversibly between first and second scans. Furthermore, the energy required to remove water from a membrane sample often overwhelms the energy involved in morphological changes in the material, making first scans difficult to interpret.

All DSC scans were taken on a , with a dry nitrogen purge constantly flowing through the heating chamber. Standard aluminum pans (Rheometric Scientific X1021, average mass 31 mg) were used, and each pan sealed by manually pressing them together. The mass of each sample was recorded and used to obtain heat in J/g; sample masses ranged from 5-10 mg.

3.3.3 Atomic Force Microscopy

Atomic force Microscopy (AFM) rasters a physical tip along a surface of a material to probe its topography, as well as other properties. For soft materials such as polymers, the tip is tapped along the surface to prevent damage; the amplitude of tapping is directly correlated to the height of the sample at a given point. This "tapping mode" gives additional information about the surface of the material through comparing the applied tapping phase to the responding phase of the tip. Increased phase lag corresponds to a softer surface. Thus, features such as phase separation or crystallinity in polymers can be viewed for sizes as small as tens of nanometers. It is important to note that the term "phase image" refers to the fact that the AFM tip experiences phase lag, and term has no root in the concept of phase separation, though this phenomenon is *one* type of information that can be viewed with an AFM phase image. An example of both a height image and a phase images is given in Figure 3-14.

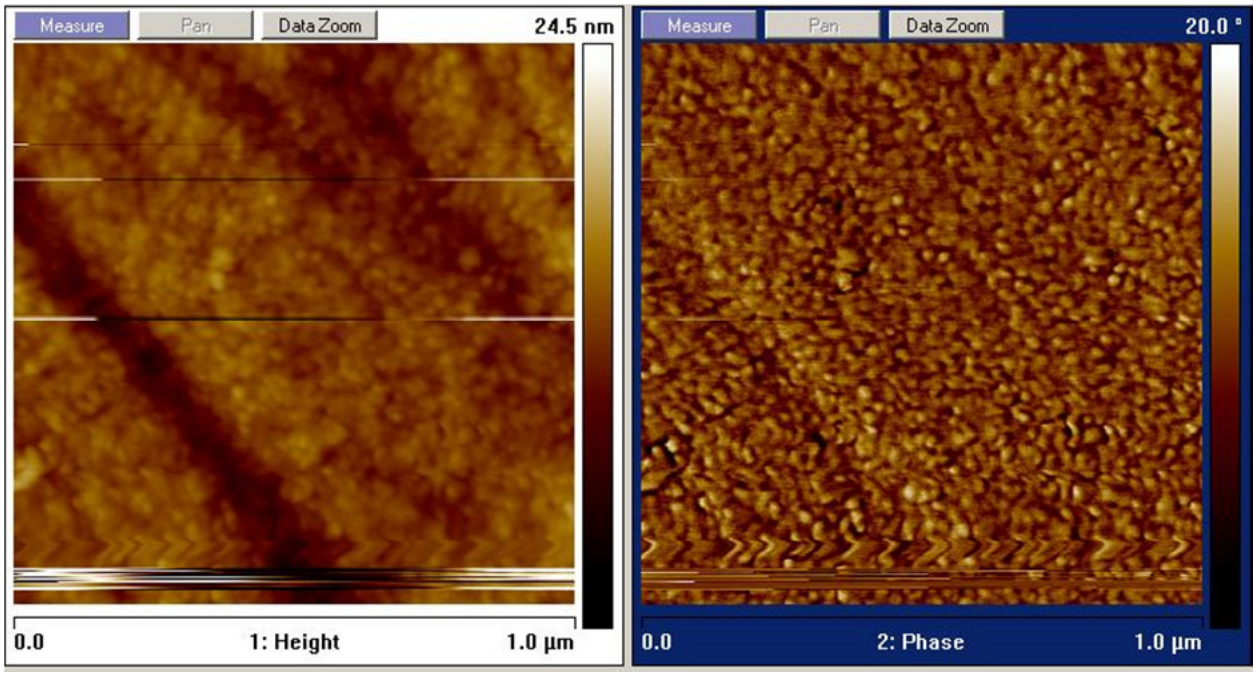

Figure 3-14: AFM height image (L) and phase image (R) of GM cast 30% KF/ 70% TAKS

In these images, the information in the phase image is slightly convoluted with height information. For instance, where the height of the sample dips dramatically, the phase image appears brighter. However, in general, the bright regions of the phase image correspond to hard areas of polymer, and dark regions correspond to softer material.

All AFM scans were performed on a Veeco Multimode Atomic Force Microscope. The free air RMS for every sample was 3±.05 mV, and the tapping RMS was 2.15±.05 mV. A high k tip was used for every sample. Every sample was run under ambient conditions.

3.3.4 Fourier Transform Infrared Spectroscopy (FTIR)

Fourier Transform Infrared Spectroscopy (FTIR) is a commonly used technique for evaluating chemical bonds. It involves bombarding a specimen with infrared radiation, and observing which wavelengths of photons or absorbed in a sample. Many chemical bonds oscillate at frequencies near that achieved by infrared photons. Thus, if many photons of a certain frequency are absorbed in a sample, a bond with the associated with that frequency

oscillation is present. The identification of IR peaks is generally well documented in the literature. For the purposes of this study, two main modes of FTIR were used: transmission and attenuated total reflectance modes.

Transmission mode simply passes an infrared beam of wavenumber from 400 to 4000 cm^{-1}, where wavenumber is the inverse of the frequency. Attenuated total reflectance mode aims the beam at the surface of a sample at a low angle. The beam then reflects off the sample and attenuator element several times before being led to the detector. Figure 3-15 visually represents this process.

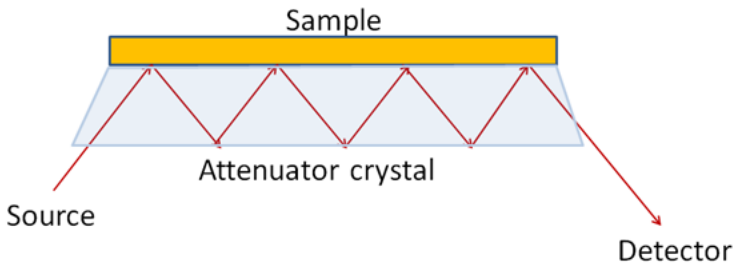

Figure 3-15: Schematic of ATR-FTIR

Each of these modes has its advantages and shortcomings. ATR mode can be used on any kind of sample, regardless of the thickness, and regardless of whether it is in powder, solid, liquid, or another form. However, the beam does not penetrate very far into the sample, on the order of a few microns, dependent on the samples' chemistry. Transmission mode gives information about the bulk of the sample. However, only very thin samples can be used, or a range of wavelengths may be completely absorbed, preventing peaks from accurately appearing.

In both of these modes, the type of spectroscopy used is Fourier transform infrared spectroscopy (FTIR). In direct ("dispersive") spectroscopy, the wavenumber of radiation is swept through every frequency, one at a time. In FTIR, a collection of the entire range of frequencies is delivered from the source simultaneously. Through use of an interferometer, the distribution of these frequencies is varied over time, which generates an interferogram, or a

plot of absorbance (or transmittance) vs. position. The Fourier transform of this interferogram gives plot of absorbance vs. inverse position, or absorbance vs. wavenumber.

All FTIR data was collected on a Resolutions Pro Varian UM 600, using Resolutions Pro Software. A background of 32 scans was collected, and all samples were collected over 32 scans as well.

3.3.5 Solvent Dissolution

Various membranes were exposed to the solvent from which they was cast, N,N-Dimethylacetamide (DMAc), in order to assess the gel fraction of material (wt% solid after solvent exposure).

First, the samples were massed, and 9 times the membrane mass of DMAc was added to the sample (resulting in a 10 wt% solution if membranes fully dissolved). The membrane's appearance (gel-like or dissolved) was noted. Next, excess DMAc was added to the membrane, and the membrane's appearance noted. Finally, the entire mixture was ultrasonicated for 1 hour, and its appearance noted. Examples of membrane appearance are given in Figure 3-16.

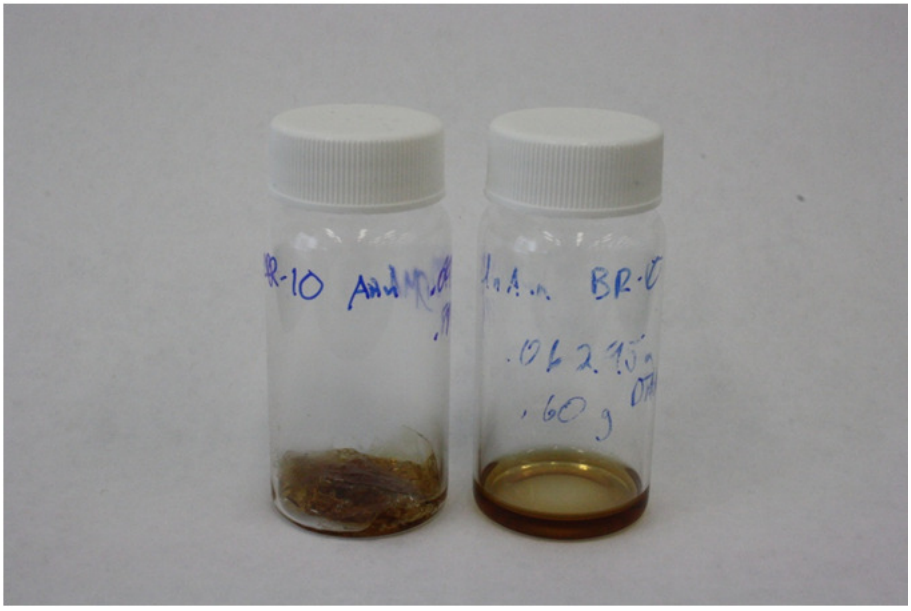

Figure 3-16: BR-10 (30% KF/ 70% TAKS, GM cast) 1 hr. after exposure to 9x mass of DMAc; annealed (L), unannealed (R)

This study yields solely qualitative, comparative results intended to highlight a significant chemical difference between annealed and unannealed samples.

Chapter 4:

4.1 Pure PFCB Materials

The first studies conducted were those used to determine the morphology of pure S-PFCB. Our priorities were the shape and prevalence of the block copolymer phase separation, and the size and prevalence of ionic aggregation. In order to understand these features, we have compared several forms of PFCB, sulfonated and non-sulfonated.

4.1.1 SAXS, PFCB Materials

Small angle x-ray scattering data was collected for VT cast pure S-PFCB, for samples cast at a thickness of 100, 12, and 5 μm (Figure 4-1).

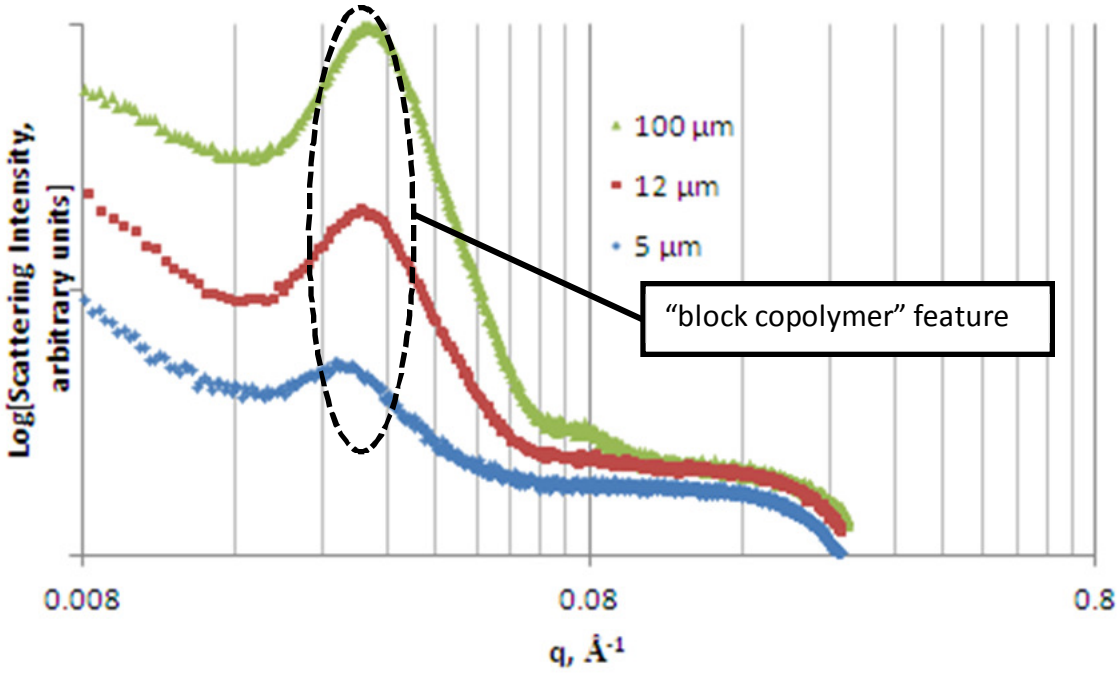

Figure 4-1: SAXS profile of VT cast pure S-PFCB, for three different membrane thicknesses

Most significant is the peak occurring in every sample at approximately q = .028, the "block copolymer" feature. This q range corresponds to an average feature size of 22 nm. SAXS profiles of different thicknesses, but identical morphologies will be different by a factor,

representing the ratio of thicknesses between the samples; this appears graphically as a vertical shift on a plot of log[intensity]. In this case, the profiles are not related by a vertical shift, and thus represent different morphologies. In particular, the block copolymer peak becomes more prominent with increases in thickness. Because the prominence in a given peak indicates the order of the structure present, we conclude that thicker samples contain a higher degree of order. If the surface of a membrane (the one exposed to air or substrate during casting) develops a less ordered morphology than the bulk of the polymer, we would expect increasing thickness would bring the SAXS response closer to that of bulk response. The existence of a surface defect layer is supported by AFM (Section 4.4.2).

However, in order to understand the nature of this feature, performing SAXS on the non-sulfonated form (N-PFCB) reveals the extent to which this feature is mediated by sulfonic acid groups.

Data was also gathered for pure PFCB, in both sulfonated and non-sulfonated form. The results are shown in Figure 4-2.

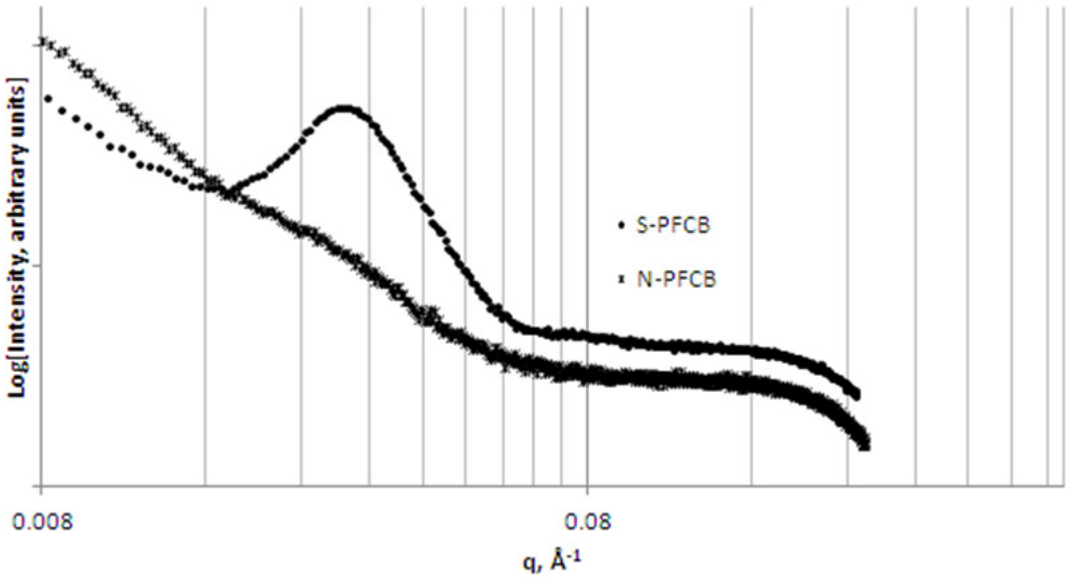

Figure 4-2: SAXS response of non-sulfonated and sulfonated PFCB

For PFCB, there is a prominent ordering peak in the sulfonated form at approximately Q=.028, representing a feature size of approximately 22 nm. However, in the non-sulfonated form, there are no notable peaks from the small angle scan, except for a small "knee" approximately centered around Q=.025.

This feature is much larger than would be anticipated for an ionic aggregate analogous to Nafion®. Instead, this represents the "block copolymer" feature of the material, or the phase separation of the 6F and BVPE-PFCB segments of polymer. Though subtly detectable in the non-sulfonated form (N-PFCB), the feature dominates the scan of S-PFCB. Whether this arises from a greater degree of ordering in S-PFCB or from an increase in scattering contrast (stemming from S-PFCB's sulfonic acid groups) is difficult to determine purely from SAXS. However, we have studied the effect of a change in scattering contrast on pure S-PFCB, as shown in Figure 4-3.

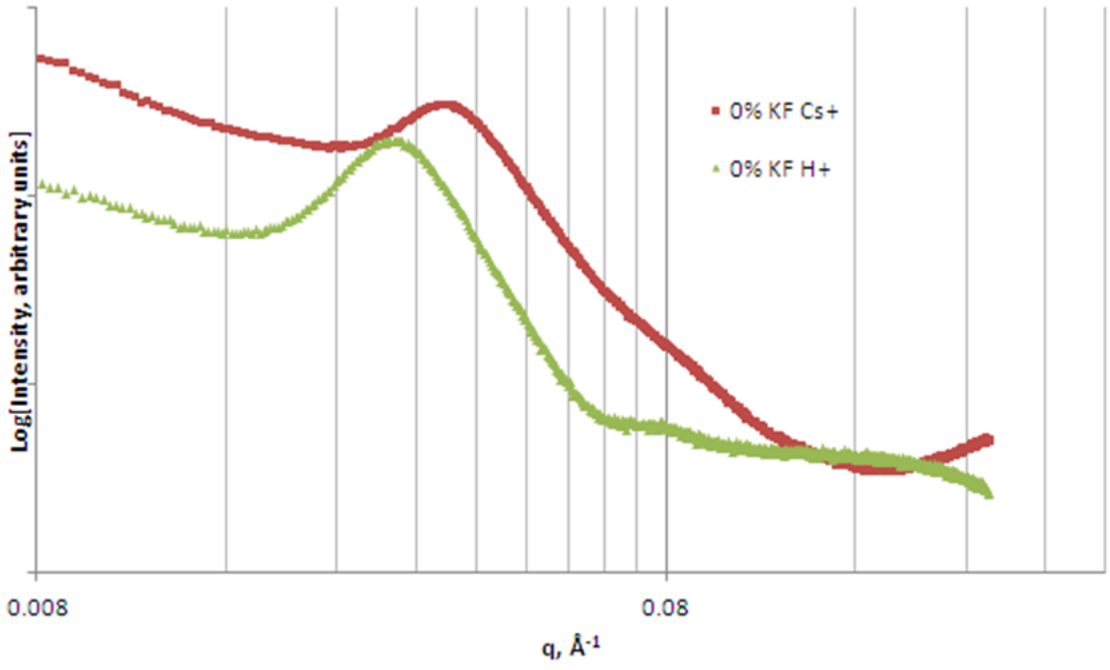

Figure 4-3: SAXs profile of pure S-PFCB, 100 μm thick, in both acid and Cs^+ form

Some stark differences appear between the scans of Cs^+ form and acid form S-PFCB. First, the "block copolymer" q_{max} position shifts from q=.0287 $Å^{-1}$ to q=.0344 $Å^{-1}$, or from an average size of 21.9 nm to 18.3 nm. Also, while the acid form's block copolymer feature ends after q=.06 $Å^{-1}$, the profile of the Cs^+ form continues dropping, though a kink at q=.06 $Å^{-1}$ suggests it is not necessarily the same feature as the block copolymer. It likely represents second order scattering, similar to that seen before in block sulfonated polymers [14]. This structure is made more obvious by the increase in scattering contrast of the cesium ions of higher electron density.

Finally, the Cs^+ profile contains a slight upturn at its end (q=.026 $Å^{-1}$), which is not present in the acid form. This upturn represents individual ionic aggregates, of a size from 2-3 nm. The entire ionomer peak is visible at higher q ranges, as shown in mid-angle x-ray scattering profiles of 30% blends (Section 4.4.1.2).

These individual aggregates form in phases rich in sulfonated BVPE-PFCB blocks, creating two degrees of ordering in the polymer, as illustrated in Figure 4-4.

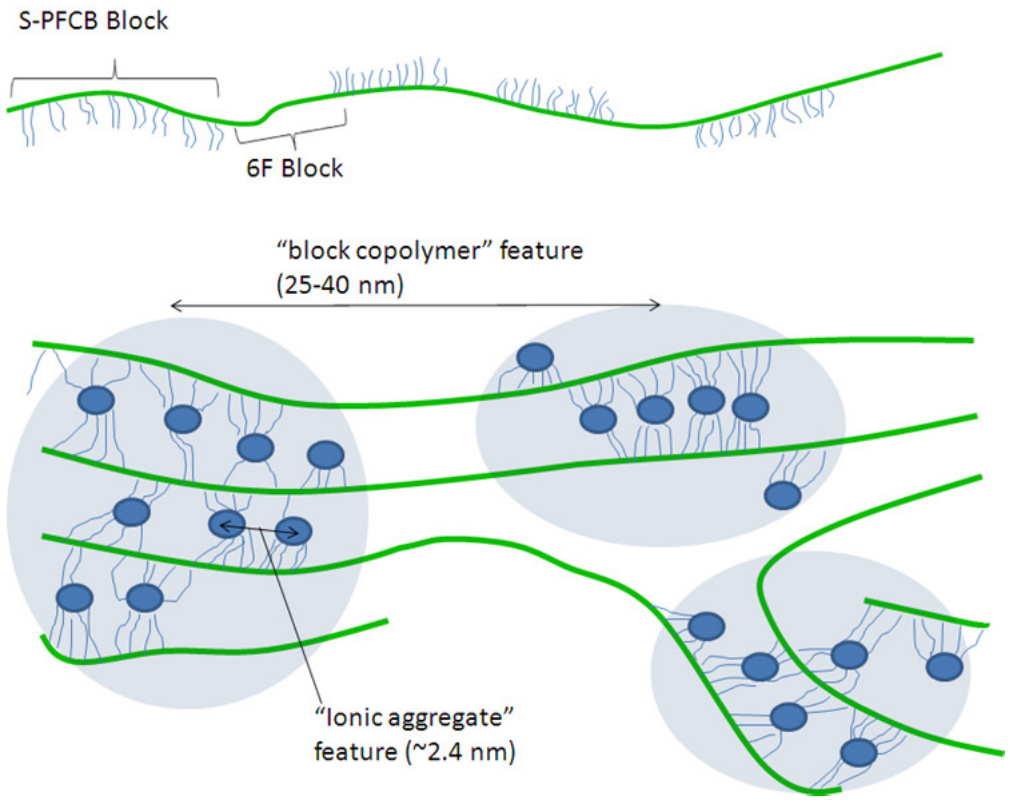

Figure 4-4: Basic understanding of S-PFCB structure

4.1.2 DSC, PFCB Polymers

DSC revealed information about the crystallinity and glass transition behavior of S-PFCB. Beginning with a simple crystalline component of S-PFCB, 6F, we study increasingly complex polymers, each incrementally closer to pure S-PFCB.

4.1.2.1 DSC, 6F Homopolymer

DSC has been performed on non-sulfonated PFCB, as well as 6F homopolymer, a single block of PFCB. For 6F, DSC scans using different cooling rates are given in Figure 4-5, Figure 4-6, and Figure 4-7.

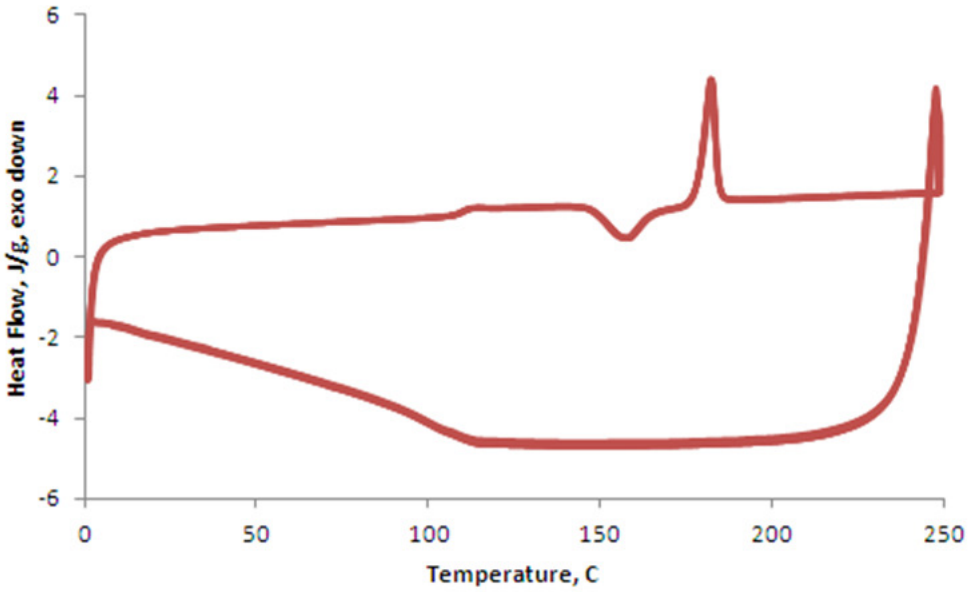

Figure 4-5: DSC, 6F homopolymer, cooling rate 50C/min, heating rate 10 C/min

At 50/C min cooling, 6F does not crystallize. Instead, it dynamically crystallizes upon heating at 148-162 C. These crystallites melt within 5 °C of 183 °C.

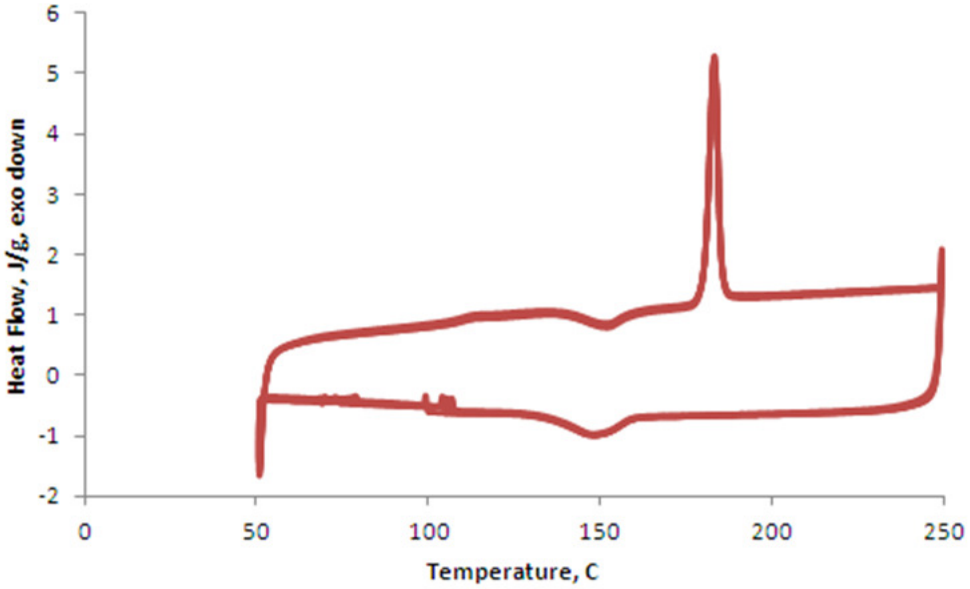

Figure 4-6: DSC, 6F homopolymer, cooling rate 10C/min, heating rate 10 C/min

At a rate of 10 C/min cooling, 6F crystallizes partially, but not completely as evidenced by an exothermic heating event for the heating ramp.

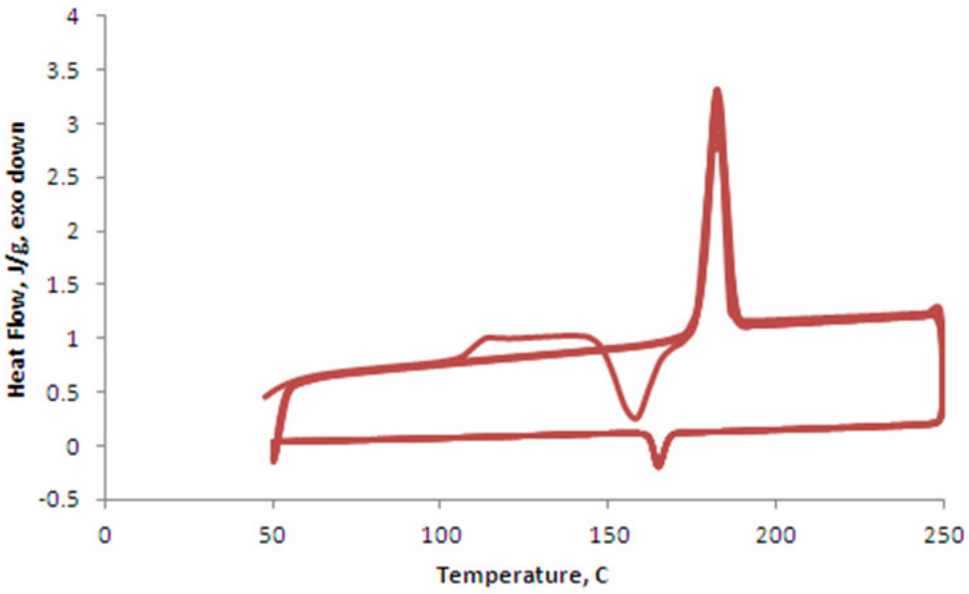

Figure 4-7: DSC, 6F homopolymer, cooling rate 1C/min, heating rate 10 C/min

At a cooling rate of 1 C/min, 6F crystallizes completely during cooling. This cooling rate represents approximately 15 minutes of crystallization, giving us an estimate for the time scale over which 6F crystallizes.

4.1.2.2 DSC, N-PFCB Multiblock Copolymer

When 6F monomer is polymerized with BVPE-PFCB oligomer blocks, N-PFCB results. We have obtained DSC profiles for N-PFCB for cooling rates of 1, 10, and 50 °C/min, and they are given in Figure 4-8, Figure 4-9, and Figure 4-10.

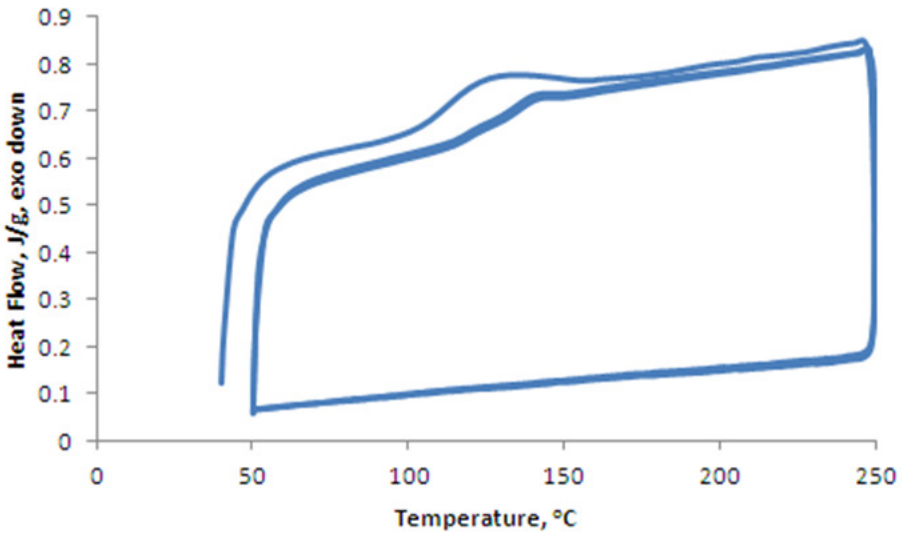

Figure 4-8: DSC scan of N-PFCB; heating rate 10 °C/min, cooling rate 1 °C/min

Even for cooling rates as low as 1 °C/min, no exothermic crystallization even is visible upon cooling, and no endothermic melting event is visible upon heating; there is likely no crystallinity resulting from cooling at these rates. No crystalline events are observed for different cooling rates.

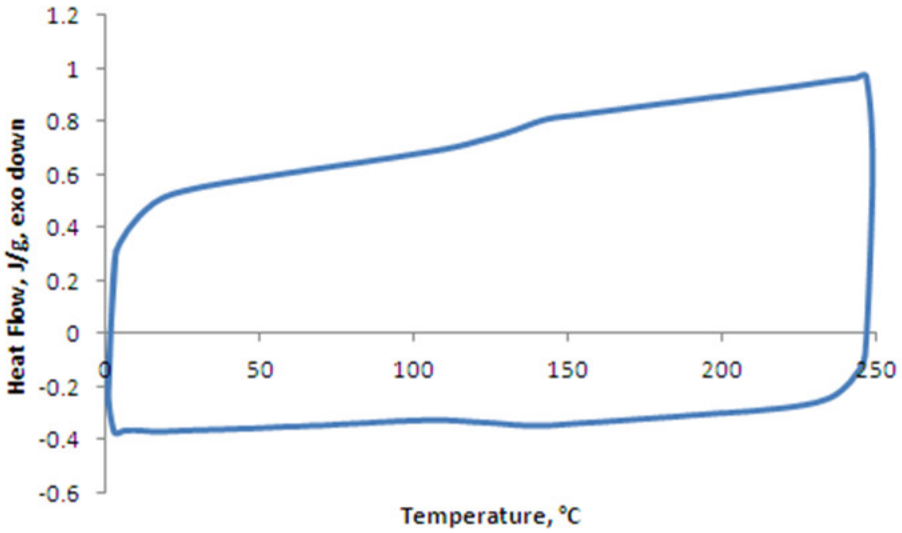

Figure 4-9: DSC scan of N-PFCB; heating rate 10 ºC/min, cooling rate 10 ºC/min

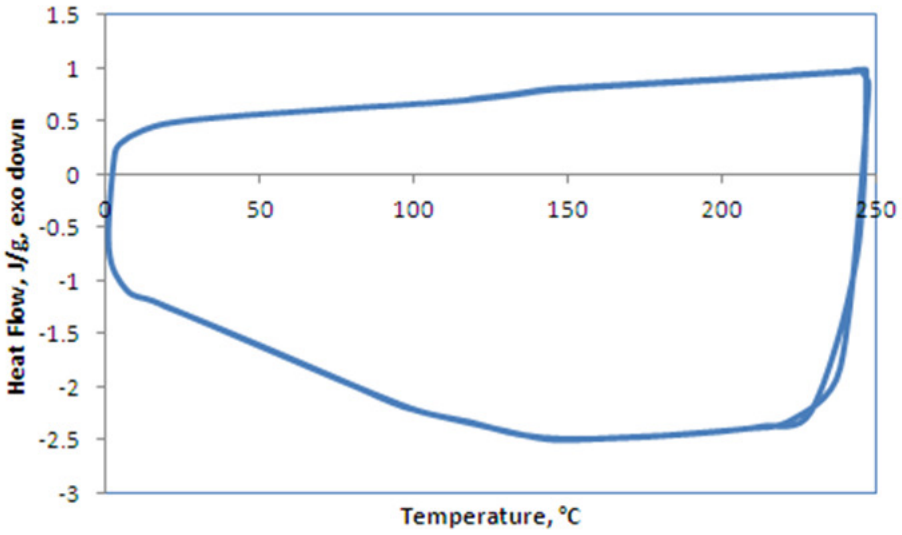

Figure 4-10: DSC scan of N-PFCB; heating rate 10 ºC/min, cooling rate 50 ºC/min

At rates of 10 and 50 ^{o}C/min cooling, no different morphological features appear, and the glass transition temperature occurs at 125 ^{o}C.

4.1.2.3 DSC, S-PFCB Sulfonated Multiblock Copolymer

The DSC response of pure S-PFCB is given in Figure 4-11, Figure 4-12, and Figure 4-13. The data includes temperature ramps of 5, 10, and 20 K/min, as well as scans of three different samples of S-PFCB: GM cast Gen 2 (TAKS 115C) 10 µm thick, VT cast (TCT 840B) 100 µm thick, and VT cast 12 µm thick.

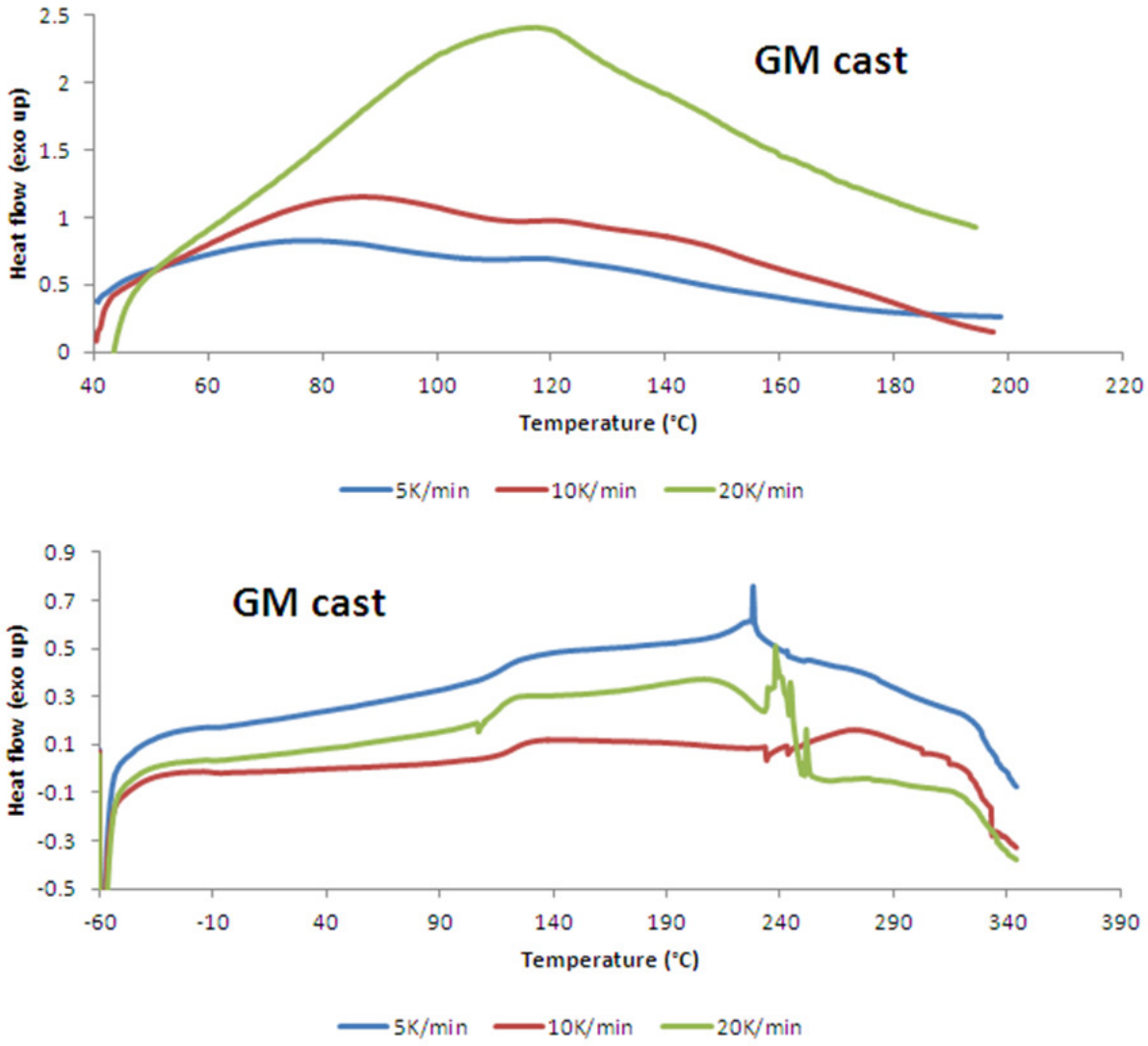

Figure 4-11: GM cast, 12 µm thick S-PFCB, first scans (top) and second scans (bottom), with three different heating rates reported

In each first scan, the shape of the profile is that of a massive endothermic event, centered around 120 ^{o}C for the 20 ^{o}C/min scan, and around approximately 80 ^{o}C for 5 and 10 ^{o}C/min scans; this event corresponds to water absorbing energy to escape the ionomer.

In second scans, thermal behavior more directly connected to polymer chains behavior rather than water evaporation. The glass transition of the polymer occurs at approximately 125

°C. Beginning at 230-250 °C, the polymer degrades extensively, and thus no notable conclusions can be drawn from the scan after this temperature range. VT cast pure S-PFCB shows largely the same behavior (Figure 4-12).

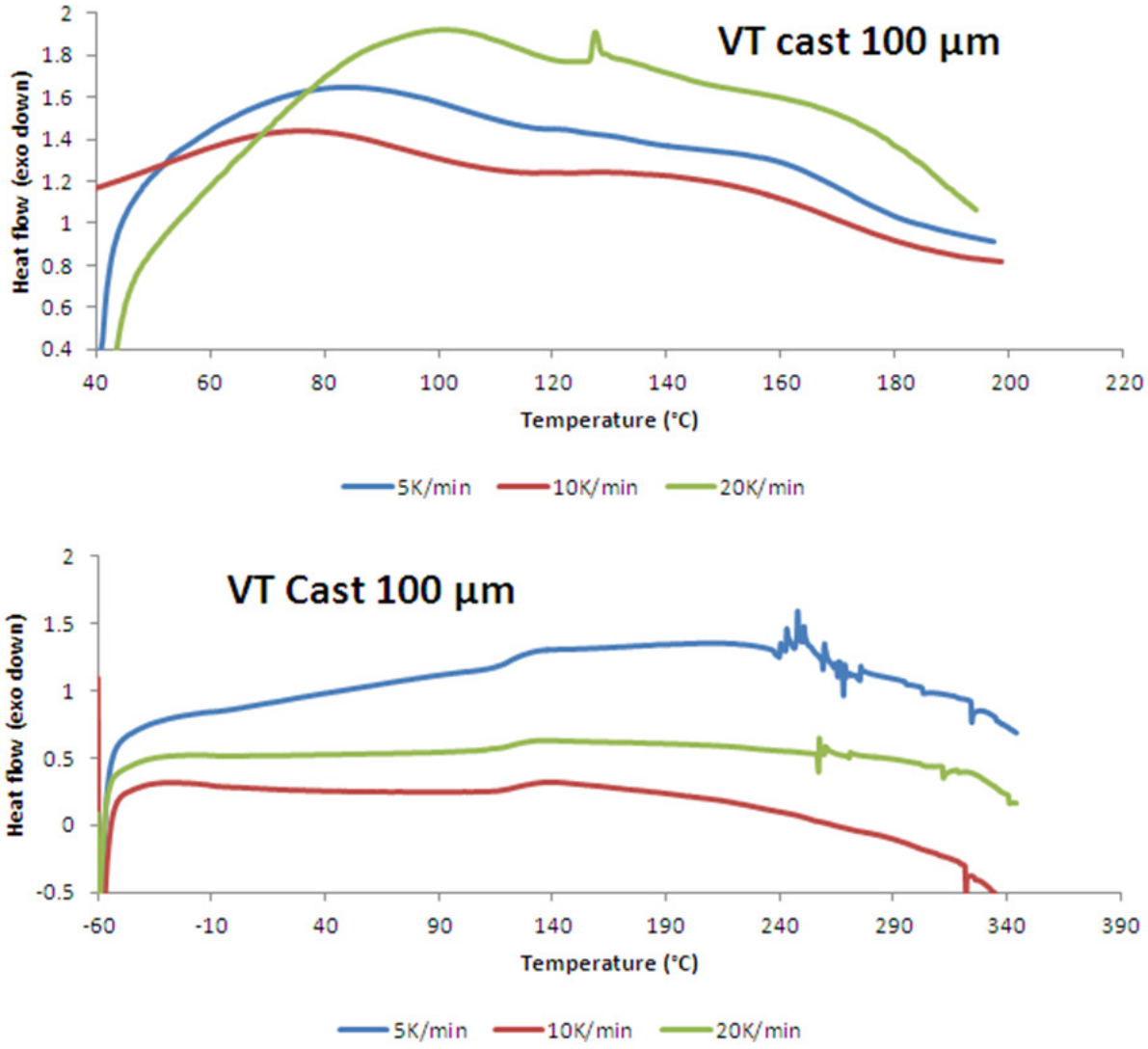

Figure 4-12: VT cast, 100 µm thick S-PFCB, first scans (top) and second scans (bottom), with three different heating rates reported

For VT cast pure S-PFCB, the response is largely the same as GM cast material. A glass transition is observed at 125 °C and degradation begins at approximately 240 °C. No crystalline melting event is observed near 180 °C (melting temperature of 6F crystallites).

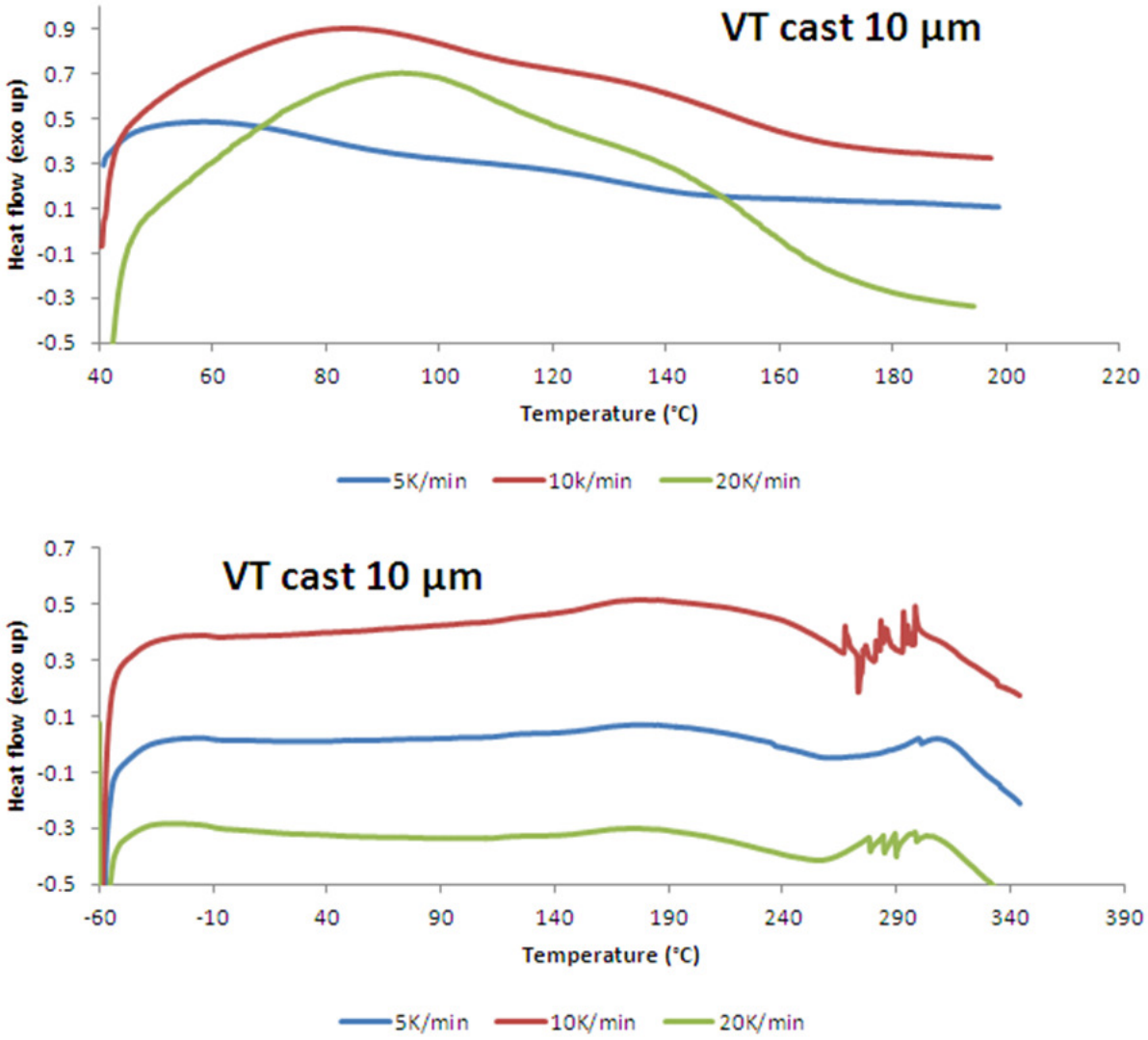

Figure 4-13: VT cast, 10 µm thick S-PFCB, first scans (top) and second scans (bottom), with three different heating rates reported

Thin VT cast samples (10 µm) do not show a clear glass transition in DSC. Also, the response does not become erratic until nearly 280 ^{o}C, 30 degrees higher than for the other two sample sets. Ultimately, these changes probably arise from the lower signal given by these smaller samples. VT cast 10 m thick samples only reached 4 mg of mass, while samples of GM cast 10 m and VT cast 100 m reach nearly 10 mg each. Therefore, we obtain more accurate material properties, such as identifying T_g and also showing a lack of crystallinity, with VT cast

100 m and GM cast 10 m. This could also suggest a less ordered arrangement in thin VT cast material, a hypothesis supported by SAXS and AFM data (Sections 4.1.1 and 4.4.2).

From these DSC studies, we have determined that the glass transition of S-PFCB occurs at 125 C. Also, we have ruled out the formation of crystallinity in pure S-PFCB despite the strong crystalline nature of one of its blocky components, 6F polymer. Finally, we have observed significant degradation of S-PFCB above 230 ^{o}C, and thus this material should not be processed at or above this temperature.

4.1.3 Atomic Force Microscopy, Pure S-PFCB

Atomic force microscopy scans were taken for VT cast pure S-PFCB, with a horizontal field width of 3 and 1 µm. These scans are given in Figure 4-14 and Figure 4-15.

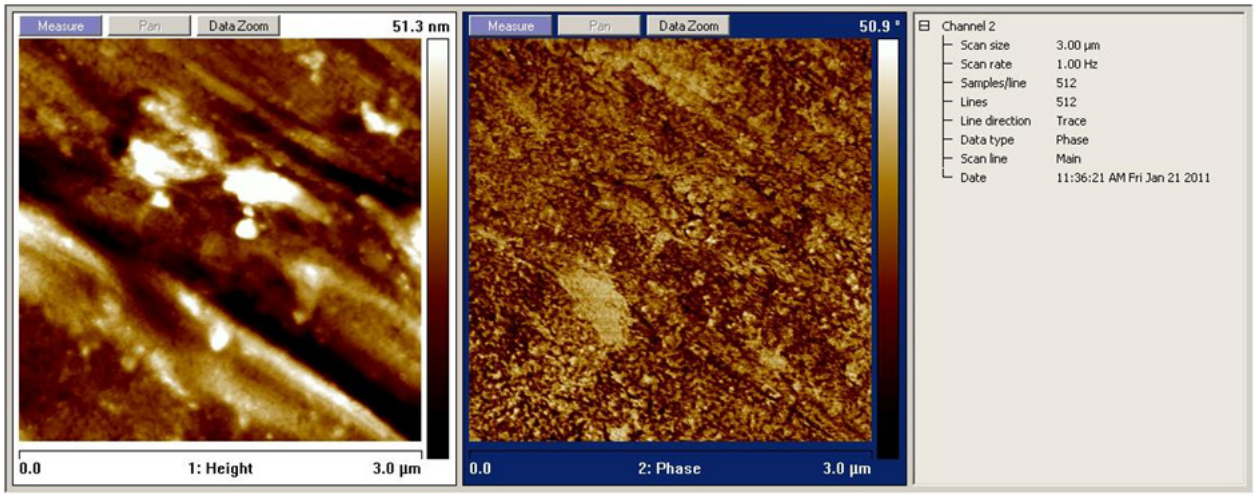

Figure 4-14: AFM scan of pure VT cast S-PFCB, HFW 3 µm; height image left, phase image right

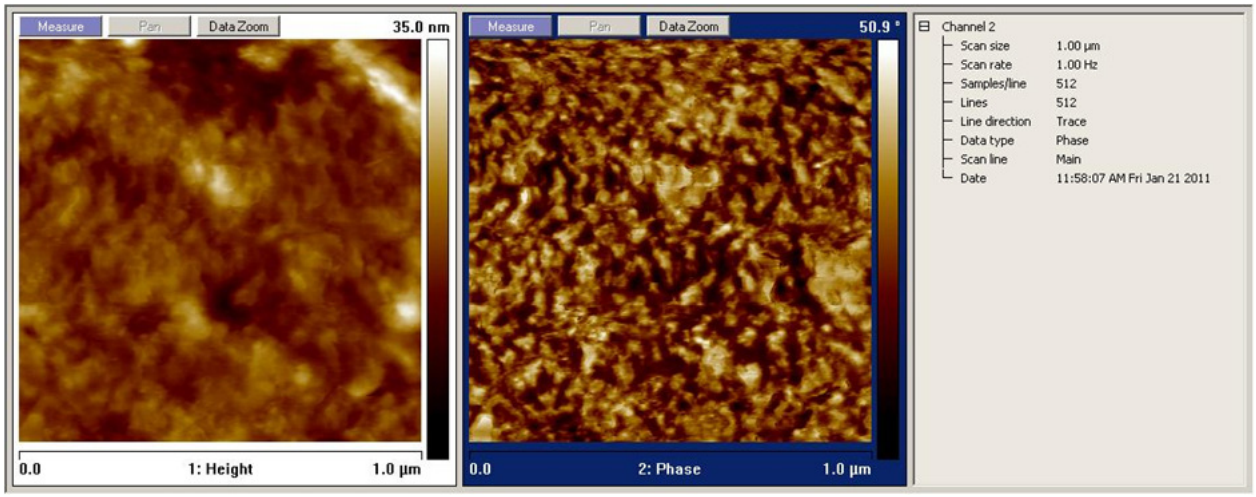

Figure 4-15: AFM scan of pure VT cast S-PFCB, HFW 1 µm; height image left, phase image right

In both scans, the phase image shows nanoscale heterogeneity. These features vary in shape and size, but the hard (bright) features are roughly 32 nm across. Also, it is difficult to distinguish to what extent these domains are interconnected. However, upon close examination, it appears to be a bicontinuous structure- one where both the soft and hard phases are continuous among each other.

This feature appears to have a similar size as the "block copolymer" phase separation observed in SAXS. However, while SAXs gives a feature size of 22 nm (by q_{max} method), AFM features appear to be 32 nm. This difference could represent a discrepancy between the surface morphology and bulk morphology, as AFM only probes the surface, while SAXS scans the bulk material. This may also represent a shortcoming in interpreting SAXS data, and the SAXS intensity function as predicted by our current model should be derived to evaluate this possibility.

4.1.4 Solvent Dissolution, Pure PFCB Materials

Several pure PFCB samples were treated in this method:

- VT cast unsulfonated PFCB, water bathed (50 °C, 1 hour)
- VT cast unsulfonated PFCB, water bathed, annealed (100 °C, 2 hours)

- VT cast TCT, water bathed, annealed and unannealed
- GM cast Gen 1 S-PFCB (main chain sulfonated), water bathed, annealed (2 and 24 hours, 100 and 140 °C) and unannealed

For all membrane varieties, unannealed samples dissolved quickly in DMAc, as did samples annealed at 100 ^{o}C for up to 24 hours. Samples annealed at 140 ^{o}C for at least one hour remained in a gel state both with 9x mass of DMAc as well as with excess DMAc. However, after ultrasonication, all samples entered the solution state. Notably, 100 ^{o}C is below the T_g of pure S-PFCB, and 140 ^{o}C is above it. Therefore, the morphological rearrangement that makes the material resistant to attack by solvent takes place above the material's T_g, when the polymer chains are capable of long range ordering.

Because pure ionomer could be made to not dissolve after annealing, we know that a change in properties is not solely related to crystallization of Kynar Flex. Therefore, a morphological arrangement that increases S-PFCB's chemical stability is possible, though the chemical or structural origin of this change is still under investigation. We do know with a reasonable degree of certainty that this phenomenon is not related to crystallization, from WAXS data collected on pure S-PFCB annealed at 140 ^{o}C for 6 and 24 hours (Figure 4-16).

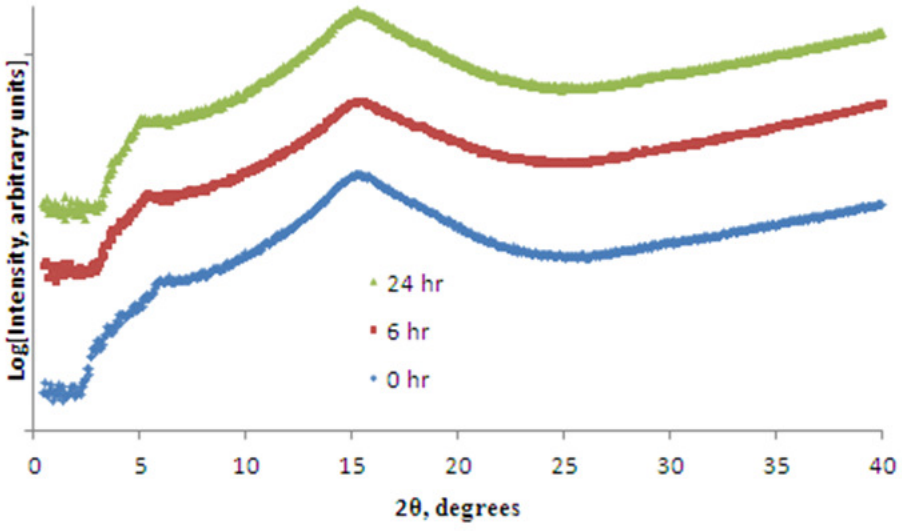

Figure 4-16: WAXS response of pure VT cast S-PFCB, annealed at 140 °C for various times

We see no change in the shape or intensities of these profiles for this amount of annealing, despite the fact that the material's chemical resistance changes drastically after 6 hours of annealing; only an amorphous halo is present. It is important to note that 6F crystallites have their peak WAXD response at $2\theta = 16^{o}$, which is within one degree of the amorphous halo peak of $2\theta = 14.9^{o}$. Still, crystallinity is very likely not the cause of this change in properties of PFCB upon annealing.

4.2 Pure Kynar Flex Studies

4.2.1 SAXS, Pure KF

The SAXS response of Kynar Flex is reported in Figure 4-17.

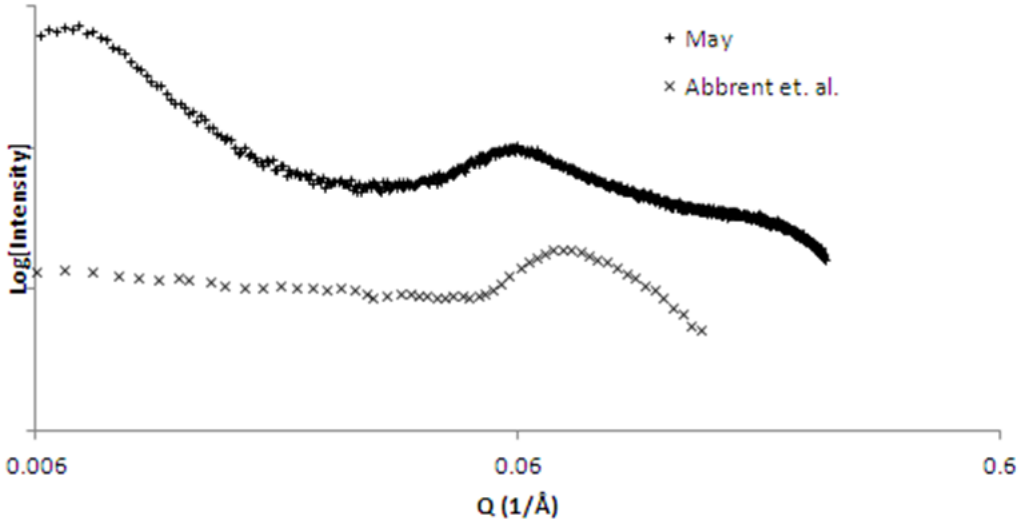

Figure 4-17: SAXS of Pure Kynar Flex taken in house and as reported in the literature [36c].

For VT cast pure Kynar Flex, a peak occurs at Q=.055, representing an average feature size of 11.4 nm. This is comparable to literature results, which put a peak at Q=.071, or d=8.85 nm. It is well known that processing parameters greatly influence polymer crystallinity [36a]. Thus,

different sample preparation techniques used in the reported results compared to the VT cast membranes account for the difference.

4.2.2 DSC, Pure KF

Pure KF was scanned in DSC in three forms: solution cast, melt processed, and precipitated. These three forms were selected to highlight crystallinity of different forms, and determine the extent to which KF crystallizes compared to traditional melt-processed forms. Melt processed samples were prepared by heating to 210 °C, and rapidly cooling to RT. Solution cast samples were cast in the traditional GM procedure, and were not water bathed. Precipitated samples were made by injecting a 10 wt% KF in DMAc solution into a container of water. A film of KF developed on the surface of the water. It was then washed extensively in water, vacuum dried at 40 °C for one hour (to remove DMAc) and desiccated for 24 hours (to remove water). The materials were heated at 10 °C/min to 250 °C, and cooled at 50 °C/min to 0 °C. The first scans of these samples are given in Figure 4-18.

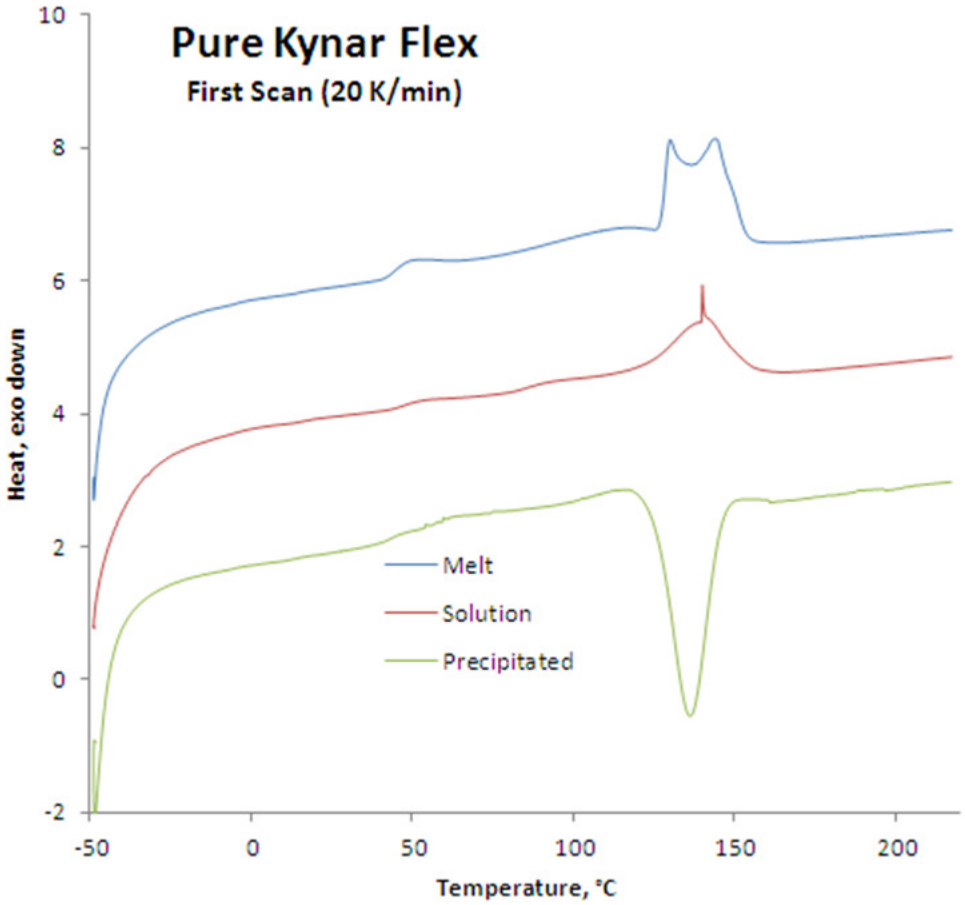

Figure 4-18: DSC scans of KF processed in three different ways

While the solution processed material shows a single crystalline melting peak, the melt-processed samples shows a bimodal distribution, which may arise from different phases of KF crystallinity. This suggests that solution cast KF films contain a different crystal structure than melt processed KF. The sample precipitated into solution shows a large, anomalous exothermic event in lieu the endothermic event associated with melting crystallites. The source of this behavior is unknown, but irrelevant to this project.

For melt-processed/quenched KF, the two crystalline melting peaks occur at 141 and 129 C. For solution cast/ air cooled samples, the single melting event is centered around 135 C. The prominent spike near this temperature likely represents removal of DMAc freed by the melting

of crystallites. It also serves to confirm the effectiveness of water-bathing membranes at 50 °C to remove DMAc; because this sharp event is not present in other samples' first scans (4.1.2 4.3.2), we can conclude that they had little to no DMAc in them when scanned. Each of these melting events occurs at a different temperature, suggesting different phases of crystals may be present depending on processing parameters.

4.2.3 Fourier Transform Infrared Spectroscopy, Pure KF

ATR-FTIR was performed on Kynar Flex processed as described in 4.2.2 . The results are shown in Figure 4-19.

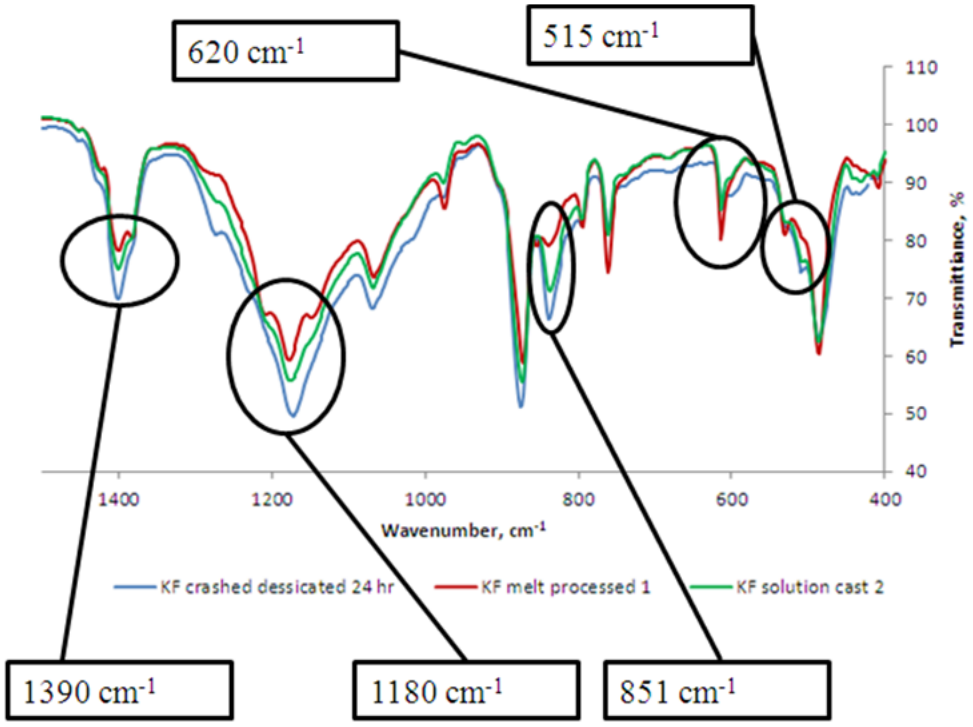

Figure 4-19: FTIR response of precipitated, melt processed, and solution cast KF

Several peaks are called out because of the large differences in them among the samples. First, the 1390 and 1180 cm^{-1} peaks appear as split peaks for melt-processed KF, while precipitated samples show single peaks for both. However, solution cast films show a behavior between the two, as if representing a single large peak with shoulder peaks. Next, in melt

processed KF, there is not a large response around 851 and 515 cm^{-1}, while in precipitated KF, there is a large peak, and in solution cast KF, though it is not as significant. Finally, melt processed KF shows a peak around 620 cm^{-1}, and the other two samples do not. In every case, the peaks associated with melt-processed KF coincide with those observed in the high energy alpha crystalline phase of KF; solution cast and precipitated samples show the peaks strongly associated with the lower energy gamma crystalline phase [36b, c]. Solution processed KF in general shows a response more consistent with a predominantly alpha crystalline structure, with some gamma crystalline characteristics.

These results show that we have developed two crystalline phases in KF, each with different properties. We have also shown FTIR as a viable method of distinguishing between the two phases.

4.2.4 Atomic Force Microscopy, Pure KF

AFM has been performed on VT cast KF, with horizontal field widths of both 3 and 1 μm, as shown in Figure 4-20 and Figure 4-21.

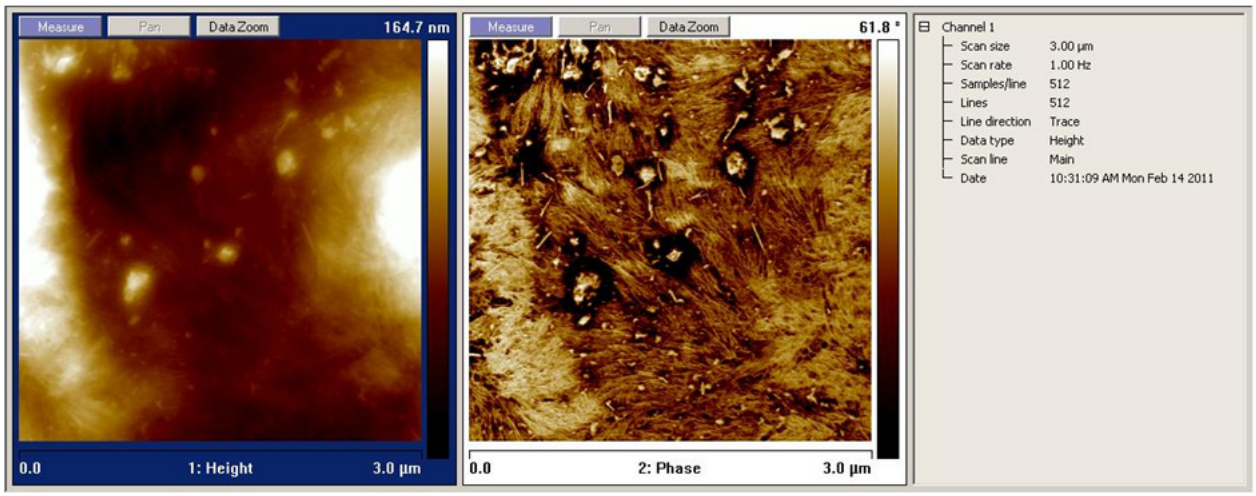

Figure 4-20: AFM scan of pure VT cast KF, 3 μm HFW

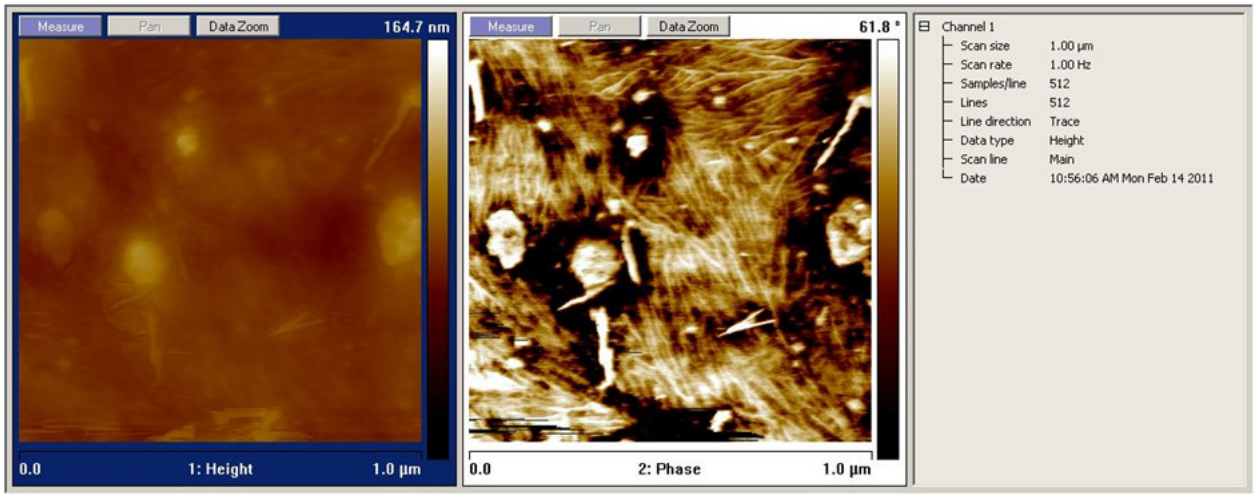

Figure 4-21: AFM scan of pure VT cast KF, 3 µm HFW

Lamellar crystallites appear in both of these scans, in the form of needle-like hard phases. These have dimensions of approximately 10-11 nm, agreeing very well with SAXS data. These lamellae are several hundred nanometers long.

4.2.5 Solvent Dissolution, Pure KF

Kynar Flex was exposed to DMAc before and after anneal at 100 ^{o}C for 2 hours. Neither sample dissolved in DMAc after 24 hours. When ultrasonicated, every sample entered solution state. This is consistent with crystallites adding to chemical resistance, as we have shown solution processed samples to be crystalline [36a, 40-41].

4.3 Various % KF

4.3.1 SAXS, Varied % KF

Small-angle x-ray scattering scans of S-PFCB with varying amounts of KF blended in were taken. The results are given in Figure 4-22 and Figure 4-23.

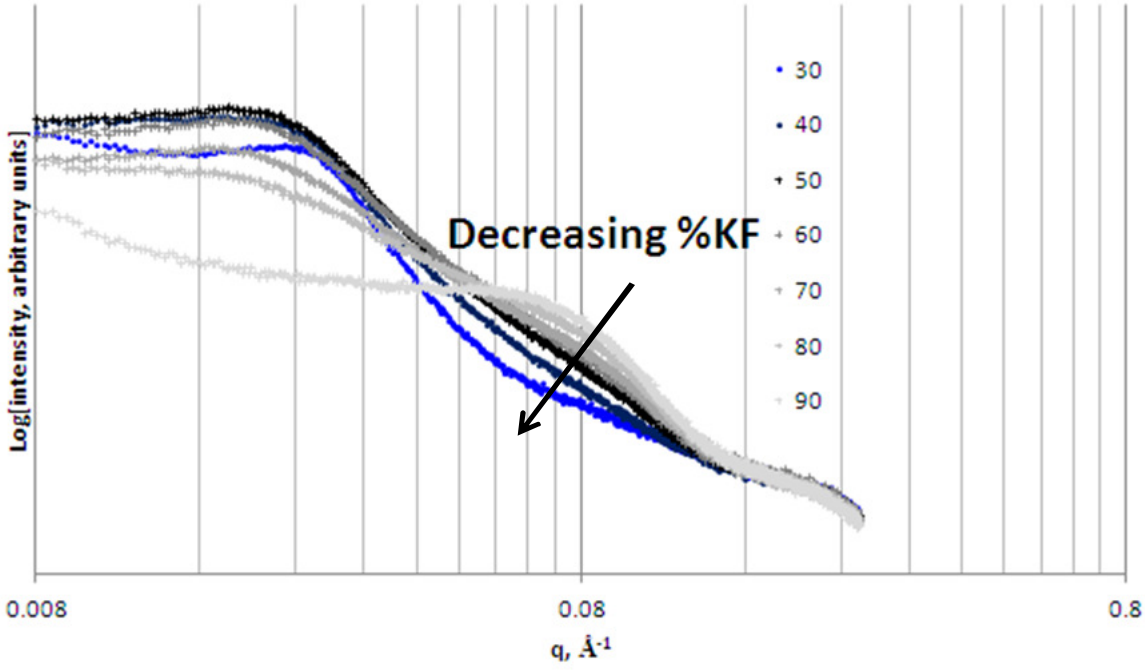

Figure 4-22: SAXS scans of VT cast S-PFCB blend membranes varying from 30-90 wt% KF, thickness 45 µm ±2

For 90 wt% Kynar Flex, the SAXS response shows a distributed peak centered on q_{max}=.069 $Å^{-1}$, or a size of 9.1 nm. The response in this region shows a steady decrease with decreased amounts of KF. Therefore, we assign the relative response in this region to Kynar Flex crystallites. At approximately 40% KF the form of this peak becomes so low as to make it blend into the gradual downward slope characteristic of SAXS scans. However, the intensities and form of the region from .033 $Å^{-1}$< q < .125 $Å^{-1}$ still shows a trend with decreasing amounts of KF. From this, we learn that we can compare differences in crystallinity of samples of like thickness (or scans represented in absolute units) from SAXS.

Besides differences in the KF crystallites-related SAXS response, a gradual change in the intensity and form of the region from .008 $Å^{-1}$ < q < .033 $Å^{-1}$ represents the size and distribution of the block copolymer structure of S-PFCB. Though not significant for 90% KF blends, this peak begins to be distinguishable for blends up to 80% KF. This peak becomes more prominent at 50% KF, and is the dominant feature on every scan for KF content below 50%, when the KF

crystallite peak diminishes. Trends for both KF crystallinity and the block copolymer peak continue for KF content lower than 30%.

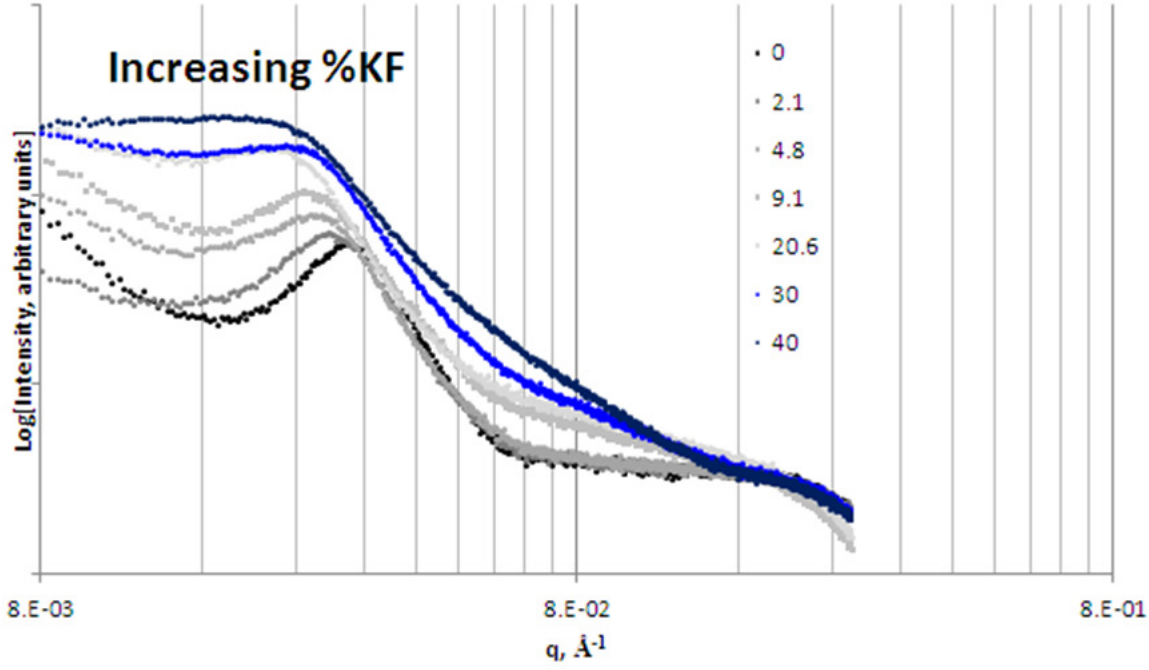

Figure 4-23: SAXS scans of VT cast S-PFCB blend membranes varying from 0-40 wt% KF, thickness 45 µm ±2

For low %KF samples, the block copolymer peak not only changes in intensity and broadness, but also in position. From q_{max} for 0 and 30% KF, we calculate d spacing of 22 and 27 nm, respectively. From modified sphere fits, we calculate an outer-shell size of 19 and 21 nm for 0 and 30% KF samples. Both estimates show a steady increase in feature size with added Kynar Flex. This fits well with our proposed morphological model (Figure 4-4), which contains ionic aggregate-rich, hydrophilic blocky phases separated by a hydrophobic matrix. However, it could also fit with an inverted structure- one with a hydrophilic continuous phase dotted with closed hydrophobic phases containing 6F and KF. In order to identify the most accurate of these models, SAXS form factors for both should be derived and fit to the data.

4.3.2 Morphological Model, Varied %KF

As shown by SAXS, the size of the block copolymer feature (proposed model Figure 4-4) becomes larger and more broadly distributed in size. This corresponds to the hydrophilic blocks, which have organized due to strong interactions among sulfonic acid groups. Added Kynar Flex, a highly hydrophobic molecule, pervades the hydrophobic phase of the ionomer multiblock, as shown in Figure 4-24.

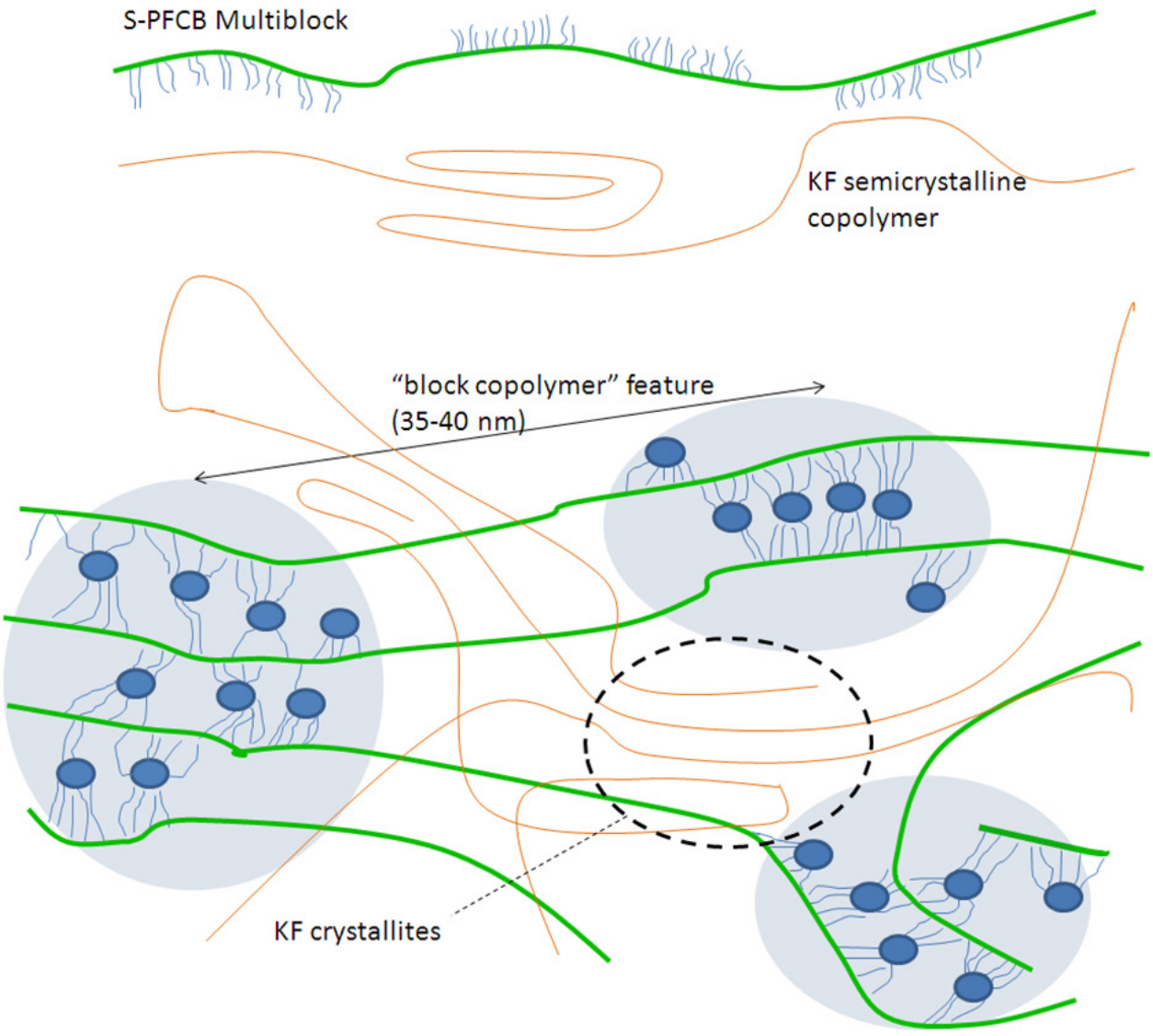

Figure 4-24: Basic understanding of S-PFCB ionomer/Kynar Flex blend morphology

4.3.3 DSC, Varied %KF

S-PFCB membranes containing varying weight% Kynar Flex were cast at Virginia Tech and scanned in DSC, with a heating ramp of 10 C/min heating and 50 C/min cooling. First heats, second heats, and first cool are given in Figure 4-25, Figure 4-26, and Figure 4-27.

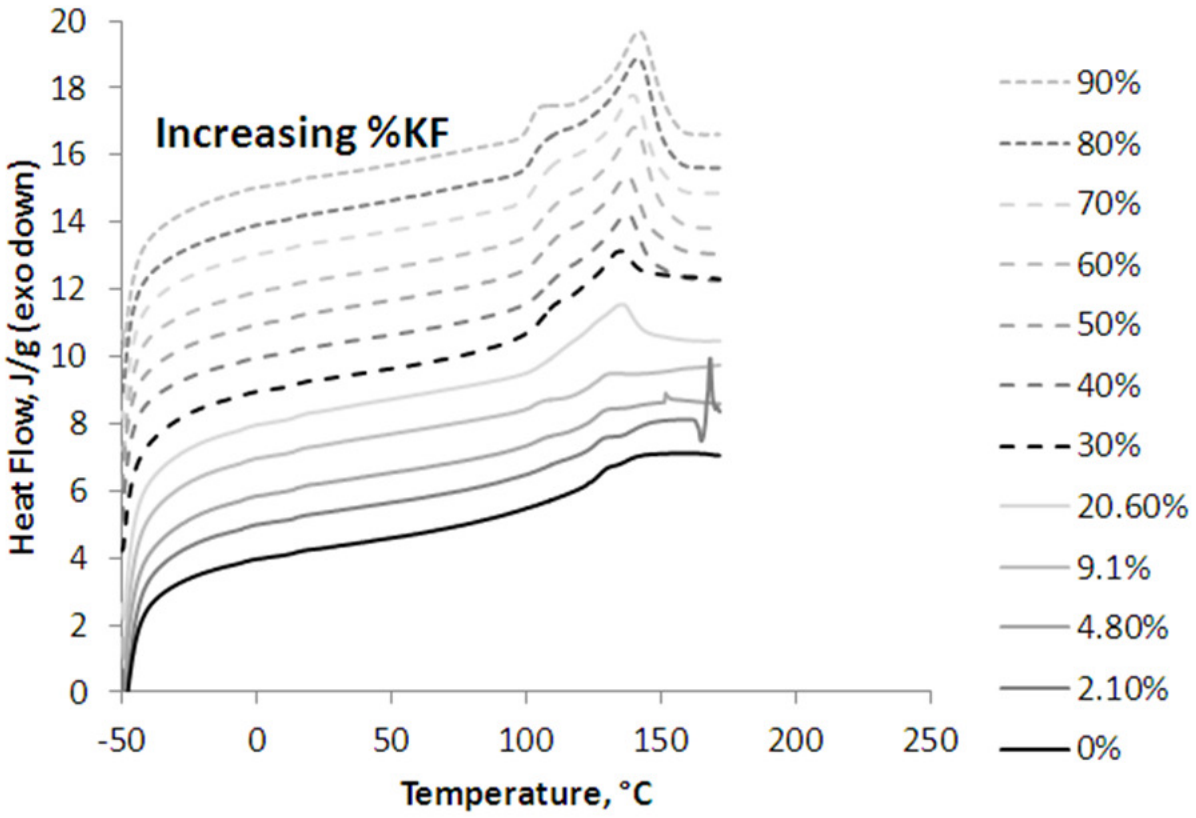

Figure 4-25: DSC scans of VT cast membranes, varying KF content (wt%); second heating of 10 ºC/min

The prominence of the crystalline peak jumps significantly above 9.1 % KF, and steadily increases thereafter with added KF. Also, unlike in the second heat, the crystals appear to melt in two distinct events for every blend composition. Finally, because the melting of KF coincides directly with the T_g of pure S-PFCB, it is difficult to determine the significance of the T_g of the blend. For samples of greater than 20% KF, there appears to be a single baseline for the entire blend. In compatible polymer blends, a single broad T_g may be observed. For incompatible (i.e. phase separated) blends, the T_g of both polymers is observable in DSC. Therefore, we can

conclude that these polymers are compatible based on the fact that we do not see a step change in the baseline of the DSC scan at 125 °C.

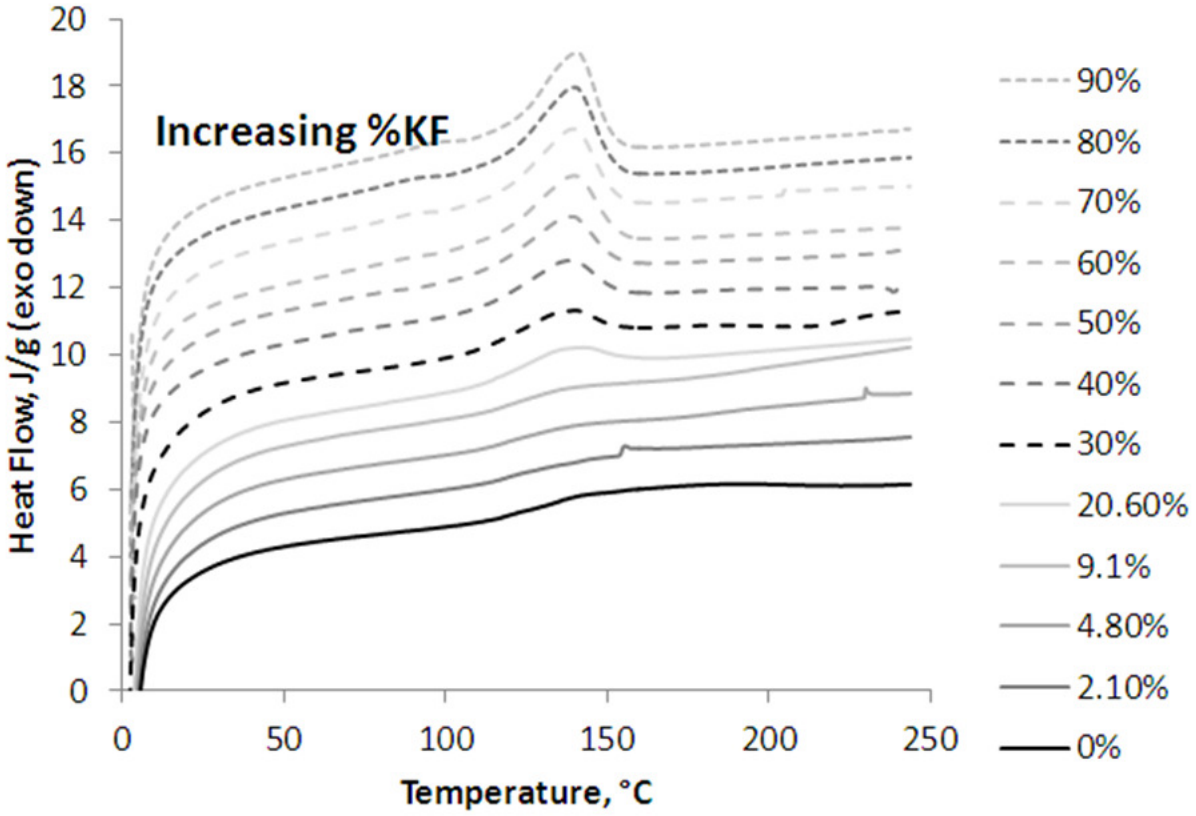

Figure 4-26: DSC scans of VT cast membranes, varying KF content (wt%); second heating of 10 ºC/min

Second heats show similar behavior, except for their single-peak melting event, rather than two peaks. The polymers still appear to be compatible, with no step change observed across 125 °C.

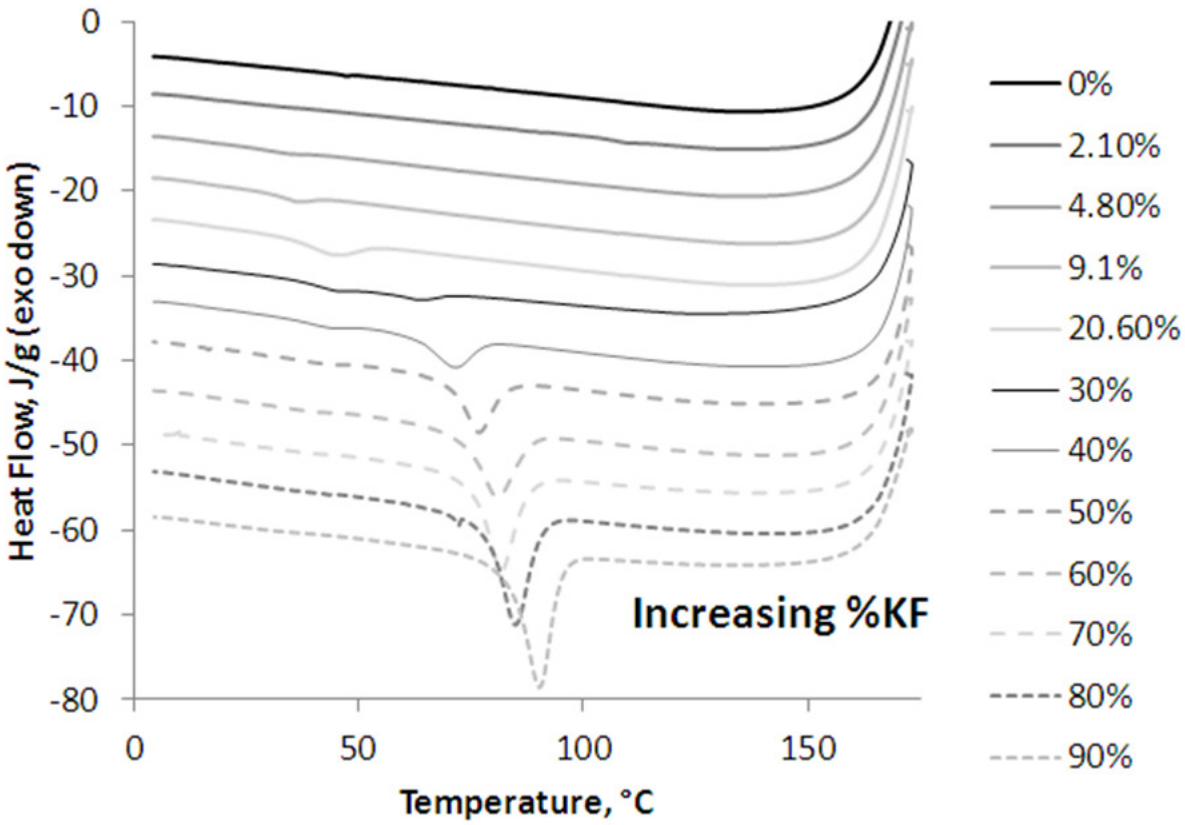

Figure 4-27: DSC scans of VT cast membranes, varying KF content (wt%); cooling scan of 50 °C/min

In the cooling scan, each blend composition contains an endothermic crystallization peak. The mean temperature of crystallization systematically decreases with lower KF content. In 40% KF, this melting event becomes visibly bimodal in nature, with a high temperature crystallization event at approximately 72 °C, and a low temperature event of 45 °C. This temperature range for samples from 50-9.1% KF is given in detail in Figure 4-28.

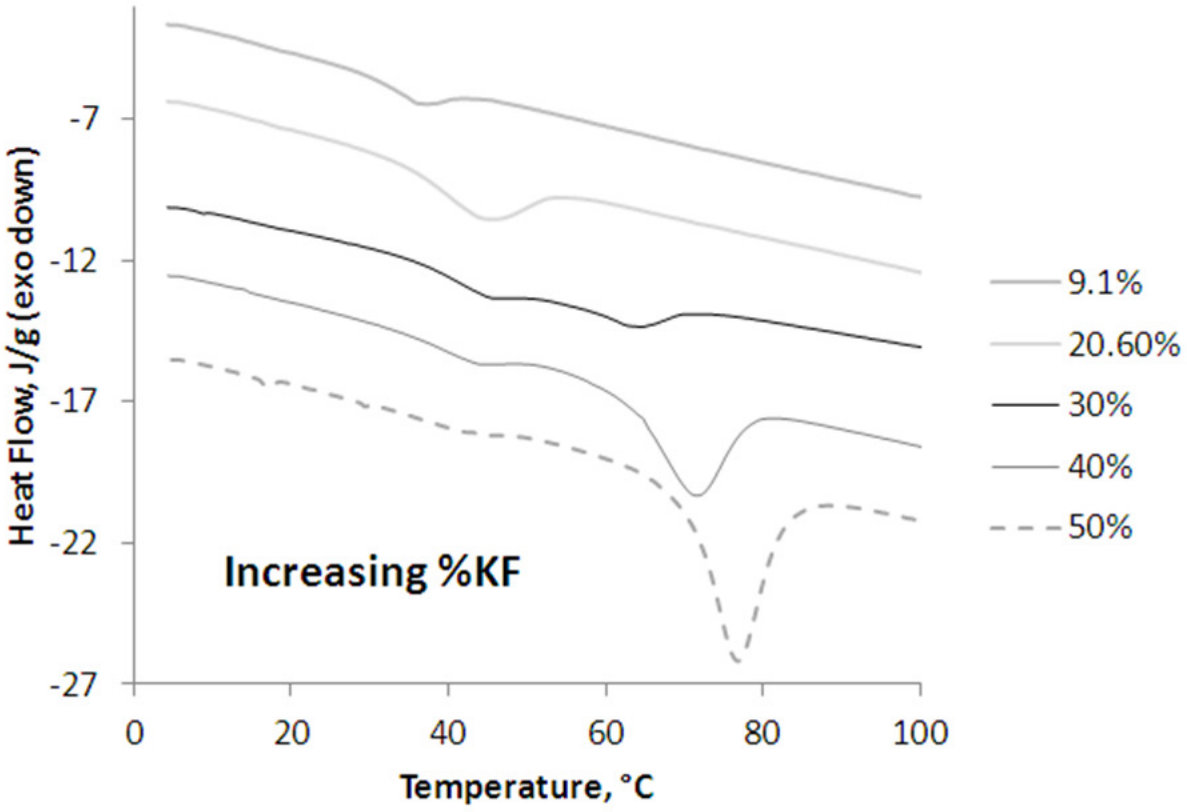

Figure 4-28: Crystallization of 50% KF to 9.1 % KF, in detail

There is a transition in the crystallization exotherm in these profiles, from the higher temperature crystallization dominated above 40% KF, to the one dominated by lower temperature crystallization below 30% KF. 30% KF appears to sit directly on a transition between the two events, with both equally represented. This reinforces that KF is at least partially miscible in S-PFCB, as its crystallization is hindered by the presence of ionomer. Also, we have discovered that the crystallization of 30% blends occurs over a range from 40-65 °C, well below the typical operation temperature of a PEM fuel cell (90 °C or higher).

This dual crystallization behavior does not appear to be dependent on cooling rate, as demonstrated by DSC of 30% KF, taken at different cooling rates (Figure 4-29, Figure 4-30, and Figure 4-48).

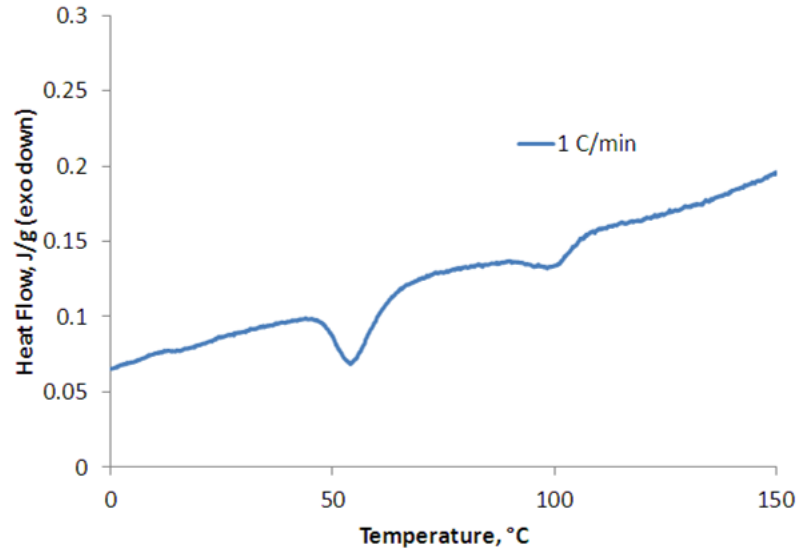

Figure 4-29: Cooling scan of VT cast 30% KF, 1 °C/min

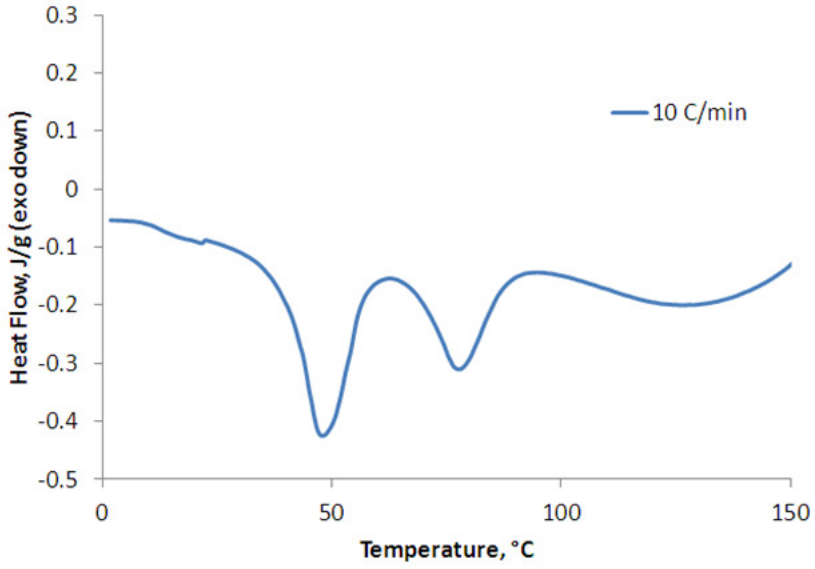

Figure 4-30: Cooling scan of VT cast 30% KF, 10 °C/min

4.4 30% KF Blends

We have performed extensive studies on the morphology of blends of S-PFCB and KF. As the blend composition of most interest to GM, 30% KF blends have been the most extensively studies. However, we have also studied varied compositions of Kynar Flex. We have varied processing parameters and studied the resulting membranes, in order to discover the extent to which we can change the morphology of this material.

4.4.1 SAXS, 30% KF Blends

In previous studies, GM has determined that 30% KF blends are those of greatest interest, due to their excellent balance of mechanical and conductive properties. Therefore, the most thorough morphological evaluations have been on various 30% KF blends. These involve comparisons of membranes thermally processed in different ways during the casting process.

4.4.1.1 SAXS, VT cast vs. GM cast 30% KF Blends

The morphologies of VT cast 30% KF and GM cast 30% KF differ notably both in the block copolymer peak and the KF crystalline region, as shown in Figure 4-31.

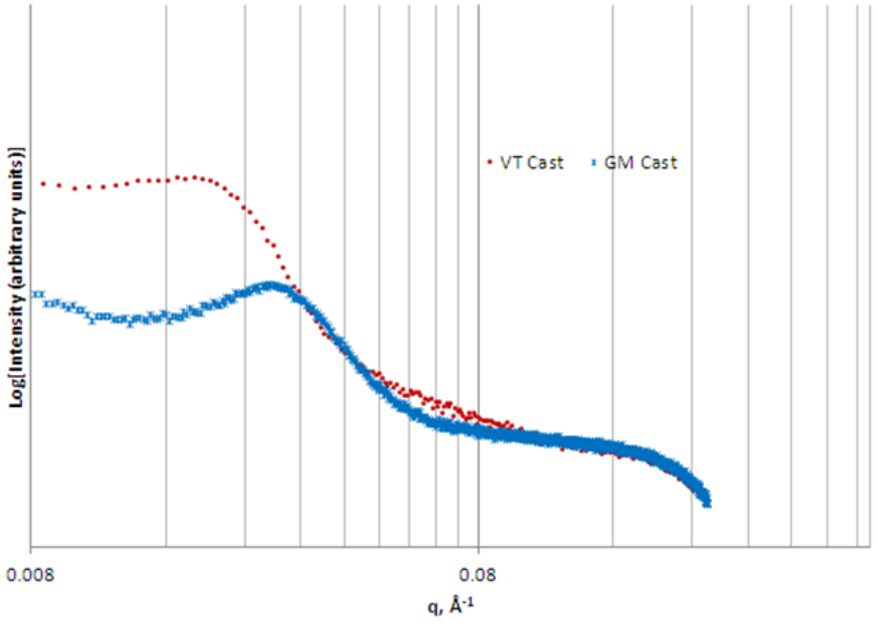

Figure 4-31: SAXS profiles of GM and VT cast 30% KF

The average block copolymer feature size for VT and GM cast 30% KF is 34 and 23 nm, respectively. Also, the VT cast membrane appears to contain more KF crystallinity, as the shoulder region is more intense. The block copolymer feature size for VT cast 30% KF is comparable both to VT cast 0% KF cast using the standard procedure (Section 4.1.1), as well as VT cast 30% KF cast at 30 C (Section 4.4.1.5). Whether these resemblances have morphological meaning has yet to be determined.

4.4.1.2 Small and Mid Angle X-ray Scattering, VT Cast 30% KF Cs^+ form

In order to study the nature of ionic aggregation in S-PFCB blends, VT cast 30% KF blends were neutralized with Cs^+ as a counterion, in order to increase contrast in ionic aggregates. The SAXS responses of the membrane before and after sulfonation are given in .

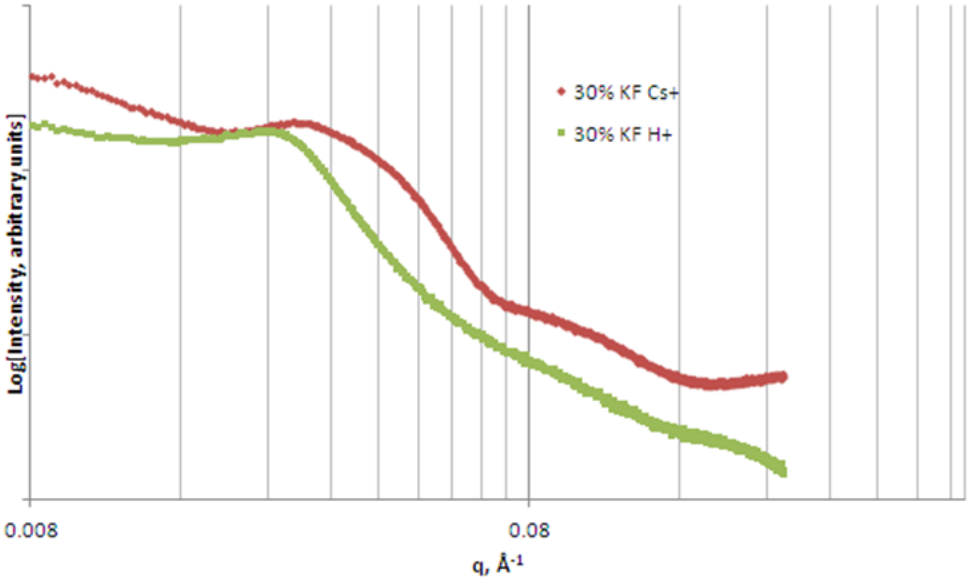

Figure 4-32: SAXS of acid and cesium form of VT cast 30% KF

As with the pure ionomer, a cesium form sample shows a more broad, higher q-range block copolymer peak, and the same second order knee appears near q=.06. Also, a slight upturn appears at the end of the profile. Mid angle scattering can accurately identify this peak more completely, as shown in Figure 4-33.

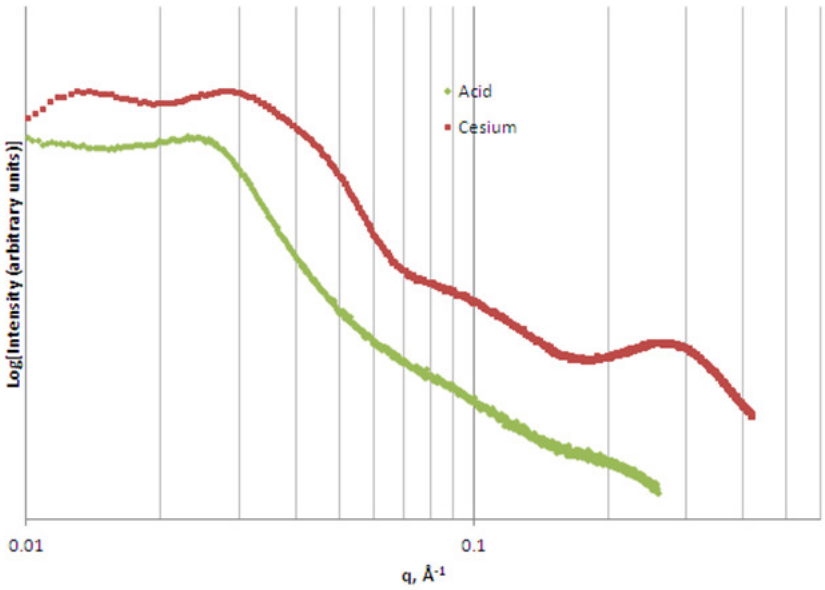

Figure 4-33: MAXS of acid and cesium form of VT cast 30% KF

We can see now that this upturn is actually the first part of a peak, centered on q = .26, or a size of 2.5 nm. This size is believed to be analogous to the ionic aggregate peak of Nafion®, representing individual ionic multiplets. The appearance of two distinct peaks, and order of magnitude separated in sizes, demands a two-level morphological model to fully describe.

4.4.1.3 SAXS, Varied Operation Temperature, 30% KF

GM cast 30% KF/70% TAKS was placed in the SAXS chamber, heated to a temperature between 40 and 140, and allowed to equilibrate for 1 hour. Data was then collected. Results are shown in Figure 4-34.

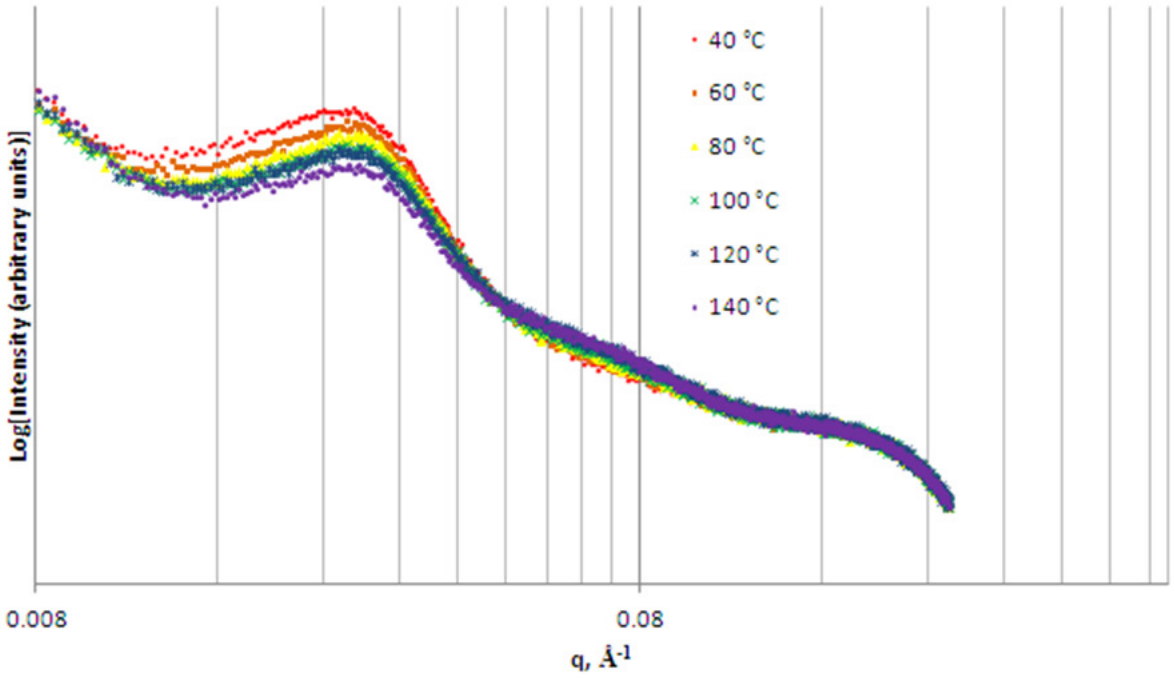

Figure 4-34: SAXS data for GM cast 30% KF, taken at varied temperature

Two trends appear in the data: with increasing temperature, the intensity of the block copolymer peak decreases, and the intensity of the KF-associated region increases. The decrease in intensity of the block copolymer peak is explained by an increase in phase miscibility as we impart greater thermal energy to polymer chains. The block copolymer peak position does not change from q = .027 (d = 23 nm) using the q_{max} method; with a modified hard sphere fit the size changes slightly from 20 nm at 40 °C to 19.5 nm at 140 °C. An increase in the amount of KF is explained as in-situ crystallization. These changes are not reversible, and the SAXS profile of the 140 C sample brought back down to room temperature is identical to it while scanned at 140 C.

4.4.1.4 Varied Anneal Temperature, 30% KF Blends

SAXS data was taken for VT cast 30% KF/70% TCT blends, for membranes cast from solution laid down at various temperatures, and then ramped to an elevated temperature. Sample temperature profiles for these membranes are given in Figure 4-35.

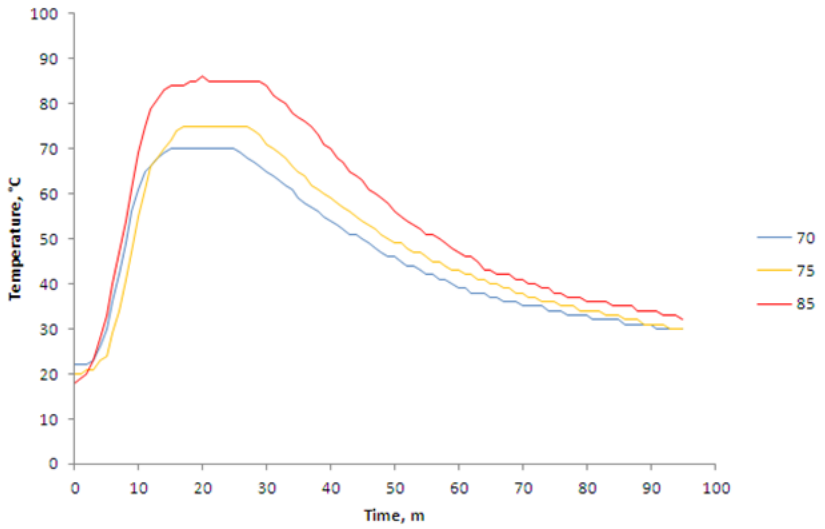

Figure 4-35: Experimental temperature profiles for VT cast membranes

Peak temperatures from 70 to 100 C were used. The SAXS response of these samples is given in Figure 4-36.

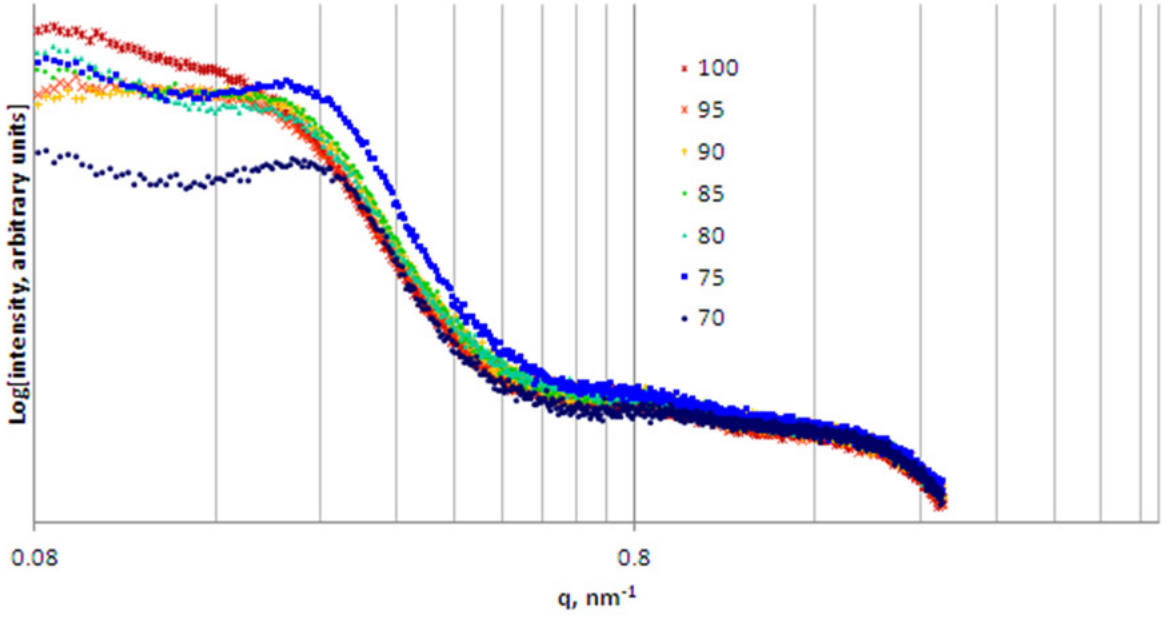

Figure 4-36: SAXS response of VT cast 30% KF annealed at various temperatures during casting (legend in °C)

The form of samples cast at elevated temperatures is slightly different than those cast at lower temperatures in the same two ways membranes at different operating temperatures vary: the block copolymer peak becomes less pronounced, and the KF region's intensity increases with higher temperature. KF crystallinity is, as with varied operating temperature, more significant when the material is exposed to higher temperature. The trend in the block copolymer peak is similar to that seen under different environmental conditions, but more pronounced. To illustrate this more clearly, the SAXS response of these materials is also presented offset in Figure 4-37.

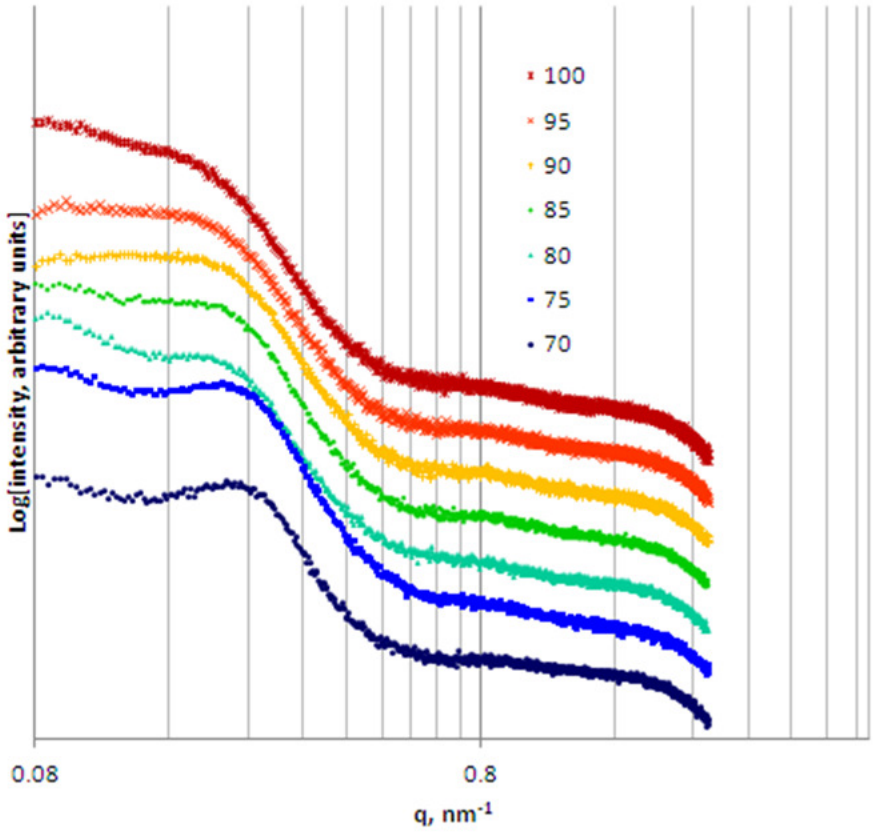

Figure 4-37: SAXS response of VT cast 30% KF annealed at various temperature during casting, offset (legend in °C)

The form of the block copolymer peak becomes significantly less prominent for samples annealed at 80 C or above. This could either represent an increase in the size of the feature (as

the peak broadens to lower q ranges), or a decrease in the intensity of its scattering due to phase mixing. Alternatively, the decrease in prominence of the block copolymer peak could result from disorder associated with a surface defect layer. When the polymer is heated during casting, one side is in contact with a heating plate, while the other is exposed to room temperature air. The change in temperature gradient as annealing temperature increases could be correlated to morphology disordering. Which of these effects is occurring can be studied either in TEM or AFM, and is the subject of proposed future work.

4.4.1.5 SAXS: Varied Casting Temperature, 30% KF

30% KF membranes were also cast at VT at different temperatures, by heating the casting block to a given temperature, and then applying solution to the surface. Solution was held for 1 hour for temperature above 60 C, for 3 hours at 50 C, 6 hours at 40 C, and 12 hours at 30 C, in order to ensure complete solidification of the membrane. The SAXS results are shown in .

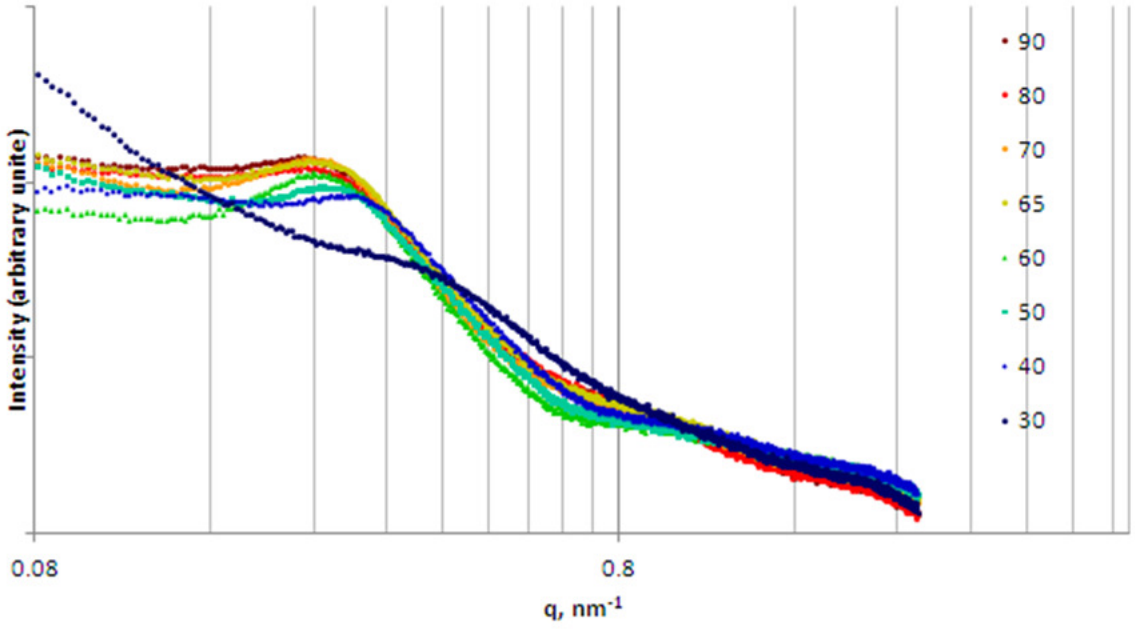

Figure 4-38: SAXS profile of VT cast 30% KF membranes, cast at various temperatures (legend in °C)

The trends for varied casting temperature are largely the same as for annealing temperature. Specifically, the block copolymer feature becomes less prominent for increased casting temperature, with little change above 65 ^{o}C. However, the block copolymer peak for every casting temperature is higher than the peak for the same temperature annealed sample. Therefore, the change in the block copolymer feature with elevated temperature anneal is less significant when the solution is laid down at elevated temperature. Kynar Flex crystallinity increases with higher temperature anneal, and does not appear to reach a maximum level.

4.4.2 Atomic Force Microscopy, 30% KF

AFM was performed on 30% KF blends, both GM cast and VT cast samples. In addition, both sides of the membrane were scanned: the side in contact with substrate during casting, and the one exposed to air while casting. For VT cast materials, data was taken for polymers cast on both glass and polypropylene-coated paper (PPP), while for GM cast membranes, only PPP samples were scanned. The results are shown in Figure 4-39 through Figure 4-45.

4.4.2.1 AFM, GM Cast 30% KF

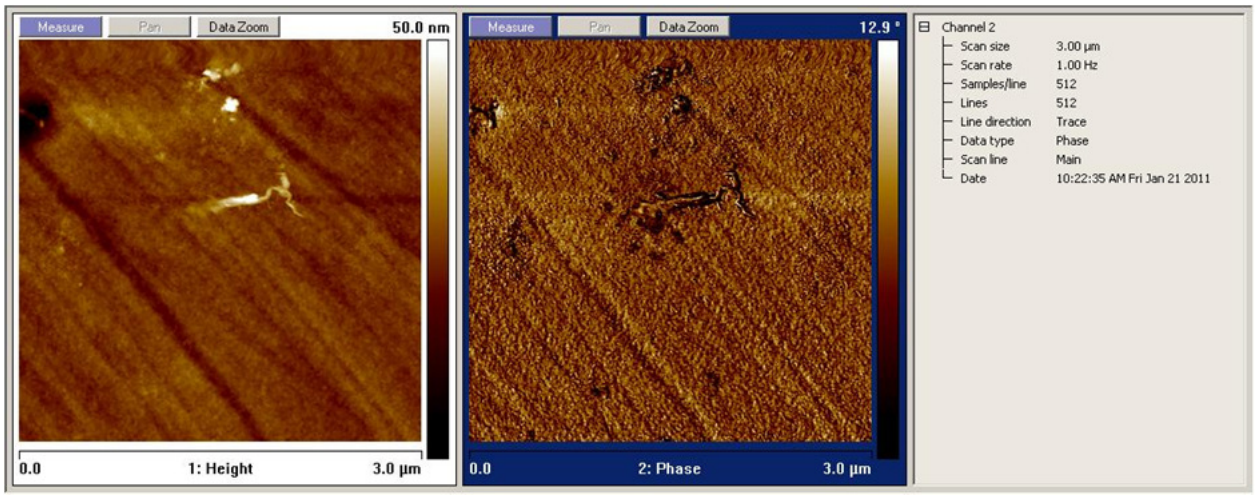

Figure 4-39: AFM of substrate side of GM cast 30% KF, 3 µm horizontal field width

For VT cast materials, we can see nano heterogeneities on the order of 25 nm, as predicted by SAXS data, but only on the substrate side. This morphology is clearer for scans with a horizontal field width of 1 µm, as shown in Figure 4-40.

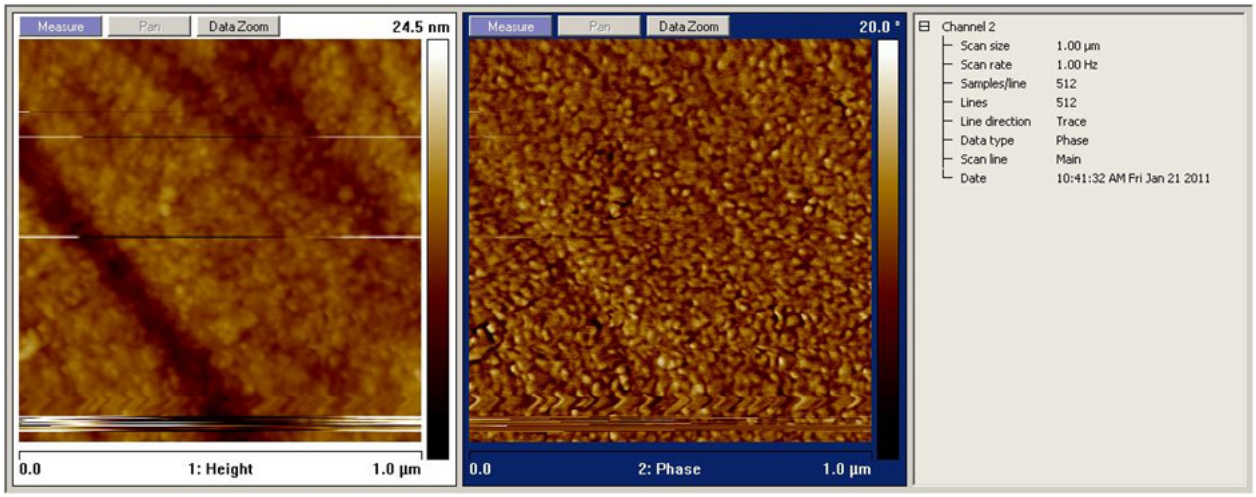

Figure 4-40: AFM of substrate side of GM cast 30% KF, 1 µm horizontal field width

This likely represents block copolymer phase separation. However, on the air exposed side of VT cast materials, we observe an extremely uniform morphology, but with some features on the order of 25 µm, as seen in Figure 4-41.

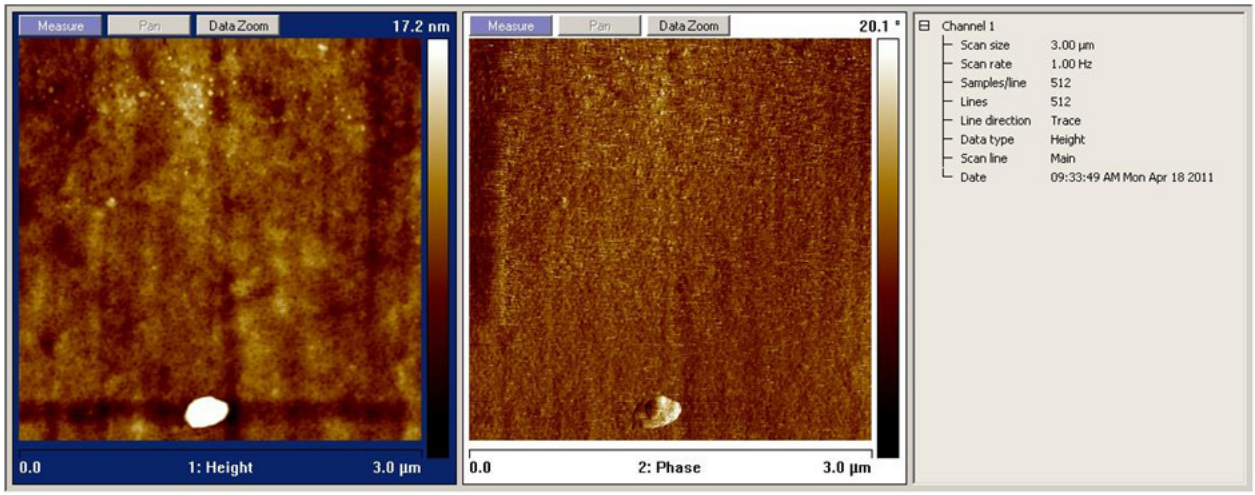

Figure 4-41: AFM of air exposed side of GM cast 30% KF, 3 µm horizontal field width

Due to tip defects, these heterogeneities appear somewhat smeared in the phase image, but are still visible upon close examination. Also, because the phase scales for both micrographs- air exposed and substrate sides- are nearly identical (20.1 and 20.0, respectively), and the contrast in the images is similar, we can conclude that the morphologies are also similar.

However, the features observed on the air-exposed side (50-70 nm) are larger than those on the substrate side (25 nm), and thus represents a different degree of ordering. This phenomenon is also observed in VT cast onto PPP 30% KF membranes.

4.4.2.2 AFM, VT cast 30% KF

AFM data for VT cast 30% KF samples includes results for samples cast on PPP substrates as well as on glass. The results for VT cast 30% KF membranes cast onto PPP are given in Figure 4-42 and Figure 4-43.

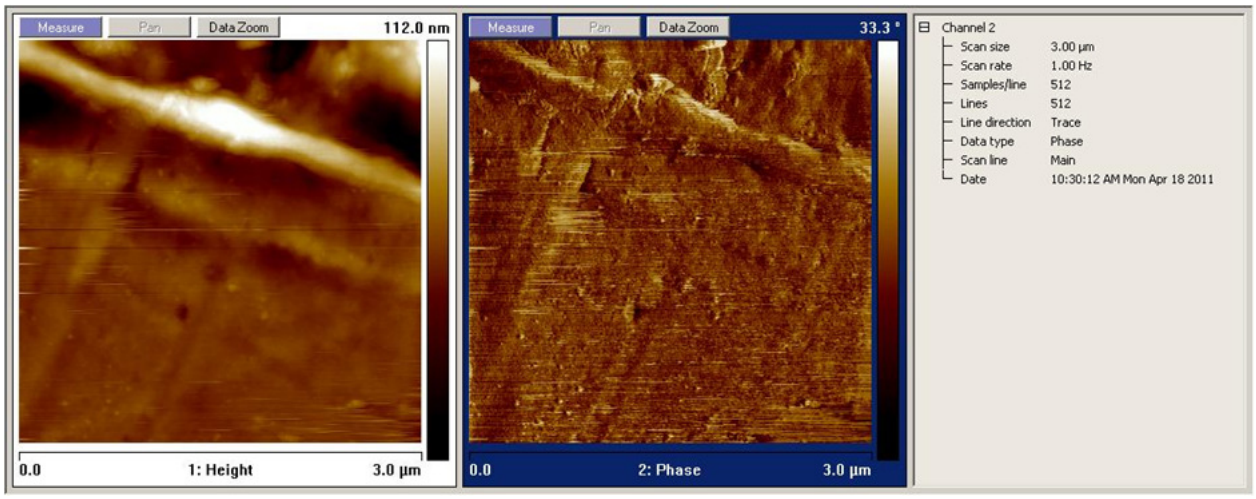

Figure 4-42: AFM of substrate side of VT cast 30% KF cast on PPP, 3 µm horizontal field width

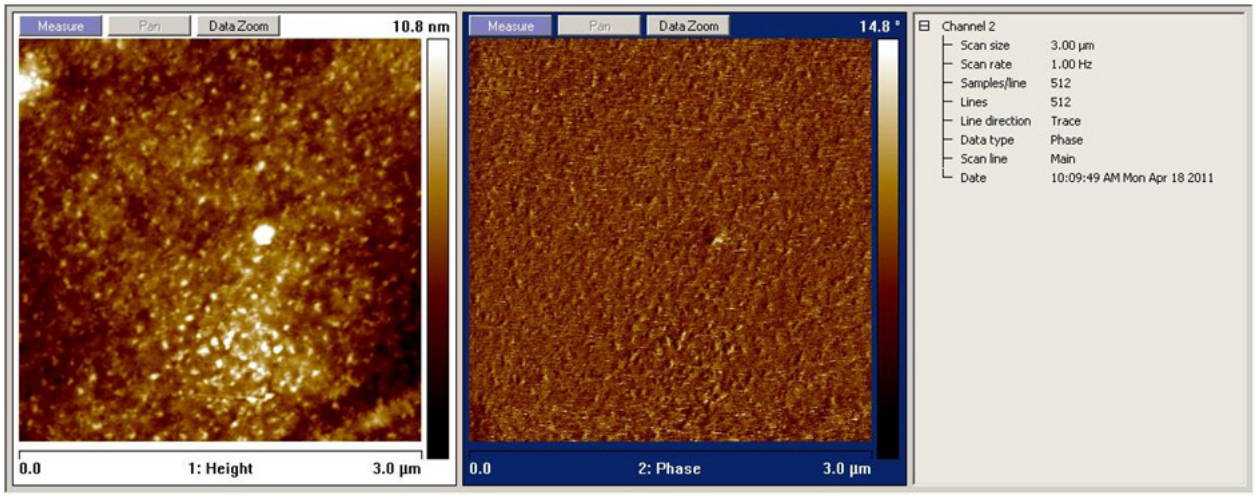

Figure 4-43: AFM of air exposed side of VT cast 30% KF cast on PPP, 3 µm horizontal field width

A similar morphology is seen in VT cast (onto PPP) 30% KF blends as for GM cast (onto PPP) 30% KF membranes. Both show a substrate side with significant topography, and some potential heterogeneities representative of phase separation. Both show, on their air-exposed sides, obvious phase heterogeneities on the order of the block copolymer peak seen in SAXS, though with sizes up to 50 nm. For VT cast materials, q_{max} method gives a size of 40 nm, still smaller than the heterogeneities seen on air side AFM scans. Therefore, the air exposed side of VT cast 30% KF does not represent a bulk morphology, but a less tightly ordered one, as with GM cast 30% KF samples.

VT materials cast onto glass show significant differences from the morphology of membranes cast onto PPP, as well as differences between the morphology of the substrate and air sides (Figure 4-44 and Figure 4-45).

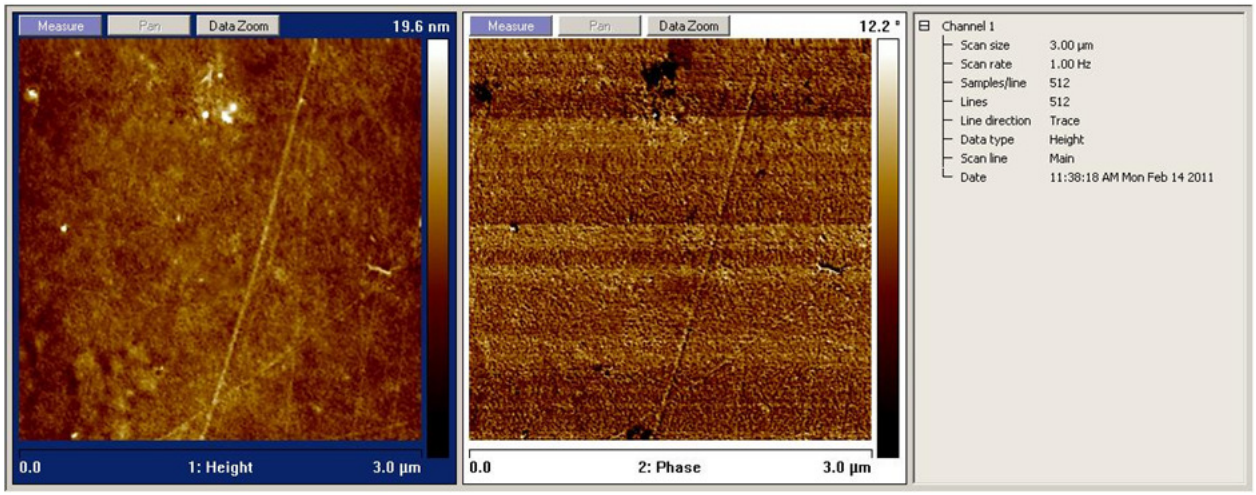

Figure 4-44: AFM of air exposed side of VT cast 30% KF cast on glass, 3 µm horizontal field width

The morphology of the air exposed side of VT cast 30% KF shows phase texture, with heterogeneities on the order of 30 nm, which agrees well with SAXS data of VT cast 30% KF blends. However, the morphology of the substrate side of the same material (cast onto glass) appears radically different than the VT and GM cast materials which were cast onto PPP.

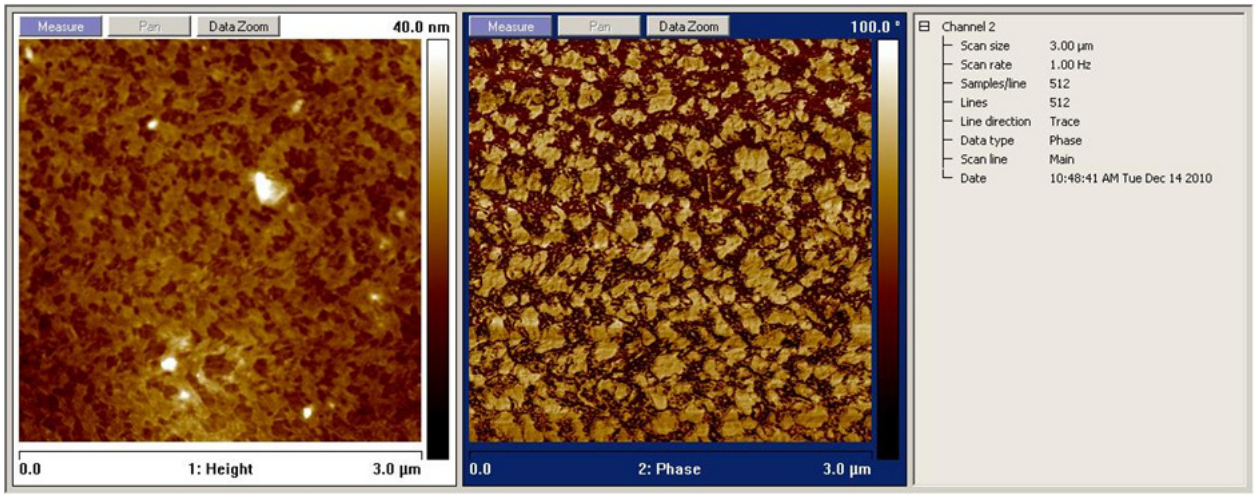

Figure 4-45: AFM scan of substrate side of VT cast 30% KF cast on glass, 3 µm horizontal field width

The heterogeneities on the substrate side of VT cast materials are approximately 240 nm in size, an order of magnitude larger than GM cast materials. This size is not detectable in SAXS, which is only useful for features up to 100 nm. This morphology does appear interconnected at a nanometer level, as seen in figure Figure 4-46.

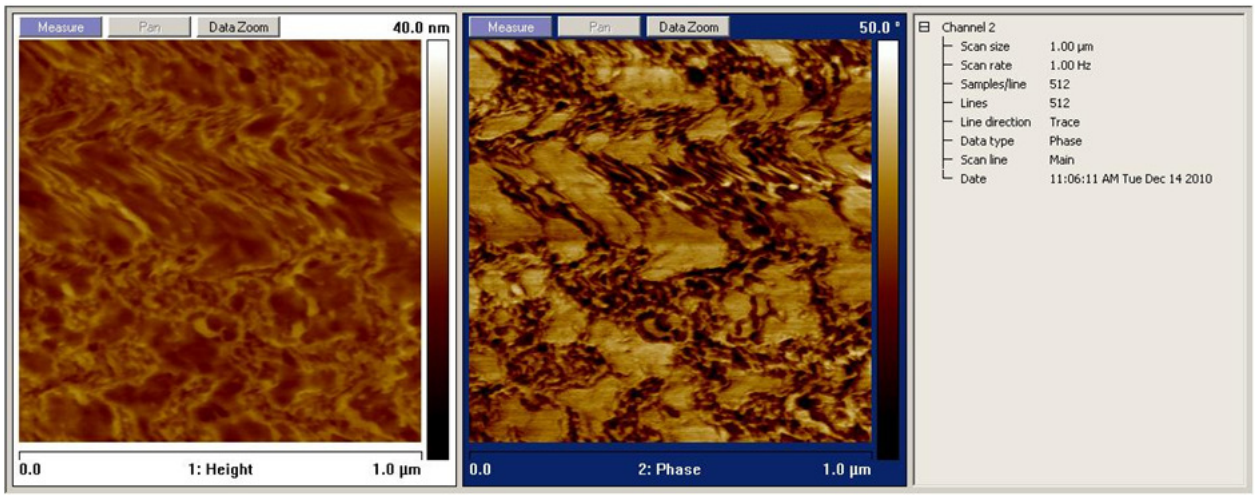

Figure 4-46: AFM of substrate side of VT cast 30% KF cast on glass, 1 µm horizontal field width

Though the larger, 240 nm heterogeneities are still visible, in these higher resolution scans, we also observe small particles or channels between the large particles. These features occur on the order of 40 nm, which corresponds well to SAXS data.

Ultimately, AFM of 30% blends has shown us that solution casting parameters, such as substrate, and the side of the membrane exposed to air during casting, can have notably different morphologies. Because the electrochemical behavior of a PEM is determined by its ionic aggregation structure, this will prove crucial to the optimization of S-PFCB in fuel cells.

4.4.3 SAXS, Varied Casting Substrate, 30% KF

In order to further probe the difference among membranes cast onto different substrates, VT cast 30% KF membranes cast onto glass, and cast onto polypropylene-coated paper, were studied in SAXS, along with GM cast onto PPP 30% KF samples. The results are given in Figure 4-47.

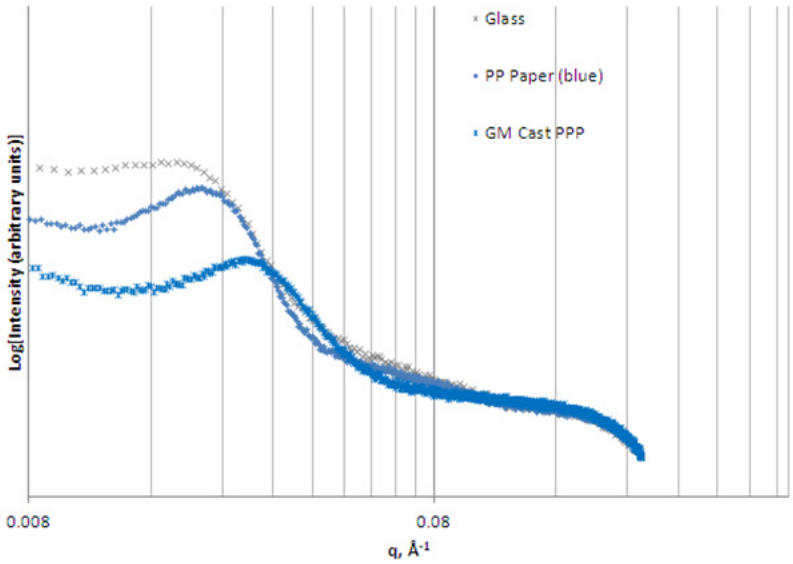

Figure 4-47: SAXS profiles of VT cast onto glass and PPP, and GM cast onto PPP

A clear difference in both the peak position and its intensity appear among these three different samples. GM cast onto PPP shows the lowest average feature size, 23 nm. VT Cast onto PPP gives block copolymer phase separation of approximately 30 nm. VT cast onto glass shows the largest block copolymer feature size, at 34 nm. Also, the region of the SAXS response related to KF crystallinity is lowest for GM cast onto PPP, and highest for VT cast onto glass. This suggests that the actual casting process is influenced by the substrate, either in substrate-

polymer solution interactions, or in the temperature gradient which the solution experiences during casting. In order to determine this more definitively, using heat lamps to heat both sides of the solution during casting is recommended for future work.

4.4.4 Solvent Dissolution, 30% KF

Several blends were exposed to DMAc after casting, in order to evaluate their chemical resistance:

- GM cast 30% KF/70% TAKS, unannealed and annealed at 100 ^{o}C for 2 hours
- GM cast 30% KF/70% TT, unannealed and annealed at 100 ^{o}C for 2 hours
- VT cast 30% KF/70% TAKS, unannealed and annealed at 100 ^{o}C for 2 hours

For every one of these, unannealed samples dissolved within 5 minutes, while annealed samples resisted dissolution. However, VT cast samples dissolved slightly, with a visible solid mass as well as a visible solution of polymer surrounding it. When ultrasonicated, all samples entered solution state.

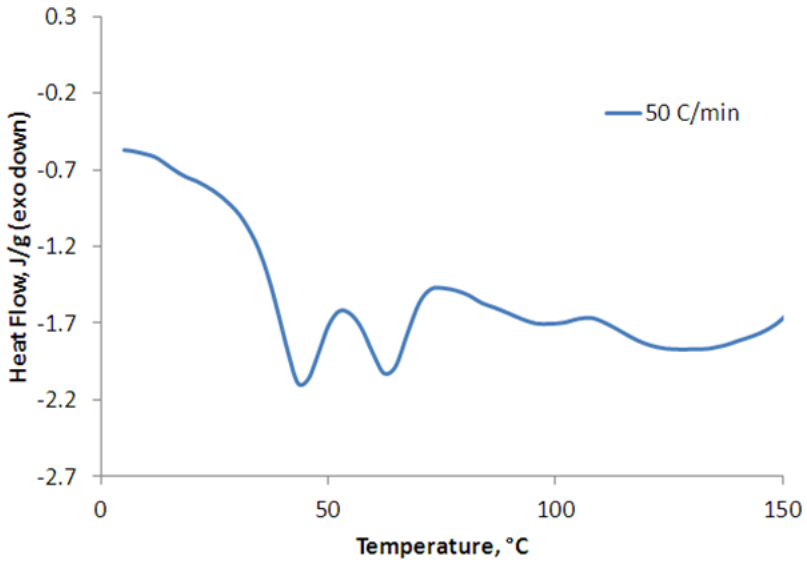

Figure 4-48: Cooling scan of VT cast 50% KF, 1 ^{o}C/min

The relative heat of each event is independent of cooling rate, while the temperature of each crystallization is highly dependent on cooling rate. For the higher temperature event, 1 ^{o}C/min cooling allows it to occur at approximately 103 ^{o}C, while for a cooling rate of 50 ^{o}C/min, it is centered on 65 ^{o}C. Likewise, the lower temperature event occurs around 53 ^{o}C for 1 ^{o}C/min cool, and 45 ^{o}C for 50 ^{o}C/min cooling. Using this knowledge, we can manipulate these crystallization events using controlled anneals and cools. Ultimately, we may be able to promote the formation of one phase of crystallinity over another.

Chapter 5: Conclusions and Future Work

Through studying S-PFCB and KF, and their blends with SAXS, DSC, and AFM, we have identified many important morphological features. First, we have shown the existence of a block copolymer-associated phase separation, which arranges itself on the order of 19-40 nm, depending on processing and blend composition; casting or annealing membranes at elevated temperature tends to increase the size of the feature. We have also identified the existence of ionic aggregate features of 2.5-3 nm. We have shown the glass transition of pure S-PFCB occurs at 125 C. We have shown that S-PFCB cannot be processed to induce crystallinity, even though one of its blocks is highly crystalline. Likewise, we have shown that KF does form crystallinity in blends of all compositions.

We have also characterized the change in the block copolymer feature as well as the ionic aggregate structure for blends of S-PFCB and Kynar Flex. The size and size distribution of the block copolymer peak becomes larger and more broad, respectively. Furthermore, we have shown that Kynar Flex can crystallize even after the membrane itself has been cast, by exposing the membrane to elevated temperature. The morphology of these blends has been shown to be most pliable during the casting phase, though it can still be changed irreversibly in the solid phase. For the most relevant blend composition, 30% KF, we have identified two crystallization events in the KF phase.

Finally, through SAXS, AFM, and DSC studies, we have shown evidence that the morphology of S-PFCB and its KF blends can form morphologies that are nonuniform through the sample. The surface morphology of 30% KF blends is not the same on the side of the membrane in contact with the substrate during casting, and the one exposed to air. Furthermore, the substrate side of a membrane cast onto glass is significantly morphologically different than the analogous side of a membrane cast onto polypropylene coated paper.

Several important studies remain to be done in order to understand the processing-morphology relationship of S-PFCB and its KF blends. First, understanding the effect of humidity on morphology will match up well with mechanical characterization of the material,

which is always performed with respect to relative humidity and temperature. This will involve the use of a unit designed to flow humidified air through the small-angle x-ray scattering chamber. Though it has been built on this project, it has not yet been used to run any systematic studies.

It runs by heating a reservoir of water in the main chamber, and flowing air through the water and out the top of the chamber. The water that leaves the chamber then has a dew point temperature of the liquid water. Next, the air is flowed through a cell meant for scanning samples in liquid. This chamber and its inlet it heated to the desired temperature of the specimen. Knowing both environmental temperature and dew point temperature, it is possible to calculate relative humidity using the following equation [43]:

$$RH = 100\left(\frac{112 - .1T + T_{DP}}{112 + .9T}\right)^8$$

Where T is environmental temperature, T_{DP} is dew point temperature, and RH is % relative humidity. SAXS scans will be performed for room temperature, 70 °C and 90 °C at several relative humidities for each temperature.

In addition to RH studies on SAXS, form factors should be developed for our given morphological descriptions, and then applied to our data. These would serve to validate or refute the models. If the models prove to be descriptive, we will know in much greater detail the specifics of phase and aggregate dimensions.

Finally, TEM should be performed on these samples. TEM has often been used to observe both block copolymer phase separation and ionic aggregation. Such a study would directly observe these structures, giving a clearer picture than the volumetric average of SAXS or DSC.

References Cited

1. Kreuer, K. D., On the development of proton conducting polymer membranes for hydrogen and methanol fuel cells. *Journal of Membrane Science* **2001,** *185* (1), 29-39.
2. H. -G. Haubold, T. V., H. Jungbluth, P. Hiller, Nano structure of NAFION: a SAXS stud. *Electrochim Acta* **2001,** *45* (10-11), 1559-1563.
3. Dennis W. Smith Jr, J. J., Hiren V. Shah, Yuan Xie, Darryl D. DesMarteau, Anomalous crystallinity in a semi-fluorinated perfluorocyclobutyl (PFCB) polymer containing the hexafluoro-i-propylidene (6F) linkage. *Polymer* **2004,** *45* (17), 5755-5760.
4. Mauritz, K. A.; Moore, R. B., State of Understanding of Nafion. *ChemInform* **2004,** *35* (50), no-no.
5. (a) Andujar, J. M., Fuel cells: History and updating. A walk along two centuries. *Renewable and Sustainable Energy Reviews* **2009,** *13* (9), 2309-2322; (b) Kerres, J. A., Development of ionomer mebranes for fuel cells. *Journal of Membrane Science* **2001,** *185* (1), 3-27.
6. O'Hayre, R., *Fuel Cell Fundamentals*. Wiley: 2006.
7. Kamaruzzaman Sopian, W. R. W. D., Challenges and future developments in proton exchange membrane fuel cells. *Renewable Energy* **2006,** *31* (5), 719-727.
8. Gierke, T. D.; Munn, G. E.; Wilson, F. C., The morphology in nafion perfluorinated membrane products, as determined by wide- and small-angle x-ray studies. *Journal of Polymer Science: Polymer Physics Edition* **1981,** *19* (11), 1687-1704.
9. (a) Casciola, M.; Alberti, G.; Sganappa, M.; Narducci, R., On the decay of Nafion proton conductivity at high temperature and relative humidity. *Journal of Power Sources* **2006,** *162* (1), 141-145; (b) Kreuer, K. D., On the development of proton conducting materials for technological applications. *Solid State Ionics* **1997,** *97* (1-4), 1-15.
10. Takeshi Kobayashi, M. R., Kohei Sanui, Naoya Ogata, Proton-conducting polymers derived from poly(ether-etherketone) and poly(4-phenoxybenzoyl-1,4-phenylene). *Solid State Ionics* **1998,** *106* (3-4), 219-225.
11. M. Rikukawa, K. S., Proton-conducting polymer electrolyte membranes based on hydrocarbon polymers. *Progress in Polymer Science* **2000,** *25* (10), 1463-1502.
12. Dennis W. SmithJr., D. A. B., Hiren V. Shah, Adrienne Hoeglund, R. Traiphol, Dvora Perahia, Harold W. Boone, Charles Langhoff, Mike Radler, Perfluorocyclobutane (PFCB) polyaryl ethers: versatile coatings materials. *Journal of Fluorine Chemistry* **2000,** *104*, 109-117.
13. Osborne, A. investigation of Phase Morphology and Blend Stability In Ionomeric Perfluorocyclobutane (PFCB)/Poly(Vinylidene Difluoride) (PVDF) Copolymer Blend Membranes. Virginia Tech, Blackburg, VA, 2010.

14. Lee, M.; Park, J. K.; Lee, H.-S.; Lane, O.; Moore, R. B.; McGrath, J. E.; Baird, D. G., Effects of block length and solution-casting conditions on the final morphology and properties of disulfonated poly(arylene ether sulfone) multiblock copolymer films for proton exchange membranes. *Polymer* **2009,** *50* (25), 6129-6138.
15. Zhao, Y.; Yin, J., Synthesis and evaluation of all-block-sulfonated copolymers as proton exchange membranes for fuel cell application. *Journal of Membrane Science* **2010,** *351* (1-2), 28-35.
16. Song Xue, G. Y., Proton exchange membranes based on poly(vinylidene diflouride) and sulfonated poly(ether etherketone). *Polymer* **2006,** *47*, 5044-5049.
17. (a) P.E. Thomas, J. F. L., C.A. Sperati and J.L. McPherson, Effects on fabrication on the properties of teflon resins. *Society of Plastic Engineers Journal* **1956,** *12*, 89-95; (b) Hu Ting-Yung, N. S. E. J., The effects of molecular weight and cooling rate on fine structure, stress-strain behavior and wear of polytetrafluoroethylene. *Wear* **1982,** *84* (2), 203-215.
18. Rae, P. J.; Brown, E. N., The properties of poly(tetrafluoroethylene) (PTFE) in tension. *Polymer* **2005,** *46* (19), 8128-8140.
19. Hensley, J. E.; Way, J. D.; Dec, S. F.; Abney, K. D., The effects of thermal annealing on commercial Nafion® membranes. *Journal of Membrane Science* **2007,** *298* (1-2), 190-201.
20. Hwang, G. S.; Kaviany, M.; Gostick, J. T.; Kientiz, B.; Weber, A. Z.; Kim, M. H., Role of water states on water uptake and proton transport in Nafion using molecular simulations and bimodal network. *Polymer* **2011,** *52* (12), 2584-2593.
21. Martin, R. B. M. a. C. R., Chemical and Morphological Properties of Solution-Cast Perflourosulfate Ionomers. *Macromolecules* **1988,** *21*, 1334-1339.
22. Goswami, M.; Sumpter, B. G.; Huang, T.; Messman, J. M.; Gido, S. P.; Isaacs-Sodeye, A. I.; Mays, J. W., Tunable morphologies from charged block copolymers. *Soft Matter* **2010,** *6* (24), 6146-6154.
23. (a) T. D. GIERKE G. E. MUNN, a. F. C. W., E.I., The morphology in nafion perfluorinated membrane products, as determined by wide- and small-angle x-ray studies. *Journal of Polymer Science: Part B, Polymer Physics* **1981,** *19* (11), 1687-1704; (b) Moore, K. A. M. a. R. B., State of Understanding of Nafion. *Chem. Rev.* **2004,** *104*, 4535-4585.
24. Marx, C. L.; Caulfield, D. F.; Cooper, S. L., Morphology of Ionomers. *Macromolecules* **1973,** *6* (3), 344-353.
25. (a) Mineo Fujimura, T. H., Hiromichi Kawai, Small-angle x-ray scattering study of perfluorinated ionomer membranes: Origin of two scattering maxima. *Macromolecules* **1981,** *14* (5), 1309-1315; (b) MacKnight, W. J., Taggart, W.P., Stein, R.S., A model for the structure of ionomers. *Journal of Polymer Science: Polymer Symposia* **1974,** *45* (1), 113-128; (c) Fujimura, M.; Hashimoto, T.; Kawai, H., Small-angle x-ray scattering study of perfluorinated ionomer membranes. 2. Models for ionic scattering maximum. *Macromolecules* **1982,** *15* (1), 136-144.

26. Eisenberg, A.; Hird, B.; Moore, R. B., A new multiplet-cluster model for the morphology of random ionomers. *Macromolecules* **1990,** *23* (18), 4098-4107.
27. Ise, M. Polymer-Elektrolyt-Membranen: Untersuchungen zur Mikrostruktur und und zu den Transporteigenschaften fur Protonen und Wasser. Dissertation, Stuttgart Universitat, Stuttgart, 2000.
28. Laurent Rubatat, A. L. R., Gérard Gebel, and Olivier Diat, Evidence of Elongated Polymeric Aggregates in Nafion. *Macromolecules* **2002,** *35* (10), 4050-4055.
29. Schmidt-Rohr, K.; Chen, Q., Parallel cylindrical water nanochannels in Nafion fuel-cell membranes. *Nat Mater* **2008,** *7* (1), 75-83.
30. Won, J.; Choi, S. W.; Kang, Y. S.; Ha, H. Y.; Oh, I.-H.; Kim, H. S.; Kim, K. T.; Jo, W. H., Structural characterization and surface modification of sulfonated polystyrene-(ethylene-butylene)-styrene triblock proton exchange membranes. *Journal of Membrane Science* **2003,** *214* (2), 245-257.
31. Isaacs Sodeye, A. I.; Huang, T.; Gido, S. P.; Mays, J. W., Polymer electrolyte membranes from fluorinated polyisoprene-block-sulfonated polystyrene: Structural evolution with hydration and heating. *Polymer* **2011,** *52* (14), 3201-3208.
32. Kim, B.; Kim, J.; Jung, B., Morphology and transport properties of protons and methanol through partially sulfonated block copolymers. *Journal of Membrane Science* **2005,** *250* (1-2), 175-182.
33. Shi, Z.; Holdcroft, S., Synthesis and Proton Conductivity of Partially Sulfonated Poly([vinylidene difluoride-co-hexafluoropropylene]-b-styrene) Block Copolymers. *Macromolecules* **2005,** *38* (10), 4193-4201.
34. Gromadzki, D.; Cernoch, P.; Janata, M.; Kudela, V.; Nallet, F.; Diat, O.; Stepánek, P., Morphological studies and ionic transport properties of partially sulfonated diblock copolymers. *European Polymer Journal* **2006,** *42* (10), 2486-2496.
35. Zhao, C.; Lin, H.; Shao, K.; Li, X.; Ni, H.; Wang, Z.; Na, H., Block sulfonated poly(ether ether ketone)s (SPEEK) ionomers with high ion-exchange capacities for proton exchange membranes. *Journal of Power Sources* **2006,** *162* (2), 1003-1009.
36. (a) Liu, F.; Hashim, N. A.; Liu, Y.; Abed, M. R. M.; Li, K., Progress in the production and modification of PVDF membranes. *Journal of Membrane Science* **2011,** *375* (1-2), 1-27; (b) Tian, X.; Jiang, X., Poly(vinylidene fluoride-co-hexafluoropropene) (PVDF-HFP) membranes for ethyl acetate removal from water. *Journal of Hazardous Materials* **2008,** *153* (1-2), 128-135; (c) Abbrent, S.; Plestil, J.; Hlavata, D.; Lindgren, J.; Tegenfeldt, J.; Wendsjö, Å., Crystallinity and morphology of PVdF-HFP-based gel electrolytes. *Polymer* **2001,** *42* (4), 1407-1416.
37. Inan, T. Y.; Dogan, H.; Unveren, E. E.; Eker, E., Sulfonated PEEK and fluorinated polymer based blends for fuel cell applications: Investigation of the effect of type and molecular weight of the fluorinated polymers on the membrane's properties. *International Journal of Hydrogen Energy* **2010,** *35* (21), 12038-12053.

38. (a) Chang, B.-J.; Kim, D. J.; Kim, J. H.; Lee, S.-B.; Joo, H. J., Sulfonated poly(fluorene-co-sulfone)ether membranes containing perfluorocyclobutane groups for fuel cell applications. *Journal of Membrane Science* **2008,** *325* (2), 989-996; (b) Kim, D.-J.; Chang, B.-J.; Kim, J.-H.; Lee, S.-B.; Joo, H.-J., Sulfonated poly(fluorenyl ether) membranes containing perfluorocyclobutane groups for fuel cell applications. *Journal of Membrane Science* **2008,** *325* (1), 217-222; (c) Zhu, Y.; Chen, H.; He, C., Novel polyelectrolytes containing perfluorocyclobutane and triazole units: synthesis, characterization and properties. *Polym J* **2011,** *43* (3), 258-264; (d) SCOTT T. IACONO, D. E., AMIT SANKHE, ARNO RETTENBACHER, and DENNIS W. SMITH, JR., Sulfonated fluorovinylene aromatic ether polymers for proton exchange membrane. *High Performance Polymers* **2007,** *19*, 581-591; (e) Iacono, S. T.; Budy, S. M.; Jin, J.; Smith, D. W., Science and technology of perfluorocyclobutyl aryl ether polymers. *Journal of Polymer Science Part A: Polymer Chemistry* **2007,** *45* (24), 5705-5721.
39. Timothy J. Fuller, M. S. Sulfonated Pefluorocyclobutane Polyelectrolyte Membranes for Fuel Cells. June 23, 2008, 2011.
40. Iwai, Y.; Yamanishi, T., Thermal stability of ion-exchange Nafion N117CS membranes. *Polymer Degradation and Stability* **2009,** *94* (4), 679-687.
41. (a) Kratky, O.; Pilz, I.; Schmitz, P. J., Absolute intensity measurement of small angle x-ray scattering by means of a standard sample. *Journal of Colloid and Interface Science* **1966,** *21* (1), 24-34; (b) Pilz, I.; Kratky, O., Absolute intensity measurement of small-angle X-ray scattering by means of a standard sample, II. *Journal of Colloid and Interface Science* **1967,** *24* (2), 211-218; (c) Pilz, I., Absolute intensity measurement of small-angle x-ray scattering by means of a standard sample, III. *Journal of Colloid and Interface Science* **1969,** *30* (1), 140-144; (d) Lixin Fan, M. D., Scott Bendle, Nick Grupido and Jan Ilavsky, Rigaku Innovative Technologies Inc., Auburn Hills, MI 48326, USA, Advanced Photon Source, Argonne National Laboratory, Argonne, IL 60439, USA The Absolute Calibration of a Small-Angle Scattering Instrument with a Laboratory X-ray Source. *Journal of Physics: Conference Series* **2010,** *247*, 1-10.
42. (a) Wu, D. Q.; Chu, B.; Lundberg, R. D.; MacKnight, W. J., Small-angle x-ray scattering (SAXS) studies of sulfonated polystyrene ionomers. 2. Correlation function analysis. *Macromolecules* **1993,** *26* (5), 1000-1007; (b) Mineo Fujimura, T. H., Hiromichi Kawai, Small Angle X-ray Scattering Study of Perflourinated Ionomer Membranes: 2. Models for Ionic Scattering Maxima. *Macromolecules* **1981,** *1982* (15).
43. Martin Wanielista, R. K. a. R. E., *Hydrology Water Quantity and Quality Control*. 2 ed.; John Wiley & Sons.